Aalto University
School of Engineering

Department of Applied Mechanics

Matias Mattila

EXPERIMENTAL METHODS FOR DETERMINING THE RESIDUAL STRESSES OF COMPOSITE LAMINATES

Master's thesis for the degree of Master of Science in Technology submitted for inspection, Espoo, 25 February, 2013.

Supervisor **Professor Olli Saarela**

Instructor **M.Sc. Tuomas Pärnänen**

Aalto University
School of Engineering

Aalto University, P.O. BOX 11000, 00076
AALTO
www.aalto.fi

Abstract of master's thesis

Author	Matias Mattila
Title of thesis	Experimental methods for determining the residual stresses of composite laminates
Department	Department of Applied Mechanics
Professorship	Aeronautical Engineering
Code of professorship	Kul-34
Thesis supervisor	Professor Olli Saarela
Thesis advisor	Tuomas Pärnänen, M.Sc.
Date	25.2.2013
Number of pages	76+5
Language	English

Abstract

The object of the thesis was to find experimental methods for determination of cure induced residual stresses in composite materials. The stresses develop because of the differences in the thermal and elastic properties of the constituents of a composite. The residual stresses may affect the strength of a composite material. The stresses may also cause delamination and matrix microcracking, which means degradation of the material properties.

Many of the residual stress determination methods have been developed for isotropic materials in first place. Later on, the methods have been extended for orthotropic materials such as composites. Both destructive and non-destructive and also semi-destructive methods have been developed. Some of the methods are suitable only for a specific shaped specimen.

In the experimental section of the thesis some of the residual stress determination methods were evaluated. The experiments were done mainly in the facilities of Aalto University at the Department of Applied Mechanics. The results of the experiments were partly evaluated by comparing them to thermal stresses taking place due to cooling to the ambient temperature from the cure temperature and partly by using FEM modelling.

As a conclusion, some of the tested experimental methods showed their potential in residual stress measurement. Some methods, such as hole-drilling method could be developed further to be an efficient tool for finding the residual stresses of composite materials. Combining some experimental measurements to FEM modelling could provide opportunities for determination of residual stresses.

Keywords residual stresses in composite, experimental method, hole-drilling

Aalto-yliopisto
Insinööritieteiden
korkeakoulu

Aalto-yliopisto, PL 11000, 00076 AALTO
www.aalto.fi
Diplomityön tiivistelmä

Tekijä Matias Mattila

Työn nimi Kuitulujitteisten komposiittien jäännösjännitysten kokeellinen määrittäminen

Laitos Sovelletun mekaniikan laitos

Professuuri Lentotekniikka **Professuurikoodi** Kul-34

Työn valvoja Professori Olli Saarela

Työn ohjaaja Tuomas Pärnänen, DI

Päivämäärä 25.2.2013 **Sivumäärä** 76+5 **Kieli** Englanti

Tiivistelmä

Tässä työssä esitellään komposiittien jäännösjännitysten kokeellisia määritysmenetelmiä ja jännityksiin johtavia tekijöitä. Komposiittimateriaaleissa esiintyy jäännösjännityksiä materiaalin ainesosasten kemiallisten ja elastisten ominaisuuksien, sekä lämpölaajenemiserojen johdosta. Jäännösjännitykset voivat vaikuttaa komposiittimateriaalin lujuuteen. Jäännösjännitykset voivat myös aiheuttaa delaminaatiota ja matriisin mikrosäröilyä, jotka johtavat materiaaliominaisuuksien heikkenemiseen.

Useat jäännösjännitysten määritysmenetelmät on kehitetty alun perin isotrooppisia materiaaleja silmälläpitäen. Myöhemmin näitä menetelmiä on jatkokehitetty komposiittimateriaaleja varten. Jäännösjännitysten määrittämiseen on olemassa sekä ainetta rikkovia, että ainetta rikkomattomia menetelmiä. Jotkut menetelmistä soveltuvat ainoastaan tietyn muotoiselle kappaleelle.

Tämän työn kokeellisessa osuudessa testattiin joitakin jäännösjännitysten määritysmenetelmiä. Kokeet tehtiin pääosin Aalto-yliopistossa, Sovelletun mekaniikan laitoksen tiloissa. Kokeellisia tuloksia arvioitiin vertaamalla niitä kovetuslämpötilan ja huoneen lämpötilan lämpötilaerosta aiheutuviin laskennallisiin jännityksiin. Osassa kokeista arviointiin käytettiin myös elementtimenetelmään perustuvaa laskentaa.

Osa menetelmistä osoitti potentiaalinsa ja käytettävyytensä jäännösjännitysten määrittämiseen. Joitakin menetelmiä, kuten reiänporausmenetelmää, voitaisiin kehittää edelleen soveltamalla eri tekniikoita porauksen aikana vapautuvien jännitysten aiheuttamien venymien mittaukseen ja jännitysten laskentaan. Myös kokeellisten tulosten ja FEM-mallinnuksen yhdistäminen voisi tuoda uusia mahdollisuuksia jäännösjännitysten määrittämiseen.

Avainsanat komposiitin jäännösjännitykset, kokeelliset menetelmät

Preface

The thesis was done in the Laboratory of Lightweight Structures at Aalto University. The thesis was a part of the LIGHT project (Low density material solutions), funded by the Finnish Funding Agency for Technology and Innovation (Tekes) and Finnish partner companies mainly from the branch of reinforced plastic industry. Relating to the residual stress measurements, the company Stresstech Oy demonstrated their devices.

I express my gratitude to Professor Olli Saarela for interesting thesis topic and to M.Sc. Tuomas Pärnänen and M.Sc. Markus Wallin for developing comments on the thesis and technical support. I also want to thank the Stresstech Oy and Markus Laakkonen for introducing their company and facilities and demonstrating the hole-drilling residual stress measurement device. Visiting Stresstech was rewarding and hopefully this initiates the cooperation between the Laboratory and the company. Finally I want to thank my colleagues and friends at the University for a pleasant working environment and support.

Espoo, 25 February, 2013

Matias Mattila

Table of contents

Preface I
Table of contents II
Abbreviations IV
List of symbols V
1 Introduction 1
2 Shrinkage of plastics 2
2.1 Chemical shrinkage of a thermoset 3
2.2 Thermal shrinkage of a thermoset 4
2.3 Shrinkage of thermoplastics 4
3 Residual stresses of a composite 5
3.1 Formation of residual stresses 5
3.2 Residual stress effects 10
4 Measurement of the residual stresses 13
4.1 Ring slitting method 13
4.2 Hole drilling method 15
4.3 Moiré interferometry 19
4.4 Layer removal method 23
4.5 Cut cylinder bending test 26
4.6 X-Ray Diffraction, Micro Raman Spectroscopy and fiber Bragg gratings 29
5 Affecting residual stresses 33
6 Experiments 36
6.1 Materials and manufacturing 36
6.2 Hole-drilling method 41
6.2.1 Theory 41
6.2.2 Test procedures 45
6.2.3 Results and discussion 46
6.2.4 Electronic Speckle Pattern Interferometry (ESPI) 49
6.3 Layer-removal method 51
6.3.1 Theory 51
6.3.2 Test procedures 53
6.3.3 Results and discussion 53

6.4 Unsymmetrical laminate....56
6.4.1 Theory....56
6.4.2 Test procedures....58
6.4.3 Results and discussion....59
7 Case study: Ring slitting method for a composite tube....61
8 Conclusions....70
9 References....72
10 Appendices....76

Abbreviations

CLT	Classical Lamination Theory
FEM	Finite Element Method
VCM	Vinyl Chloride Monomer
TFE	Tetrafluoroethylene
CTE	Coefficient of Thermal Expansion
UP	Unsaturated Polyester
EP	Epoxy
PF	Phenolic
PI	Polyimide
RTM	Resin Transfer Molding
CF	Carbon Fibre
PE	Polyethylene
PP	Polypropylene
PEEK	Polyetheretherketone
CRM	Cure Referencing Method
ILTS	Interlaminar Tensile Strength
XRD	X-Ray Diffraction
MRS	Micro Raman Spectroscopy
DSC	Differential Scanning Calorimetry
SG	Strain Gage
CNC	Computer Numerical Control
UD	Unidirectional
ESPI	Electronic Speckle Pattern Interferometry
CCD	Charge-Coupled Device

List of symbols

$\Delta V_{\%}$	Percentual change in volume
V	Volume
ρ	Density
ΔL	Change in the length
L	Length
L_0	Initial length
α	Coefficient of thermal expansion
T	Temperature
S	Chemical shrinkage
$\Delta\theta$	Angular change of a corner of a laminate
$\emptyset$	Cure shrinkage
Ψ	Stress function of a curved bar under pure bending
A	Constant in the stress function Ψ, Calibration constant
B	Constant in the stress function Ψ, Calibration constant
C	Constant in the stress function Ψ, Calibration constant
D	Constant in the stress function Ψ, Calibration constant
r	Radius of the ring
σ	Stress
τ	Shear stress
a	Inner radius of the ring
b	Outer radius of the ring
M	Moment
n	Coefficient, Number of moiré fringes
E	Elastic modulus
δ	Displacement
ε	Strain
θ	Strain gage angle in hole-drilling method
G	Shear modulus
ν	Poisson´s ratio
C	Influence coefficient
u	Displacement field in in-plane axis direction
v	Displacement field in perpendicular direction to u
δ_m	Distance between moiré fringes
l_g	Gage length
d_m	Reference grating line density
d_s	Specimen grating line density
p_m	Reference grating pitch
p_s	Specimen grating pitch
β	Angle between gratings

a_l	Measure of length in moiré fringe pattern
α	Angle between moiré fringes
U	Displacement in x-direction, Potential energy
V	Displacement in y-direction
ΔN	Change in the fringe order, change in the normal force
f	Frequency
z	Coordinate in thickness direction
$[A]$	Extensional stiffness matrix
$[B]$	Coupling stiffness matrix
$[D]$	Bending stiffness matrix
κ	Curvature
x	In-plane coordinate
y	In-plane coordinate perpendicular to x
a	Constant in the potential energy approach and hole-drilling method
b	Constant in the potential energy approach and hole-drilling method
c	Constant in the potential energy approach and hole-drilling method
d	Constant in the potential energy approach and hole-drilling method
e	Constant in the hole-drilling method, variable in layer-removal method
f	Constant in the hole-drilling method, variable in layer-removal method
r_i	Indicates the constants a, b, c and d
P	Force
$\emptyset_B^a$, $\emptyset_B^b$	Constants in cut cylinder bending calculation
$\emptyset_F$	Constant in cut cylinder bending calculation
$\emptyset_M^a$, $\emptyset_M^b$	Constants in cut cylinder bending calculation
c_0, c_1, c_2	Constants in cut cylinder bending calculation
$\bar{r}$	Normalized radius of the ring
$\bar{R}$	Normalized radius of the neutral surface
X	Integration constant
K	Constant in cut cylinder bending calculation
$E(\bar{r})$	Elastic modulus as a quadratic function of $\bar{r}$
$[\tilde{Q}]$, $[\bar{Q}]$	Stiffness matrix in laminate coordinate system
$[Q]$	Stiffness matrix in local (ply) coordinate system
$[T]$	Transformation matrix
$[S]$	Compliance matrix
$[C]$	Influence matrix
$[a^*]$	Normalized stiffness matrix
$F_{1,2}(\theta)$	Functions in hole-drilling method
$f_{1,2}(x, y)$	Functions in hole-drilling method
$\zeta_{1,2}(x, y)$	Functions in hole-drilling method
$\mu_{1,2}$	Complex parameters
$[\bar{E}]$	Dimensionless stiffness matrix
$\bar{E}$	Dimensionless elastic modulus

$\bar{G}$	Dimensionless shear modulus
N	Normal force
t	Thickness

Subscripts

p	Cured laminate, displacement measurement point
r	Resin
T	Thermal
S	Chemical
C	Internal
x	In-plane direction x
y	In-plane direction y perpendicular to x
0	Initial
r	Radial direction
θ	Tangential direction
f	Final
1	First strain gage, First layer removal, In-plane coordinate
2	Second strain gage, In-plane coordinate
3	Third strain gage, Out of plane coordinate
11	Longitudinal direction
22	Transverse direction
12	12- direction
m	Moiré
g	Gage
l	Length
D	Delamination
R	Restoring
L	Longitudinal
T	Transverse
k, i	Number of ply
xy	Laminate coordinate system
np	Neutral plane

Superscripts

0	Midplane
a	Inner radius
b	Outer radius
k	Number of ply, Number of removed layers
i	Number of ply

1 Introduction

Residual stresses build up in composite laminates due to the differences in the thermo-mechanical properties of the matrix and the reinforcing fibres. The mechanism of the residual stress formation is well studied subject by many researchers from the 20th century until today. Understanding of the mechanism is vital for developing methods to predict these stresses and also to develop such manufacturing techniques that lead to as stress free laminates as possible. Several analytical methods for predicting the laminate shape distortions due to residual stresses have been developed. By using the Classical Lamination Theory (CLT) it is possible to predict in-plane deformations and small out-of-plane deformations as well. For larger out-of-plane deformations a more accurate method based on the potential energy approach has been developed. Several FEM-software are also capable to calculate the behavior of orthotropic materials such as composites.

The purpose of this study is to present the experimental methods developed for finding out the residual stresses of polymer composites. The principles and relating equations of the methods are introduced with some examples and figures. For understanding the factors that affect formation of residual stresses, the behavior of polymers and fibres, as well as their interaction is introduced. Also a brief introduction to polymer chemistry is presented for understanding some processes that take place during the cure. The flow chart represents the progress of the thesis (Figure 1.1).

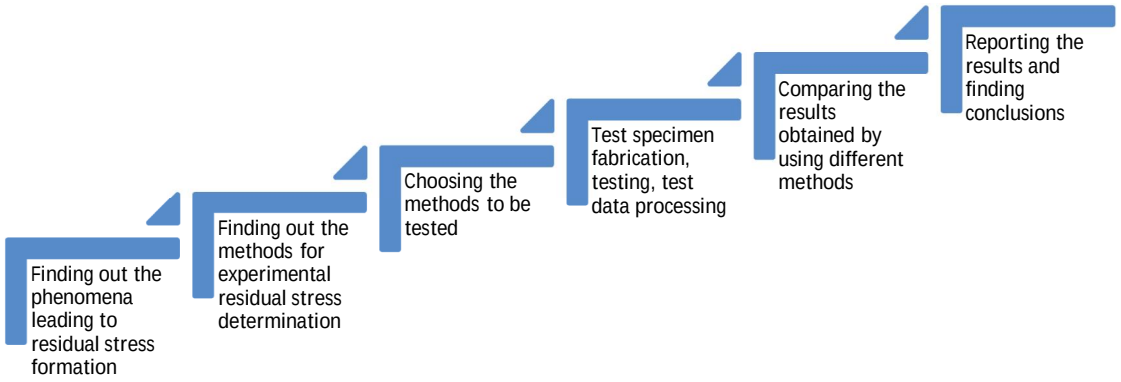

Figure 1.1. Flow chart of the thesis work.

The purpose of the experiments in the thesis was to evaluate some of the residual stress determination methods. The experiments were done mostly in Aalto University at Laboratory of Lightweight Structures. The test series were kept intentionally quite small to get only sufficient amount of results for making the conclusions about the applicability of the methods for a certain specimen. For more precise evaluation the research should be centered to only one method and test the method with different kinds of specimens.

2 Shrinkage of plastics

Volumetric changes of a plastic may cause residual stresses in a composite material. This is because the behavior of the reinforcements is usually quite different when compared to the behavior of the matrix material. The factors affecting the total cure shrinkage of plastics are introduced in the following subchapters.

Polymers are divided to two main groups which are thermoplastics and thermosets. A polymer is formed of monomers that are attached into each other by the chemical reaction called polymerisation. There are different monomers like propylene, vinyl chloride (VCM) and tetrafluoroethylene (TFE) (Figure 2.1). One thing in common with these monomers is that they all contain a carbon-carbon double bond. Monomers are basically formed of the carbon double bond and side groups. The side groups affect the polymer chain properties. [3]

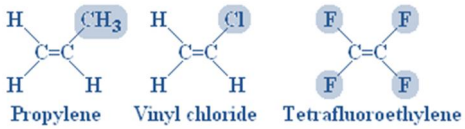

Figure 2.1. Examples of monomers (side groups are highlighted). [3]

Monomers contain different types of functional groups that react with other monomers as polymerisation takes place. As an example in Figure 2.2, the chemical structure of a monomer containing functional groups is shown.

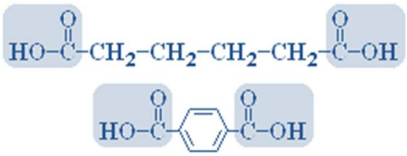

Figure 2.2. Example of a monomer that contains methylene molecules and functional carboxylic acid groups (functional groups are highlighted). [3]

A monomer is called bifunctional when it contains two functional groups. The monomer and the length of the polymer chains determines the properties of the polymer. The bifunctionality of the monomer enables the formation of long polymer chains.

2.1 Chemical shrinkage of a thermoset

The cure shrinkage of a thermoset depends highly on the resin system. If the resin is cured in a constant temperature, the shrinkage is mainly the chemical shrinkage of the resin. Shrinkage caused by the temperature change may also occur because of the exothermic reaction of the thermoset cure.

In the thermoset resin curing process, the chemical reactions lead to a cross-linked, solid material. Cross-links form the links between the polymer chains. Chemical shrinkage occurs in the thermoset resins during the cure and is a consequence of the different densities of the polymers and the low-molecular weight monomers. The Van der Waal`s distances of the monomers, meaning the distances between the reactive groups, are larger than the links that form in the cross-linking process and therefore the density of the polymer is higher. This means that the overall chemical shrinkage depends on the number of functional groups that react and form the chemical links. [2] The shrinkage is partly offset because of the thermal expansion of the resin due to the exothermic reaction and the elevated cure temperature [1].

Polymerisation shrinkage varies depending on the thermoset type. For epoxies it is around 3-6.5 %, for unsaturated polyesters 6-9 % and for urethane methacrylate 10-12.5 %. [2] A schematic graph about the formation of the total chemical shrinkage of a thermoset resin is illustrated in Figure 2.3.

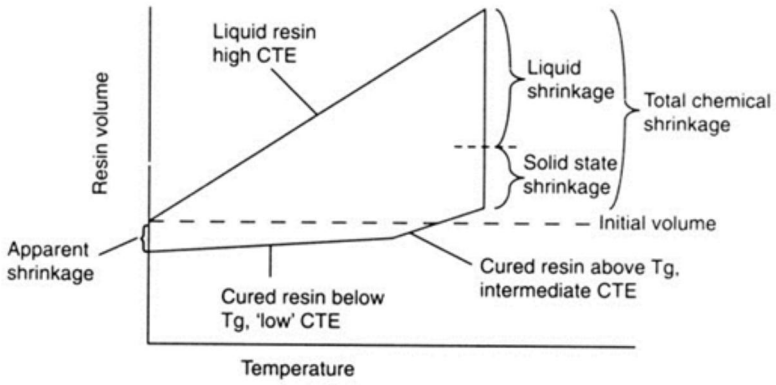

Figure 2.3. A schematic graph illustrating the overall chemical shrinkage during the cure. Apparent shrinkage is meaning the shrinkage after the curing and cooling down of the resin.

As Figure 2.3 illustrates, the shrinkage measured from the volumes before and after the cure is significantly lower than the chemical shrinkage. In other studies it is shown that chemical shrinkage is one of the main reasons in residual stress formation. [7] Thus chemical shrinkage cannot be ignored when the formation of residual stresses is investigated.

2.2 Thermal shrinkage of a thermoset

When a resin is cured at elevated temperature, the change in the temperature between the curing and cooling down to ambient temperature causes shrinkage in the thermoset. A temperature change may also occur because of the exothermic reaction of the thermoset curing process. The coefficient of Thermal Expansion (CTE) of different plastic types varies a lot being somewhere in between 1 - $100 \cdot 10^{-6}$ 1/°C. Some suggestive CTE values for different plastics are shown in Table 2.1.

Table 2.1. Suggestive CTE values for different polymers [4].

Material	CTE [1/°C]	Type
Unsaturated Polyester (UP)	$30 \cdot 10^{-6}$	Thermoset
Epoxy (EP)	$50 \cdot 10^{-6}$	Thermoset
Phenolic (PF)	$40 \cdot 10^{-6}$	Thermoset
Polypropylene (PP)	$90 \cdot 10^{-6}$	Thermoplastic
Polyamide (Nylon)	$66 \cdot 10^{-6}$	Thermoplastic
Polyimide (PI)	$40 \cdot 10^{-6}$	Thermoplastic

CTE value of a plastic depends highly on its composition. Orientations of the polymer chains can cause a difference between the CTEs in different directions. The CTE value can be varied with different kind of fillers in the resin. Particulate fillers, such as talc, silica and calcium carbonate, can reduce the shrinkage of the polymer and also even up the shrinkage differences due to the polymer chain directions. [2]

2.3 Shrinkage of thermoplastics

The behavior of thermoplastics is quite different because they are solidified in a cool mold after being in liquid form in the molding temperature. The shrinkage of thermoplastics takes place during the cooling and it is a sum of the shrinkages in liquid and solid form. Thermoplastic polymer shrinkage depends on the morphology of the polymer matrix, meaning if the polymer is amorphous or semi-crystalline. For amorphous polymers, the shrinkage is caused only by the temperature drop during the cure. The shrinkage of semi-crystalline polymers is formed also due to the densification of the polymer during crystallization. A polymer condensates during crystallization because of crystals being of higher density than the amorphous phase. The shrinkage of semi-crystalline polymers is found to be ten times higher than the shrinkage of amorphous polymers. [18]

3 Residual stresses of a composite

The residual stresses of fibre reinforced plastic laminates are formed basically because of the non-homogenous properties of the materials used. The mechanical and chemical properties of the reinforcing fibres and the matrix are considerably different. There are basically two main factors that are affecting formation of residual stresses. The main factors are the cure shrinkage of the resin and the difference in the coefficients of the thermal expansion (CTE) of the resin and reinforcing fibres. Typically, the CTE of fibres is close to zero and the CTE of the matrix is positive and relatively high. This leads to compressive stress in the fibres and to tension in the matrix when the composite is cooled down from the cure temperature.

The residual stress formation mechanism, as well as the effect of residual stresses must be known. By understanding and knowing these matters, the residual stresses can be sometimes even used to advance the overall material properties.

3.1 Formation of residual stresses

Chemical shrinkage of a resin takes place when it is in liquid form and also after gelation occurs. The shrinkage before the gelation does not affect generally residual stresses of a laminate. That is because the chemical bond between the reinforcements and the resin is not stiff enough to carry any stresses when the resin is in liquid form. The shrinkage after the gelation is normally around 2-7 % for epoxy resins. For example in the research done by Khoun and Hubert [6], the resin shrinkage before the gelation was 6 % for the CYCOM 890 RTM epoxy. For the epoxy used in the study, the shrinkage after gelation was over 3 % which results in the total cure shrinkage of around 10 %. These values for the shrinkage were measured in a constant temperature of 170 °C. [6]

Residual stress formation due to chemical shrinkage depends on the degree of cure of the resin. Li and Potter [7] investigated the chemical shrinkage versus degree of cure for the MY750 epoxy resin. The tests were done by using the gravimetric method, which is based on the change in buoyancy of the resin being cured suspended in a fluid. As Figure 3.1 illustrates, the gradient of the chemical shrinkage of epoxy resin remains steady until the break point. After the break point, the gradient is smaller but steady again. The break point where the gradient of cure shrinkage changes is somewhere close to the gel point of the resin. Gel point means the point where first infinite polymer network appears. In their study, the gel point was at 25 % degree of cure and the break point at 28 %, respectively. From the results it can also be noted that chemical shrinkage does not depend on the cure temperature. The experiments were done at constant temperatures of 90 °C, 100 °C and 110 °C. The chemical shrinkage is somewhat equal between these test samples. Lower gradient of the chemical shrinkage after the gelation suggests that the three-dimensional polymer network hinders the shrinkage. [7]

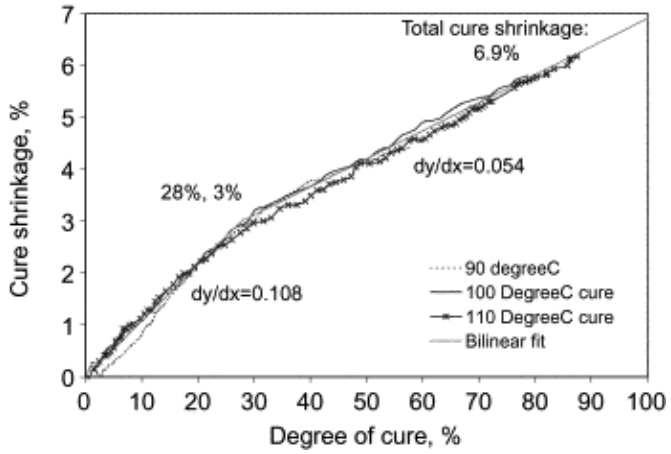

Figure 3.1. Chemical shrinkage versus degree of cure of the MY750 epoxy resin. [7]

For the residual stresses, the interesting and affecting part of the shrinkage is the one that takes place after the gelation. In situ cure strains can be measured with embedded strain gages. Measurable strains begin to develop in the composite as the gelation occurs. This is because the strain gages are not bonded to the material before gelation. [8] As well as the strain gages, the reinforcements begin to bond to the resin after gelation occurs. At this point also the development of the internal cure stresses begins.

During the cure, the physicochemical characteristics, meaning the degree of cure, glass transition temperature and fibre volume fraction should be homogeneous throughout the thickness of the laminate. This is usually the case with thin laminates consisting of roughly less than 100 plies. In the case of thicker laminates, the characteristics may vary within the thickness and this leads to the formation of additional residual stresses. According to P. Olivier and M. Cavarero [9], the curing stresses develop in different ways. In thick laminates, internal thermal gradients induce gradients in the degree of cure and fibre volume fraction. The gradients may result in residual stresses because of the differences in the material properties between the core and the surfaces. In the end of the cure, the degree of cure and fibre volume fraction are somewhat homogeneous throughout the laminate, but thermal gradients during the cooling may occur and may cause residual stresses to the laminate. Due to this, the thermal gradient should be avoided. This basically means that the manufacturer recommendations for a cure cycle may not be compatible for thick laminates and thus the cure cycle must be optimized in some way. Olivier and Cavarero investigated the cure cycle optimization in their study. The optimization concentrated mainly on the temperature optimization. The differences between the optimized and the recommended cure cycles can be seen in Figure 3.2. The significant difference between the exotherm, when recommended and optimized cure cycles are used, is noteworthy. [9]

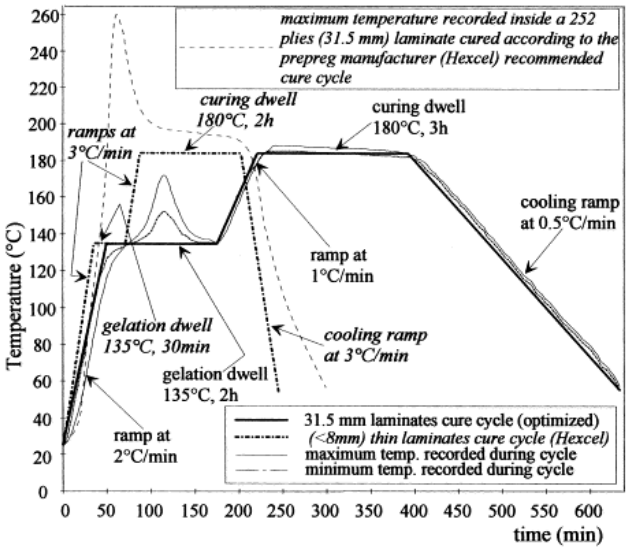

Figure 3.2. A cure cycle recommended by the prepreg (T300/914) manufacturer (Hexcel) and an optimized cure cycle in the research done by Olivier and Cavarero. [9]

Despite the optimized cure cycle, it is presumable that the physical characteristics will not remain fully homogeneous throughout the thickness of the thick laminate. Olivier and Cavarero discovered that the variation of fibre volume fraction may not, after all lead to significant residual stresses. If the cure cycle is optimized for a thick laminate, significant thermal gradients between the core and surface are avoided. The degree of cure is then homogenous throughout the laminates thickness and it is also similar with the degree of cure of a thin laminate. Therefore the residual stresses of a thick laminate are identical with the residual stresses of a thin laminate with a similar stacking sequence. [9]

The cooling rate affects considerably the residual stresses of thermoplastic composites. In the case of a thick laminate, the surfaces of the laminate may have been solidified before the inner plies. As the thermoplastic solidifies from outside in, it bonds to the outer layers ply by ply. This results in a compressive residual stress inside the laminate and tensile residual stress in the outer plies of the laminate. With a slower cooling rate, the polymer has more time to relax and thus the final residual stresses end up being lower. Considering the amorphous polymers, it has been found out that the cooling rate around the glass transition temperature mainly affects the formation of residual stresses. The lower the cooling rate is, the smaller is the range where residual stresses can form. This is because the lower cooling rate lowers the glass transition temperature as well. This is illustrated in Figure 3.3, where the free volume refers to the volume between the molecules and the occupied volume stands for the volume of the molecules. [18]

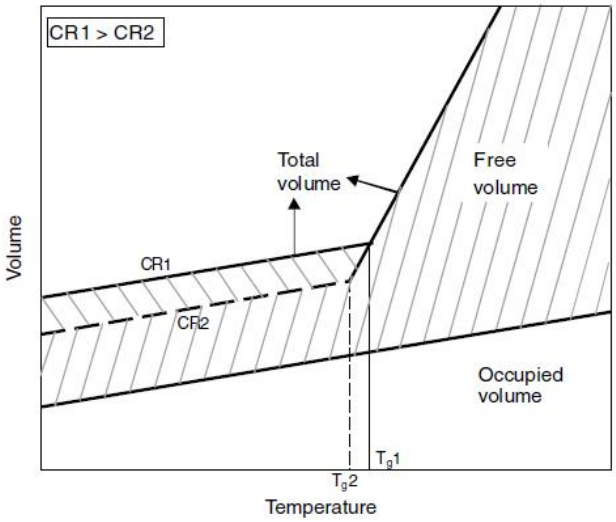

Figure 3.3. The effect of cooling rate on the glass transition temperature. CR stands for cooling rate. [18]

The higher cooling rate leads to a lower peak crystallization temperature and lower crystallinity levels in semi-crystalline thermoplastics. Because of this, the stress-free temperature is lower and the shrinkage is lower. However, when crystallinity level is lower, the amorphous content of the polymer is higher. As earlier was noticed, high cooling rate of the amorphous phases leads to higher residual stresses. Because of this an optimal cooling rate must be found taking into account these two residual stress formation mechanisms. Thus a relation between the visco-elastic behavior and crystallization need to be established. [18]

There is a big difference between the crystallization behaviors of different semi-crystalline polymers. In some semi-crystalline polymers, such as polyethylene (PE), a constant level of crystallinity can be found with any practical cooling rate. On the other hand, some semi-crystalline polymers can even be amorphous when the cooling rate is high enough. Nielsen and Pyrz [19] found out in their study of residual strains and crystallization of carbon fibre/polypropylene (CF/PP) that a low cooling rate leads to higher residual strains in this kind of composite. The reason for this was the higher crystallization temperature and higher level of crystallinity caused by the low cooling rate. High crystallinity level increased the residual stress relaxation in this case and thus the residual strains increased as well. For polyetheretherketone (PEEK) composites there is a limiting cooling rate, i.e. there is no significant difference in residual stresses in composites cooled down with lower cooling rates than the limiting cooling rate. [18]

The elastic modulus of semi-crystalline polymers is higher when the level of crystallinity is higher. That is because of the high elastic modulus of crystals. As earlier was mentioned, the lower cooling rate may lead to higher level of crystallinity and thus to higher residual stresses. Because of this, for some semi-crystalline polymers, higher elastic modulus means higher residual stresses. [18]

It has been also found out that higher interfacial bond strength between the matrix and the fibre leads to higher residual stresses. If the interfacial strength is high, the stresses

formed by the matrix shrinkage cannot relieve. On the other hand, if the interfacial strength is low, the fibre slips during the curing of the composite and this results in lower residual stresses. However, in order to achieve better mechanical properties, it is desirable that the interfacial strength is high. The interfacial strength is improved by chemical sizing of the fibres, which results in a better adhesion between the fibre and the matrix in molecular level. In respect of mechanical properties and residual stresses an optimum interfacial strength can be formed for every fibre-matrix system. [18]

Epitaxial spherulites may form in the fibre-matrix interface when semi-crystalline polymers are used. These spherulites create a trans-crystalline region around the fibre. According to some studies this region increases the interface strength and thus the stress transfer efficiency of the interface, which leads to higher residual stresses. Nuriel et al. [20] discovered that the mechanical properties of trans-crystalline regions may be 30 % higher compared to the surrounding matrix. They used aramid fibre reinforced polyamide (Nylon) in their study. On the other hand, some other studies concluded that the trans-crystalline interface relieves the stresses because of the orientation of the crystallites. The latter was based on some experimental tests, which were made for this type of a composite. It seems that there is not enough knowledge about the mechanism and effects of this phenomenon. [18]

Some findings of residual stress studies apply for many different composite laminates where thermoplastics are used as matrix material:

- Higher number of plies leads to larger residual strains in reinforcing fibres
- Higher fibre volume fraction decreases residual strains of fibres
- Residual stresses for cross-ply laminates are higher with a higher fibre volume fraction
- Fibre waviness equalizes the CTE between the fibre direction and transverse direction
- Highest interlaminar shear stresses are found in laminates with ±30° fibre angles

The properties of the mould material used in the cure process of a laminate may have an effect on the residual stress formation in the laminate. The heat transfer properties and CTE of the mould are affecting the curing of the laminate. The CTE of a laminate often differs from the CTE of the mould being used. The CTE of the mould is often larger than the CTE of the laminate. This may lead to compressive residual stresses in the laminate after the cure. The formation of these residual stresses depends also on the friction in the interface of the mould and the laminate when the laminate is turning to solid state. The heat transfer properties of the mould material affect the local temperature of the laminate during the cure. This results in local differences in the degree of cure of the laminate and in the cooling rate. These are possible factors leading to the formation of residual stresses. [18]

3.2 Residual stress effects

In some publications, the sources of residual stresses are classified as intrinsic and extrinsic sources. The intrinsic sources are related to material, lay-up and part shape and the extrinsic are the sources related to processing and tooling. Intrinsic sources generate residual stresses between the constituents of the laminate. Extrinsic sources generate stresses at the boundaries of the laminate and these stresses have also an effect on the internal stress level of the laminate.

Generally any kind of residual stress existing in a laminate may have an effect on mechanical properties of the laminate. Because of that, the internal residual stresses must be superimposed to the stresses caused by an external loading to find out the real stress state. Internal stresses may cause degradation of a laminate quality or change dimensions or shape of a laminate. Residual stress effects can be divided to two main groups which are microscopic and macroscopic effects.

Microscopic residual stresses may induce effects such as local yielding, microcracking and fibre breaking. Microcracking may affect mechanical and thermal properties of a laminate and may also form pathways to corrosive agents to reach the internal structure of the laminate. Microcracks also act as initial points for delamination and longitudinal splitting. These are possible events that lead to final failure of the laminate. [11]

The distorted shape of a cured laminate is often a result of residual stresses. The most common shape distortions are spring-in (Figure 3.4) and warping (Figure 3.5). These phenomena occur basically because of the different CTE of the matrix and the reinforcing fibres.

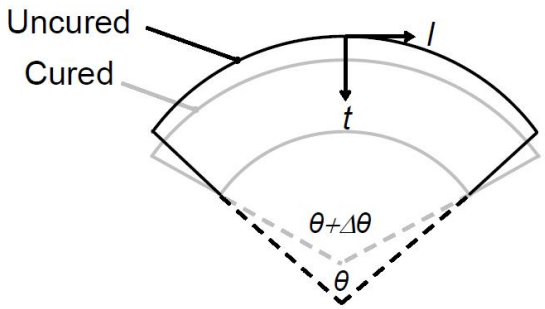

Figure 3.4. A schematic of the spring-in phenomenon, caused by the laminate shrinking during the cure. The laminate is forming a corner, with a change in its angle due to residual stresses. [29]

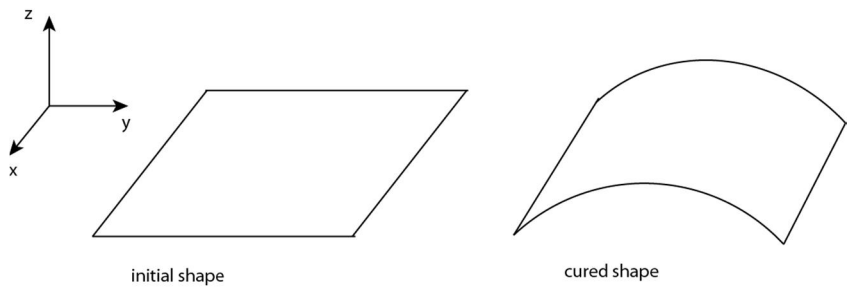

Figure 3.5. Schematic of the cure induced warping phenomenon of a laminate.

Total cure shrinkage of a thermoset depends on CTE values of the liquid resin and cured resin, as well as on the cure temperature. Shrinkage can be expressed as a percentual change in volume:

$$\Delta V_{\%} = -\frac{100(V_p - V_r)}{V_r} = 100(1 - \rho_r/\rho_p) \quad 2.1$$

where V_p is the volume of the cured thermoset, V_r is the volume of the resin and ρ_p and ρ_r are the densities, respectively. [2]

The shrinkage of a laminate can be considered as a change in the length of the laminate:

$$\Delta L_x = L_x\left[\alpha_x\left(T_{ref} - T_c\right) - S_x\right] \quad 2.2$$

where L_x is the initial length of the laminate, α_x is the CTE of the cured laminate, T_{ref} is the reference temperature, T_c is the cure temperature and S_x is the chemical shrinkage per unit length in the x- direction. [5]

Shrinkage may also have an effect on the shape of a laminate. For example we can consider the angular change of a corner of a laminate as follows:

$$\Delta\theta = \Delta\theta_T + \Delta\theta_S + \Delta\theta_C \quad 2.3$$

where the subscripts stand for the angular change due to different reasons. The idea of the angular shape is shown in Figure 3.4. The subscript T refers to thermal expansion, S to chemical shrinkage and C to internal stresses. The dominant term is the angular change due to thermal expansion. That is because of the difference between the CTE values in the thickness direction and in the plane of the laminate. The CTE is normally considerably larger in the thickness direction. [5]

If a laminate is assumed to be homogeneous, the angular change due to thermal expansion is:

$$\Delta\theta_T = \theta_0\left(\frac{(\alpha_x - \alpha_z)\Delta T}{1 + \alpha_z \Delta T}\right) \quad 2.4$$

where θ_0 is the initial value of the angle, α_x and α_z are the CTEs of the cured laminate in the longitudinal and thickness directions, respectively, and ΔT is the temperature change. [5]

The angular change because of the cure shrinkage can be expressed as follows:

$$\Delta\theta_S = \theta_0 \left(\frac{\emptyset_x - \emptyset_z}{1+\emptyset_z}\right) \quad 2.5$$

where x and z refer to longitudinal and thickness directions, respectively, and $\emptyset$ is the cure shrinkage.

The last part ($\Delta\theta_C$) of Equation 2.3 is formed due to the internal residual stresses in the laminate. The effect of the residual stresses for the final shape of the laminate would be higher if the laminate was cured without tooling. The tooling prevents the laminate deforming during the cure. After curing, the final deformation of the laminate is smaller than it would be without tooling. Thus the spring-in deformation of a laminate can be predicted quite accurately with the first two parameters of Equation 2.3. [29]

Warping of a laminate may occur due to non-uniform properties through the thickness of a laminate. Analytical methods have been developed for predicting warping of a laminate. With the CLT it is possible to predict warping of the laminates in case of small deformations. Because the CLT does not take into account the non-linear effects of deformation, it cannot be used in case of large deformations. [22] A calculation method based on the potential energy approach has been developed for predicting large out-of-plane deformations of orthotropic materials. [24] Warping due to part-tool interaction has been studied by curing laminates with uniform properties through the thickness. Fernlund et al. [29] studied this phenomenon by curing laminates with uniform through the thickness properties on aluminum tooling. The laminates were cured in an autoclave and the tool was coated with release agent and fluorinated ethylene propylene sheet. Laminates were made of carbon/epoxy prepreg. As a result, they compared the effect of dimensions on the dimensionless warping. They concluded that increasing of the part length leads to larger deformations and increasing of part thickness leads to smaller deformations due to larger bending stiffness of a thicker laminate. They also noticed that the tool surface treatment and cure cycle affect the amount of warping. In some studies it has been noted that certain cure cycles lead to larger deformations when the laminate is cooled down to room temperature. If the cure cycle has two hold temperatures, the resin may be in gelled or solid form before the final hold temperature. The increased stiffness leads to thermal stress formation when the laminate is heated to its final hold temperature. These stresses relax again during the cooling. The stress free temperature of the laminate is lower and the residual stresses end up to be lower when compared to a laminate which is cured only in the higher hold temperature. [29]

4 Measurement of the residual stresses

Since residual stresses may degrade mechanical properties of a laminate, it is important to find out the magnitude of them. Several methods have been developed for determining the residual stresses of laminates with different shape. Some of them are destructive, some are non-destructive and some are semi-destructive. Non-destructive and semi-destructive residual stress measurement methods may be useful when the material and manufacturing costs of the final product are high and residual stresses cannot be found out from a test specimen. Often there is a possibility to manufacture test specimens for residual stress measurements. Many of the residual stress measurement methods have been developed for isotropic materials in first place, but since the use of composites is increasing in advanced structural solutions, the methods are modified to be valid for determining the residual stresses of orthotropic materials as well.

4.1 Ring slitting method

The ring slitting method is suitable for measuring residual stresses of filament wound tubes. The method enables to find out the tangential (hoop) stresses and the radial stresses of a tube. It is destructive since the tube needs to be cut open so that the displacement caused by the residual stresses can be measured. It has been found out in previous studies that the maximum tangential residual stresses occur at the inner and outer radius of the tube and maximum radial stresses occur near the mean radius of the tube. The test specimen used in this method is a ring sliced from the tube. The ring is slit open from one side and the displacement of the ends caused by the residual stresses is measured. The displacement can be measured with optical equipment or manually, for example with a slide caliper. For determining the residual stresses we need to know the inner and outer radius of the ring, the distance from the center of the ring to the point where the displacement is measured and the displacement after cutting the ring open. The geometry of the ring used in this method is shown in Figure 4.1.

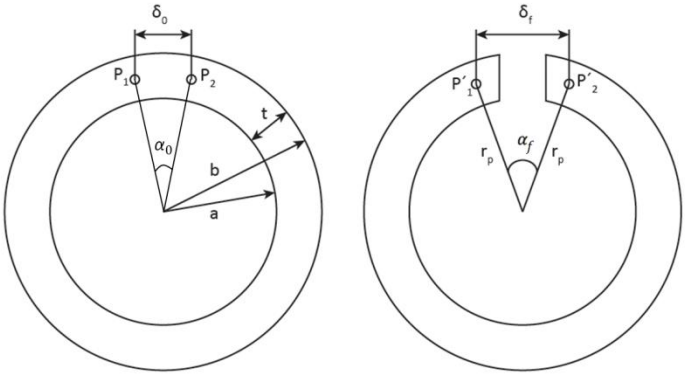

Figure 4.1. Geometry of the ring, used in the measurement of the residual stress driven displacement.

The stress distribution is expected to be equal in all radial cross-sections of the ring and the stress function Ψ is only dependent on the radius r. The calculation is based on the equations of pure bending of curved bars originally introduced by Timoshenko and Goodier [33] in the early 20th century. The stress function for this case is given as follows:

$$\Psi = Alog(r) + Br^2 \log(r) + Cr^2 + D \quad 4.1$$

where A, B, C and D are constants and r is the radius of the ring. Values of the constants are determined from the boundary conditions.

Tangential and radial stress components are determined from Equations 4.2 and 4.3:

$$\sigma_r = \frac{1}{r}\frac{\partial \Psi}{\partial r} = \frac{A}{r^2} + B(1 + 2\log(r)) + 2C \quad 4.2$$

$$\sigma_\theta = \frac{\partial^2 \Psi}{\partial r^2} = \frac{A}{r^2} + B(3 + 2\log(r)) + 2C \quad 4.3$$

$$\tau_{r\theta} = 0 \quad 4.4$$

where σ_r is the radial stress component and σ_θ is the tangential stress component. The shear stress component $\tau_{r\theta}$ is zero.

Boundary conditions for this case are:

$$\sigma_r = 0 \; \forall \; r = a \quad or \quad r = b \quad 4.5$$

$$\int_a^b \sigma_\theta \, dr = 0 \quad and \quad \int_a^b \sigma_\theta r \, dr = M_r \quad 4.6$$

$$\tau_{r\theta} = 0 \quad 4.7$$

According to Equation 4.5, the radial stress component at the inner and outer surface is zero. Tangential stress at the ends gives rise to the residual moment M_r (4.6).

Using the boundary condition equations for the tangential stress σ_r and radial stress σ_θ we obtain:

$$\sigma_r = -\frac{4M_r}{n}\left(\frac{a^2b^2}{r^2} log\left(\frac{b}{a}\right) + b^2 log\left(\frac{r}{b}\right) + a^2 log\left(\frac{a}{r}\right)\right) \quad 4.8$$

$$\sigma_\theta = -\frac{4M_r}{n}\left(\frac{-a^2b^2}{r^2} log\left(\frac{b}{a}\right) + b^2 log\left(\frac{r}{b}\right) + a^2 log\left(\frac{a}{r}\right) + b^2 - a^2\right) \quad 4.9$$

where a is the inner radius of the ring and b is the outer radius of the ring. The coefficient n and residual moment M_r can be obtained as follows:

$$n = (b^2 - a^2)^2 - 4a^2b^2\left(log\left(\frac{b}{a}\right)\right)^2 \quad 4.10$$

$$M_r = -\frac{\alpha E}{8\pi}\left(\frac{\left(b^2-a^2\right)^2 - 4a^2b^2\left(log\left(\frac{b}{a}\right)\right)^2}{2(b^2-a^2)}\right) \quad 4.11$$

where α is the angle measuring the displacement (see Figure 4.1) and E is the modulus of elasticity of the material.

The displacement δ of the ends of the ring after slitting is obtained from Equation 4.12:

$$\delta = \delta_0 - \delta_f \quad 4.12$$

where δ_0 is the distance between the measuring points before slitting and δ_f is the distance after slitting the ring.

The angle α is obtained from Equation 4.13:

$$\alpha = \frac{\delta}{r_p} \quad 4.13$$

where r_p is the radius to the point where the displacement is measured. [10]

This method also enables to find out the residual stresses of a laminate which has alternating modulus of elasticity E along the thickness. In the case of alternating modulus, the piecewise constant modulus E is used in calculating the residual moment M_r.

4.2 Hole drilling method

The hole drilling method is used for finding out residual stresses of isotropic and orthotropic materials. The method was invented by Mathar in 1934 [34] to study isotropic materials and it was developed for orthotropic materials by Prasad and Prabhakaran in 1987 [35]. G.S. Schajer and L. Yang proved that the method invented in 1987 is not valid for orthotropic materials and they introduced a new residual stress calculation method which is valid for orthotropic materials with any degree of orthotropy. [12, 13] With this method it is possible to define only the in-plane stresses of the material.

The hole drilling method is based on the phenomenon where drilling a hole to a laminate causes residual stress relaxation around the hole. The method has shown its advantages in use: it is easy to use, reliable and causes only limited damage to the specimen. [12] Since the damage caused to the specimen is relatively small, this method can be called semi-destructive. The hole can be made with water jet to reduce deformations caused by mechanical drilling.

In the method, a strain gage rosette is attached to the surface of the specimen. Strain gages normally locate in 0°, 90° and 225° directions, in the strain gage rosette for the hole-drilling method (Figure 4.2). A circular hole is drilled at the geometrical center of the strain gage rosette. The hole relaxes the residual stresses locally and the strain gage rosette measures the strains caused by relaxation. [13]

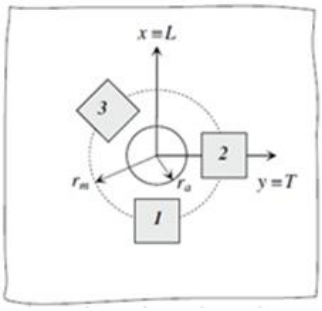

Figure 4.2. The locations of the strain gages in a conventional strain gage rosette for the hole-drilling method. [39]

For calculating the stresses we need to define influence coefficients, which are dependent on the material properties, geometry of the rosette and the depth of the hole. For an isotropic material the released strains are expressed with Equation 4.14 [13]:

$$\varepsilon_r = A(\sigma_x + \sigma_y) + B(\sigma_x - \sigma_y)\cos(2\theta) + C\tau_{xy}\sin(2\theta) \quad 4.14$$

where A, B and C are calibration constants, σ_x, σ_y and τ_{xy} are the residual stresses in the specimen and θ is the angle of each strain gage direction in respect to x-axis. If the strain gages are located in 0°, 90° and 225° directions in the rosette, Equation 4.14 can be expressed as [13]:

$$\begin{bmatrix} A+B & 0 & A-B \\ A & C & A \\ A-B & 0 & A+B \end{bmatrix} \begin{Bmatrix} \sigma_x \\ \tau_{xy} \\ \sigma_y \end{Bmatrix} = \begin{Bmatrix} \varepsilon_1 \\ \varepsilon_2 \\ \varepsilon_3 \end{Bmatrix} \quad 4.15$$

In the case of orthotropic materials, the influence coefficients are dependent on five elastic constants, which are shear modulus G_{xy}, elastic moduli in the longitudinal and transverse direction of the laminate E_x and E_y, and Poisson´s ratios ν_{xy} and ν_{yx}. If x and y point to the principal elastic directions of the material, strains can be written in the form of Equations 4.16, 4.17 and 4.18 using the Hooke´s law [13]:

$$\varepsilon_x = \frac{\sigma_x}{E_x} - \nu_{yx}\frac{\sigma_y}{E_y} \quad 4.16$$

$$\varepsilon_y = \frac{\sigma_y}{E_y} - \nu_{xy}\frac{\sigma_x}{E_x} \quad 4.17$$

$$\gamma_{xy} = \frac{\tau_{xy}}{G_{xy}} \quad 4.18$$

Four of the elastic constants are independent because of the elastic symmetry relationship 4.19 [12]:

$$\frac{\nu_{xy}}{E_x} = \frac{\nu_{yx}}{E_y} \quad 4.19$$

If the material behavior is assumed to be linear elastic, Equation 4.15 can be generalized to the form of Equation 4.20 for orthotropic materials [12]:

$$\frac{1}{\sqrt{E_x E_y}}\begin{bmatrix} C_{11} & C_{12} & C_{13} \\ C_{21} & C_{22} & C_{23} \\ C_{31} & C_{32} & C_{33} \end{bmatrix}\begin{Bmatrix} \sigma_x \\ \tau_{xy} \\ \sigma_y \end{Bmatrix} = \frac{1}{\sqrt{E_x E_y}}\begin{bmatrix} C_{11} & C_{12} & C_{13} \\ C_{21} & C_{22} & C_{23} \\ C_{31} & C_{32} & C_{33} \end{bmatrix}\begin{Bmatrix} \sigma_{11} \\ \sigma_{12} \\ \sigma_{22} \end{Bmatrix} = \begin{Bmatrix} \varepsilon_1 \\ \varepsilon_2 \\ \varepsilon_3 \end{Bmatrix} \quad 4.20$$

where C_{ij} are the influence coefficients.

Schajer and Yang calculated the influence coefficients for a wide range of different orthotropic materials by using an analytical solution. [13] The solution is based on Equations 4.21 and 4.22, which are used for defining the displacement field around the hole. [12] The method for defining the displacement field with Equations 4.21 and 4.22 is originally introduced by Smith in his work considering the effect of holes on stress distribution of wood or plywood [15]:

$$u = \frac{\alpha^2 m^2 + \nu_{xy}}{m(\alpha-\beta)E_x(1-\alpha m)}\left[Y_1(1+\beta m)\tau_{xy} - X_1\left(\sigma_x - \beta m \sigma_y\right)\right]$$

$$+ \frac{\beta^2 m^2 + \nu_{xy}}{m(\beta-\alpha)E_x(1-\beta m)}\left[Y_2(1+\alpha m)\tau_{xy} - X_2\left(\sigma_x - \alpha m \sigma_y\right)\right] \quad 4.21$$

$$v = \frac{1+\alpha^2 m^2 \nu_{yx}}{\alpha m^2(\alpha-\beta)E_y(1-\alpha m)}\left[X_1(1+\beta m)\tau_{xy} - Y_1\left(\sigma_x - \beta m \sigma_y\right)\right]$$

$$+ \frac{1+\beta^2 m^2 \nu_{xy}}{\beta m^2(\beta-\alpha)E_y(1-\beta m)}\left[X_2(1+\alpha m)\tau_{xy} - Y_2\left(\sigma_x - \alpha m \sigma_y\right)\right] \quad 4.22$$

where:

$$m = \sqrt[4]{\frac{E_x}{E_y}} \quad 4.23$$

$$\kappa = \sqrt{E_x E_y}\left(\frac{1}{G_{xy}} - \frac{2\nu_{xy}}{E_x}\right)/2 \quad 4.24$$

$$\alpha = \sqrt{\kappa + \sqrt{(\kappa^2 - 1)}} \quad 4.25$$

$$\beta = \sqrt{\kappa - \sqrt{(\kappa^2 - 1)}} \quad 4.26$$

$$W_1 = \sqrt[4]{(x^2 - r_a^2 - \alpha^2 m^2 (y^2 - r_a^2))^2 + (2\alpha m x y)^2} \quad 4.27$$

$$W_2 = \sqrt[4]{(x^2 - r_a^2 - \beta^2 m^2 (y^2 - r_a^2))^2 + (2\beta m x y)^2} \quad 4.28$$

$$\psi_1 = \tan^{-1}\left[\frac{2\alpha m x y}{x^2 - r_a^2 - \alpha^2 m^2 (y^2 - r_a^2)}\right]/2 \quad 4.29$$

$$\psi_2 = \tan^{-1}\left[\frac{2\beta m x y}{x^2 - r_a^2 - \beta^2 m^2 (y^2 - r_a^2)}\right]/2 \quad 4.30$$

$$X_1 = x - W_1 \cos\psi_1 \quad 4.31$$

$$X_2 = x - W_2 \cos\psi_2 \quad 4.32$$

$$Y_1 = \alpha my - W_1 \sin\psi_1 \quad 4.33$$

$$Y_2 = \beta my - W_2 \sin\psi_2 \quad 4.34$$

The calibration constants C_{ij} calculated by Schajer and Yang are shown in Appendix A. [12] In Section 6.1 of this study, another approach for calculating the influence coefficients is introduced.

The constants can also be defined using Finite Element Method (FEM). Shokrieh and Ghasemi [14] defined the constants using a FEM-software (Ansys). They simulated the hole by reducing the stiffness of the elements by a factor of 10^{-6} in the area of the hole. They applied a known stress in the direction of strain gages one direction at a time. Strain gages were located in directions of 0°, 90° and 225° of the unidirectional ply. With Ansys they defined the strains ε_1, ε_2 and ε_3, when the applied stress σ_{11} was affecting in the direction of the strain gage no. 1 and σ_{12} and σ_{22} were zero. Now they could obtain the values for C_{11}, C_{21} and C_{31} (4.35-4.37) by using Equation 4.20:

$$C_{11} = \sqrt{E_x E_y}\,\frac{\varepsilon_1}{\sigma_{11}} \quad 4.35$$

$$C_{21} = \sqrt{E_x E_y}\,\frac{\varepsilon_2}{\sigma_{11}} \quad 4.36$$

$$C_{31} = \sqrt{E_x E_y}\,\frac{\varepsilon_3}{\sigma_{11}} \quad 4.37$$

The constants C_{13}, C_{23} and C_{33} (4.38-4.40) can be defined in the same manner by applying the stress in the direction of the strain gage no. 2 while σ_{11} and σ_{12} are zero:

$$C_{13} = \sqrt{E_x E_y}\,\frac{\varepsilon_1}{\sigma_{22}} \quad 4.38$$

$$C_{23} = \sqrt{E_x E_y}\,\frac{\varepsilon_2}{\sigma_{22}} \quad 4.39$$

$$C_{33} = \sqrt{E_x E_y}\,\frac{\varepsilon_3}{\sigma_{22}} \quad 4.40$$

The constants C_{12}, C_{22} and C_{32} (4.41-4.43) can be defined in the similar manner. Now shear stress $\tau_{xy} = \sigma_{12}$ is applied to the specimen:

$$C_{12} = \sqrt{E_x E_y}\,\frac{\varepsilon_1}{\sigma_{12}} \quad 4.41$$

$$C_{22} = \sqrt{E_x E_y}\,\frac{\varepsilon_2}{\sigma_{12}} \quad 4.42$$

$$C_{32} = \sqrt{E_x E_y}\,\frac{\varepsilon_3}{\sigma_{12}} \quad 4.43$$

There are different variations of the hole drilling method. In other versions the hole is drilled in small increments and the strains are measured after each drilling increment. This way the stresses of a laminate can be calculated in different depths of the specimen

and the stress profile is obtained. The other approach is to drill a through hole after which the strains are measured from the surface and the through the thickness stress profile is calculated.

There is often a limiting depth of the hole, after which the strain-stress relation changes when the measured surface strains do not give sufficient information about the internal stress state. According to Schajer and Yang, the limiting depth of the hole for orthotropic materials depends on the ratio of the out-of-plane shear modulus to the in-plane axial modulus. The lower this ratio is the smaller is the limiting depth of the hole. [13] According to Pagliaro and Zuccarello [39], the limiting depth depends also on the ratio of the laminate thickness and the mean radius of the strain gage rosette. The meaning of the mean radius r_m is shown in Figure 4.2.

4.3 Moiré interferometry

There is often a need for a non-destructive method for measuring the residual stresses. For this purpose P. G. Ifju et al. [16] developed a method, which is based on the moiré interferometry. This non-destructive residual stress measurement method is called Cure Referencing Method (CRM). In the interferometry process a grating is attached or created to the surface of the specimen under investigation. Using interferometer, it is possible to reflect a reference grating on the top of the grating on the specimen. This leads to formation of moiré fringe patterns, which are recorded with a camera. With these moiré fringe patterns the strains of the specimen can be calculated and using these strains the stress state of the specimen can be defined. [16]

It is possible to detect very small strains with high-sensitivity moiré techniques. In the geometric moiré techniques, the gratings to be used usually consist of equally spaced parallel lines. Other possible gratings are in the form of concentric equally spaced circles, cross gratings and dots made of two sets of equally spaced lines perpendicular to each other.

The strain measurement technique is presented here by using the grating in the form of equally spaced parallel lines. For creating the moiré fringe patterns, two gratings are needed. The needed gratings are the one in the specimen and the reference (master) grating. The distance between the lines in these gratings is called pitch and it is denoted by the symbols p_m in the master grating and p_s in the specimen grating. The number of lines in the gratings is considered as the density of lines (e.g. lines/mm) and it is denoted by the symbols d_m in the reference grating and d_s in the specimen grating. The density and pitch of the grating are illustrated in Figure 4.3. For the grating with parallel lines the primary direction is the one parallel to the lines and the secondary direction is the one perpendicular to the lines. [17]

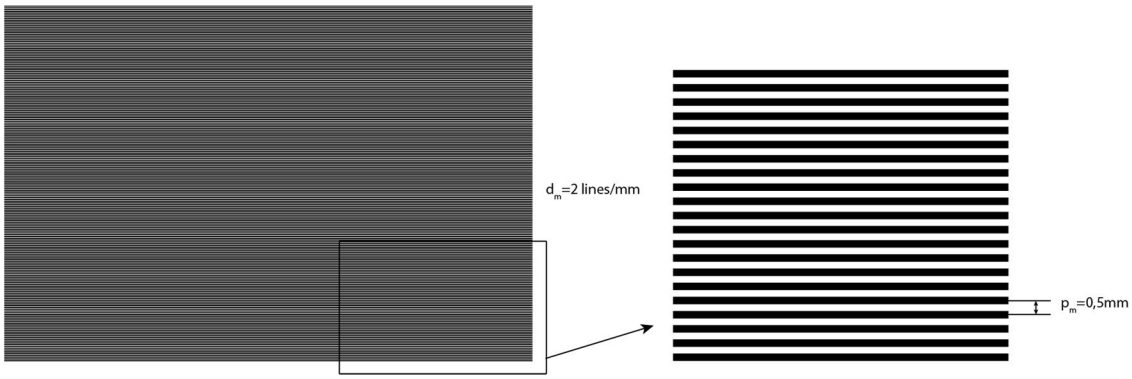

Figure 4.3. Line grating for moiré interferometry.

The idea of the interference technique can be explained most easily with interference of two parallel gratings. The pitches of these gratings are different and the difference can be considered as a uniform deformation of the specimen. A light fringe is observed in the area where opaque lines coincide and dark fringes in the areas where lines are side by side, as shown in Figure 4.4. The distance between the fringes (light or dark) is here denoted by δ_m. If the pitches of the specimen grating and the reference grating were originally similar, the change in the specimen pitch is due to specimen deformation.

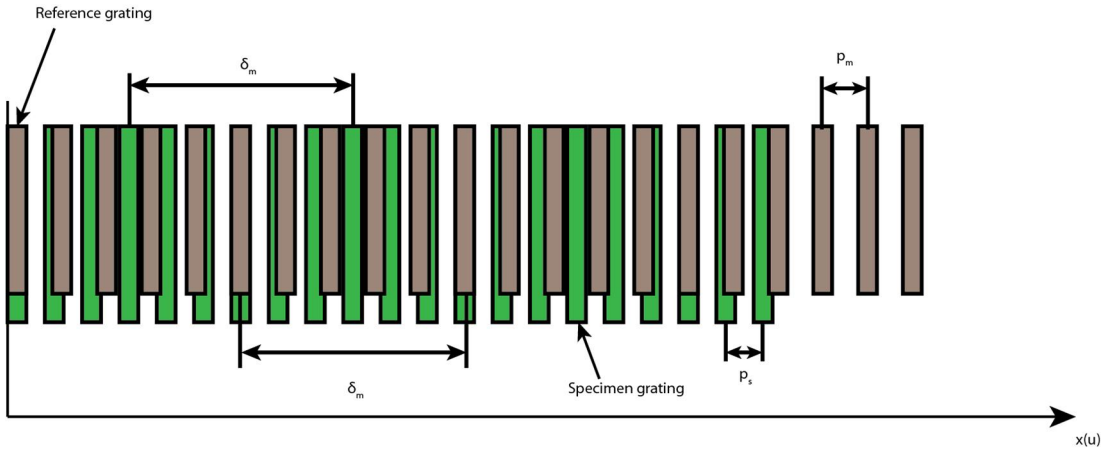

Figure 4.4. Moiré fringe formation due to change of the pitch in specimen grating.

In a uniform deformation case, the strain of the specimen can be calculated as follows:

$$\varepsilon = \frac{\Delta L}{L_0} = \frac{p_m}{p_m - \delta_m} \cong \frac{p_m}{\delta_m} \qquad 4.44$$

where p_m is the pitch of the reference grating and δ_m is the distance between the moiré fringes.

When the number of moiré fringes is n on the length of the gage l_g, the strain can be defined as follows:

$$\varepsilon = \pm \frac{\Delta L}{L_0} = \frac{np_m}{l_g - np_m} \quad 4.45$$

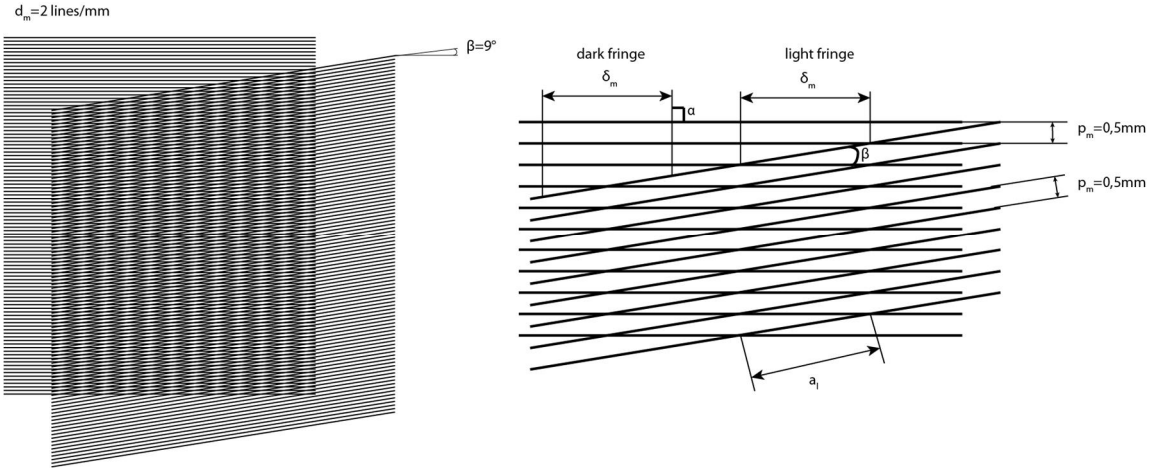

Figure 4.5. Moiré fringe formation due to pure rotation of the specimen grating.

In the case of pure rotation illustrated in Figure 4.5, where the pitch of the both gratings is equal p_m and the angle between the gratings is β, the distance between the fringes can be defined with Equation 4.46:

$$\delta_m = a_l \cos\left(\frac{\beta}{2}\right) = \frac{p_m \cos\left(\frac{\beta}{2}\right)}{\sin\left(\frac{\beta}{2}\right)} = \frac{p_m}{2\sin\left(\frac{\beta}{2}\right)} \quad 4.46$$

where a_l is the length of the side defined with Equation 4.47 and β is the angle between the gratings:

$$a_l = \frac{p_m}{\sin(\beta)} \quad 4.47$$

The small angle β can be defined as follows:

$$\beta \cong \frac{p_m}{\delta} \quad 4.48$$

The angle between the moiré fringes and the reference grating is denoted by α and it is defined as:

$$\alpha = \frac{\pi}{2} \pm \frac{\beta}{2} \quad 4.49$$

When we consider two gratings with different pitches under pure rotation, it can be noted that the fringes form sloping lines through the area where gratings are overlapping (Figure 4.6).

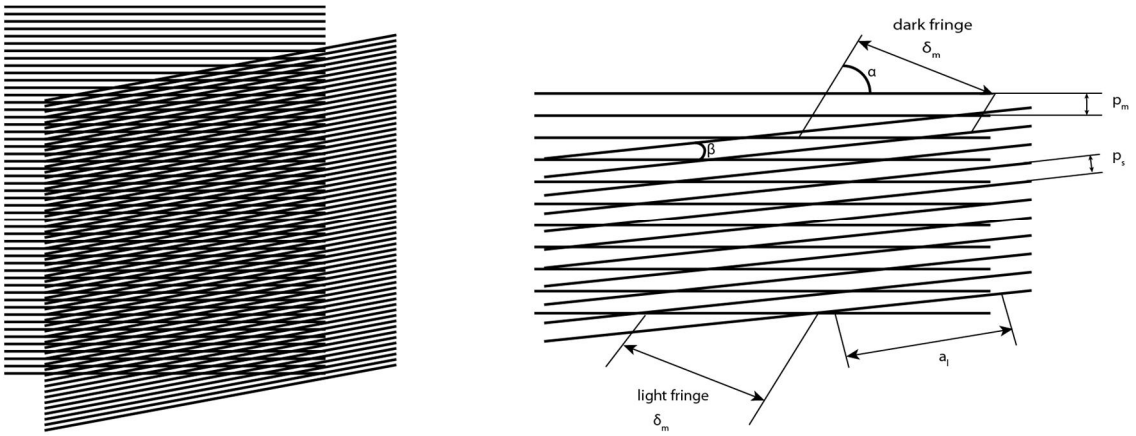

Figure 4.6. Moiré fringes of two overlapping gratings with different pitches.

The length a_l can be stated as:

$$a_l = \frac{p_m}{\sin(\beta)} = \frac{\delta}{\sin(\alpha-\beta)} \quad 4.50$$

and the rotation angle β can be solved as follows:

$$\beta = \tan^{-1}\frac{\sin\alpha}{\frac{\delta}{p_m}+\cos\alpha} \quad 4.51$$

The pitch of the specimen grating can be solved from the following relation:

$$\frac{p_s}{\sin(\alpha-\beta)} = \frac{p_m}{\sin\alpha} \quad 4.52$$

Thus, the following is obtained:

$$p_s = \frac{p_m \sin(\alpha-\beta)}{\sin\alpha} = \frac{\delta \sin\beta}{\sin\alpha} \quad 4.53$$

Using Equation 4.51 we get the following form for Equation 4.53:

$$p_s = \frac{\delta}{\sqrt{1+\left(\frac{\delta}{p_m}\right)^2+2\left(\frac{\delta}{p_m}\right)\cos\alpha}} \quad 4.54$$

With the deformed pitch p_s, the strain ε can be defined with Equation 4.55:

$$\varepsilon = \frac{p_s-p_m}{p_m} \quad 4.55$$

P. G. Ifju et al. [16] created the grating to the specimen laminate in the curing phase. The reference grating made of aluminum coated epoxy was placed under another layer of epoxy and the prepreg layup. The aluminum coating was made for making the separation of the layers easier after the cure. When the laminate and the grating in the bottom of the laminate were cured, they were removed from the mold and left into autoclave to cool slowly. The replicated grating was now able to deform freely during the cool down. [16] The moiré fringes were formed and examined using interferometer.

The average normal and shear displacements were measured from the fringe patterns. The strains were calculated using the measured displacements with Equations 4.56-4.58 as follows:

$$\varepsilon_x = \frac{\partial U}{\partial x} = \frac{1}{f}\left(\frac{\Delta N_x}{\Delta x}\right) \quad 4.56$$

$$\varepsilon_y = \frac{\partial V}{\partial y} = \frac{1}{f}\left(\frac{\Delta N_y}{\Delta y}\right) \quad 4.57$$

$$\gamma_{xy} = \frac{\partial U}{\partial y} + \frac{\partial V}{\partial x} = \frac{1}{f}\left(\frac{\Delta N_x}{\Delta y} + \frac{\Delta N_y}{\Delta x}\right) \quad 4.58$$

where ΔN_x and ΔN_y are the changes in fringe order over the length Δx and Δy, f is the frequency (lines/mm) of the reference grating. The fringe orders N_x and N_y are defined by the displacements in the x- and y-directions and the frequency of the reference grating (4.59-4.60):

$$N_x = fU \quad 4.59$$

$$N_y = fV \quad 4.60$$

where U is the displacement in the x-direction and V is the displacement in the y-direction.

Ifju et al. noticed in their study that an error may occur during the analyzing of the fringe pattern for strain measurement. The amount of error may be reduced by observing the fringes over larger length. They achieved reliable strain information for strains within 20 με. The stress state of each ply is obtained from the in plane strains, which were achieved with the moiré fringe interferometry technique. The stresses can be calculated by using the Classical Lamination Theory (CLT). The overall results were consistent and thus they believed that this method could be used in determining the residual stresses, as well as the mechanical and machining stresses of multidirectional laminates. [16]

4.4 Layer removal method

The stress calculations in the layer removal method are based on the deformations measured after removing a layer from the laminate. Considering a symmetric composite laminate with the stacking sequence [0/90]s the idea of the layer removal technique can be explained with Figure 4.7. The case (1) illustrates the stresses and deformations before and after the layer removal. In the case (2) an unsymmetrical laminate with the stacking sequence [90/90/0] is cured in elevated temperature and the residual stresses occur after cooling down, which causes the deformation of the laminate. In both cases, the unsymmetrical stress distribution leads to a similar deformation of the laminate. [22]

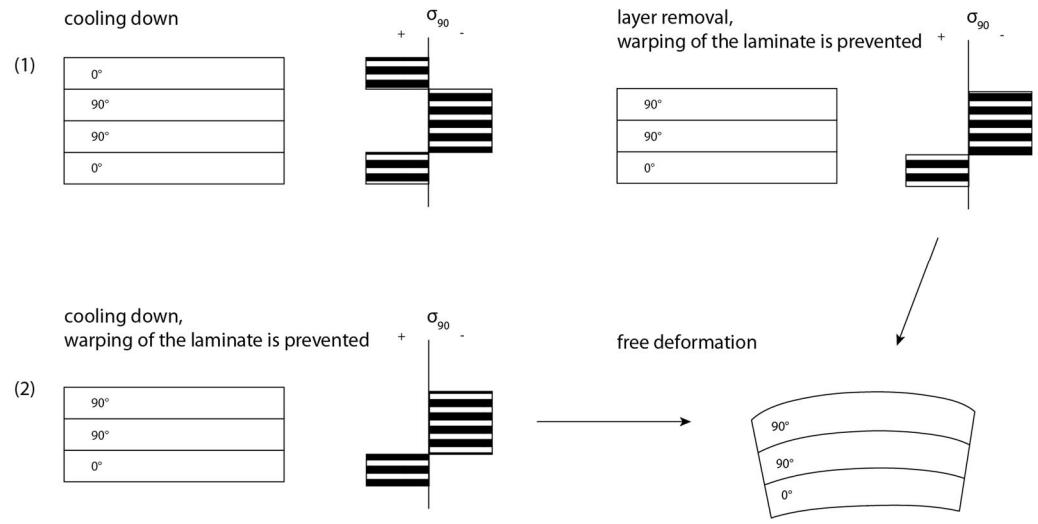

Figure 4.7. Deformation of the laminate due to uneven stress distribution. Case (1) illustrates layer removal and case (2) cooling down of an unsymmetrical laminate.

In the layer removal method, the curvature is measured after removing a layer mechanically. This curvature builds up after removing a layer and the force equilibrium is restored at the same time. With the known curvature and thickness change, the stress profile of the original laminate can be solved. The curvature can be considered being induced by the resultant moment acting on the free edges of the laminate. With the resultant moment, the corresponding stress of an orthotropic laminate can be calculated with the following Equations derived by Treuting and Read [20]:

$$\sigma_x(z_1) = \frac{2}{z_0+z_1}\frac{dM_x(z_1)}{dz_1} + \frac{2M_x(z_1)}{(z_0+z_1)^2} - 4\int_{z_0}^{z_1}\frac{M_x(z)}{(z_0+z)^3}\mathrm{dz} \qquad 4.61$$

$$\sigma_y(z_1) = \frac{2}{z_0+z_1}\frac{dM_y(z_1)}{dz_1} + \frac{2M_y(z_1)}{(z_0+z_1)^2} - 4\int_{z_0}^{z_1}\frac{M_y(z)}{(z_0+z)^3}\mathrm{dz} \qquad 4.62$$

where M_x and M_y are the resultant moments, z_0 is the coordinate at the top of the laminate before layer removal and z_1 is the coordinate at the top of the laminate after layer removal. The coordinate system is illustrated in Figure 4.8. [22]

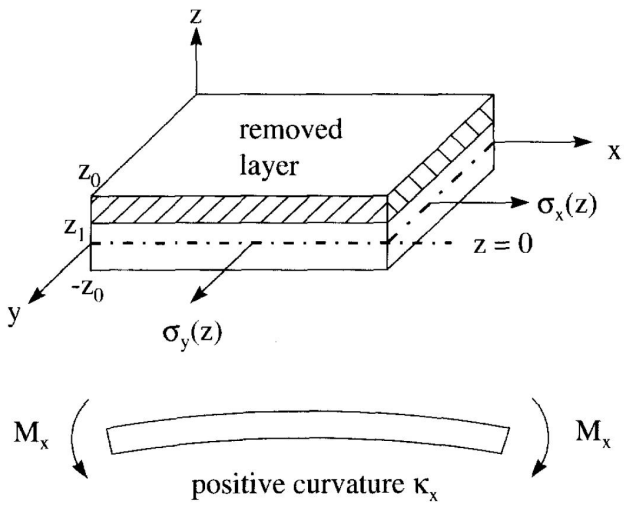

Figure 4.8. The coordinate system of the layer removal method.

In the case of small deformations, the resultant moments M_x and M_y can be solved with the CLT using Equations 4.63 and 4.64:

$$M_x = B_{11}\varepsilon_x^0 + D_{11}\kappa_x + D_{12}\kappa_y \quad 4.63$$

$$M_y = B_{11}\varepsilon_y^0 + D_{11}\kappa_y + D_{12}\kappa_x \quad 4.64$$

where B_{11}, D_{11} and D_{12} are the stiffness coefficients defined by the CLT, κ_x and κ_y are the curvatures, and ε_x^0 and ε_y^0 are the midplane strains after each layer removal.

The CLT is not applicable for solving the moments in case of large deformations. The nonlinear terms in the strain-displacement relations in the CLT are neglected which leads to an error in calculations in case of large deformations. [22] For large deformation cases, an energy approach has been developed by several researchers in multiple steps over the years. This energy approach is based on the idea that the laminate, being thought as a system, is in a stable state when the potential energy is in its minimum. Dano and Hyer [24] developed a method where the modeling is done by using approximations of the midplane strains. This method is based on the Rayleigh-Ritz minimization of total potential energy. The potential energy is defined with the following equation:

$$U = \iint \left(\frac{1}{2}A_{ij}\varepsilon_i^0\varepsilon_j^0 + B_{ij}\varepsilon_i^0\kappa_j + \frac{1}{2}D_{ij}\kappa_i\kappa_j - N_j\varepsilon_j^0 - M_j\kappa_j\right)dxdy \quad 4.65$$

where $i, j, ij = x, y, xy$ and A_{ij}, B_{ij} and D_{ij} are the stiffness coefficients, ε and κ are the midplane strains and curvatures, N_j and M_j are the force and moment resultants, respectively, induced by the layer removal.

The strain-displacement relations can be expressed as follows:

$$\varepsilon_x(z) = \frac{du^0}{dx} + \frac{1}{2}\left(\frac{dw^0}{dx}\right)^2 + z\frac{d^2w^0}{dx^2} \quad 4.66$$

$$\varepsilon_y(z) = \frac{dv^0}{dy} + \frac{1}{2}\left(\frac{dw^0}{dy}\right)^2 + z\frac{d^2w^0}{dy^2} \quad 4.67$$

$$\varepsilon_{xy}(z) = \frac{du^0}{dy} + \frac{dv^0}{dx} + \left(\frac{dw^0}{dx}\frac{dw^0}{dy}\right) + 2z\frac{d^2w^0}{dxdy} \quad 4.68$$

where u^0, v^0 and w^0 are the midplane displacements in the x-, y- and z-directions, ε_x and ε_y are the strains in the x- and y-directions and ε_{xy} is twice the shear strain. [22]

The midplane displacements of the laminate can be expressed with the following equations:

$$u^0(x,y) = cx - \frac{a^2x^3}{6} - \frac{abxy^2}{4} \quad 4.69$$

$$v^0(x,y) = dy - \frac{b^2y^3}{6} - \frac{abx^2y}{4} \quad 4.70$$

$$w^0(x,y) = \frac{1}{2}(ax^2 + by^2) \quad 4.71$$

where a, b, c and d are constants to be determined. [25]

By substituting Equations 4.69-4.71 into Equations 4.66-4.68, the midplane strains can be calculated. The minimum potential energy can be expressed with Equation 4.72:

$$\frac{\partial U}{\partial r_i} = 0 \quad 4.72$$

where r_i indicates the unknown constants a, b, c and d. Solving 4.72 leads to four equilibrium equations.

The equations for solving these unknown constants are derived by Hyer and Jilani in their study considering of predicting the deformation characteristics of rectangular unsymmetrically laminated piezoelectric materials.[25] When the strains are known, Equation 4.72 can be solved to yield the resultant moments M_x and M_y in which case stresses can be calculated with Equations 4.61 and 4.62. When the stresses are computed for every layer removed, the stress profile of the original sample is found.

4.5 Cut cylinder bending test

If the material properties are not known, the conventional ring slitting method cannot be used. J.W. Kim and D.G. Lee [26] presented a further developed method of the conventional ring slitting method. In this method, the specimen is a ring cut from a filament wound tube, for example. The ring is cut open from one side in the radial direction (Figure 4.9). Before cutting, the strain gages are attached to the inner and outer surface of the ring. The ring is cut open from the opposite side of the located strain gages. The outer and inner hoop strains are recorded after the ring cutting. In the radial-cut-cylinder-bending test, the cut ring is attached to a universal testing machine and the loading pins are located to the free sides of the ring so that pulling the pins away from each other opens the cut in the ring (Figure 4.9). The hoop strains are measured during

the loading of the cut open ring. The ring is considered to be returned to its original shape because of the restoring moment only.

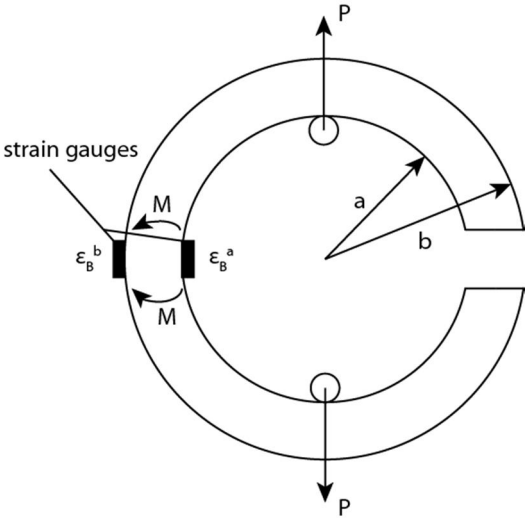

Figure 4.9. Schematic illustration of the test arrangement used in the cut cylinder bending test.

The moment M is approximated with the following equation:

$$M = \left(\frac{a+b}{2}\right) P \tag{4.73}$$

For linear elastic materials, the strains can be expressed as:

$$\varepsilon_B^a = \emptyset_B^a M \tag{4.74}$$

$$\varepsilon_B^b = \emptyset_B^b M \tag{4.75}$$

where $\emptyset_B^a$ and $\emptyset_B^b$ are constants, which consist of two parts due to force and moment components, stated as follows:

$$\emptyset_B^a = \emptyset_F + \emptyset_M^a \tag{4.76}$$

$$\emptyset_B^b = \emptyset_F + \emptyset_M^b \tag{4.77}$$

Since the strains are assumed to be developed only due to the residual moment, the change in the strains can be expressed with following equations:

$$\Delta\varepsilon_B^a = \emptyset_M^a M_R \tag{4.78}$$

$$\Delta\varepsilon_B^b = \emptyset_M^b M_R \tag{4.79}$$

where $\emptyset_M^a$ and $\emptyset_M^b$ are constants that can be solved with the following equations:

$$\emptyset_M^a = \left(\emptyset_B^a - \emptyset_B^b\right) / \left(1 - \frac{\Delta\varepsilon_B^b}{\Delta\varepsilon_B^a}\right) \tag{4.80}$$

$$\emptyset_M^a = \left(\emptyset_B^b - \emptyset_B^a\right)/\left(1 - \frac{\Delta\varepsilon_B^a}{\Delta\varepsilon_B^b}\right) \quad 4.81$$

$$\emptyset_F = \emptyset_B^a - \emptyset_M^a = \emptyset_B^b - \emptyset_M^b \quad 4.82$$

The residual moment can be expressed with the following equation:

$$M_R = \frac{\Delta\varepsilon_B^a}{\emptyset_M^a} = \frac{\Delta\varepsilon_B^b}{\emptyset_M^b} \quad 4.83$$

The residual stresses in the original uncut cylinder can be determined with the restoring moment $(-M_R)$. Kim and Lee [26] introduced the method for calculating the tangential (hoop) and radial residual stresses. Using force and moment equilibrium conditions they ended up to the following equations for tangential $\sigma_\theta(r)$ and radial residual stress $\sigma_r(r)$:

$$\sigma_\theta(\bar{r}) = (c_0 + c_1\bar{r} + c_2\bar{r}^2)K\left(1 - \frac{\bar{R}}{\bar{r}}\right) \quad 4.84$$

$$\sigma_r(\bar{r}) = \frac{K}{\bar{r}}\left[\left(c_0\bar{r} + \frac{c_1}{2}\bar{r}^2 + \frac{c_2}{3}\bar{r}^3\right) - \bar{R}\left(c_0 \log\bar{r} + c_1\bar{r} + \frac{c_2}{2}\bar{r}^2\right) + X\right] \quad 4.85$$

where c_0, c_1 and c_2 are constants which can be determined with Equations 4.86-4.88, X is an integration constant to be determined with Equation 4.89, $\bar{r}$ is the normalized radius of the ring, $\bar{R}$ is the normalized radius of the neutral surface ($\bar{R} = R/b$) and K is a constant expressed with Equations 4.90 and 4.91. $E(\bar{r})$ is approximated to be a quadratic function of the normalized radius $\bar{r}$ (Equation 4.92) [26]:

$$(1-a)c_0 + \left(\frac{1-a^2}{2}\right)c_1 + \left(\frac{1-a^3}{3}\right)c_2 + (\log a)\,\bar{R}c_0 - (1-a)\bar{R}c_1 - \left(\frac{1-a^2}{2}\right)\bar{R}c_2 = 0 \quad 4.86$$

$$\left(\frac{1-a^2}{2}\right)c_0 + \left(\frac{1-a^3}{3}\right)c_1 + \left(\frac{1-a^4}{4}\right)c_2 - (1-a)\bar{R}c_0 - \left(\frac{1-a^2}{2}\right)\bar{R}c_1 - \left(\frac{1-a^3}{3}\right)\bar{R}c_2 = \frac{M_C}{Kb^2w} \quad 4.87$$

$$(1-a)c_0 + \left(\frac{1-a^2}{2}\right)c_1 + \left(\frac{1-a^3}{3}\right)c_2 = \frac{2}{(a+1)b^2w\emptyset_F} \quad 4.88$$

$$X = -\left(c_0 + \frac{c_1}{2} + \frac{c_2}{3}\right) + \bar{R}\left(c_1 + \frac{c_2}{2}\right) \quad 4.89$$

$$R = \left(\Delta\varepsilon_B^b - \Delta\varepsilon_B^a\right)/\left(\frac{\Delta\varepsilon_B^b}{a} - \frac{\Delta\varepsilon_B^a}{b}\right) \quad 4.90$$

$$K = \left(a\Delta\varepsilon_B^a - b\Delta\varepsilon_B^b\right)/(a-b) \quad 4.91$$

$$E(\bar{r}) = c_0 + c_1\bar{r} + c_2\bar{r}^2 \quad 4.92$$

Kim and Lee also introduced another advantage of this method in addition to the fact that material properties are not needed for finding the residual stresses. The interlaminar tensile strength (ILTS) of the laminate can be measured during the same test. The test specimen is loaded in the cut-cylinder-bending test until delamination occurs. With the applied moment M_D that causes the delamination, the ILTS can be calculated by using Equation 4.93. ILTS is the radial stress just before the delamination occurs [26]:

$$ILTS = \frac{M_D}{-M_R} \max_{a<r<1} \left\{ \frac{K}{r} \left[\left(c_0 r + \frac{c_1}{2} r^2 + \frac{c_2}{3} r^3 \right) - R \left(c_0 \log r + c_1 r + \frac{c_2}{2} r^2 \right) + X \right] \right\} \quad 4.93$$

Kim and Lee verified the new residual stress measuring and calculation method by using FEM (Abaqus 6.4). They also compared the results of the new method to the results obtained by using the conventional method. The results of their study showed that the residual stresses measured with the new radial-cut-cylinder-bending method were closer to the results obtained by using FEM than the ones obtained using the conventional method. In some cases, the new method predicted the shape of the residual stress distribution similarly with FEM while the conventional method gave results where the shape of the residual stress distribution was quite different.

4.6 X-Ray Diffraction, Micro Raman Spectroscopy and fiber Bragg gratings

X-Ray Diffraction (XRD) (Figure 4.10) and Micro Raman Spectroscopy (MRS) (Figure 4.11) are used for non-destructive measuring of internal strains of a composite. For measuring the strains with these methods, embedded strain sensors are normally used in the polymer matrix. XRD is used also for some composites with a semicrystalline thermoplastic matrix.

Benedikt et al. [30] used two different types of embedded strain sensors in their study where they measured internal stresses of graphite fiber/polyimide composites with different stacking sequences. As embedded sensors for XRD measurements, they used spherical aluminum inclusions with diameters 1-20 µm and for MRS measurements they used Kevlar-49 fibres. The individual fibres were placed in the longitudinal and transverse direction to receive information about the stresses in both planar directions. Out-of-plane measurements were not done in their study. With the XRD method, they obtained only the average strain level due to the large cross section of the X-ray beam. They discovered that the accuracy of the measurements depends on the used technique and on the geometry of the embedded sensors.

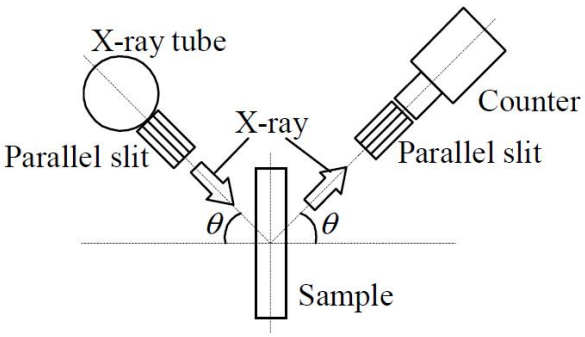

Figure 4.10. Schematic diagram of strain measurement arrangement in X-ray diffraction. [36]

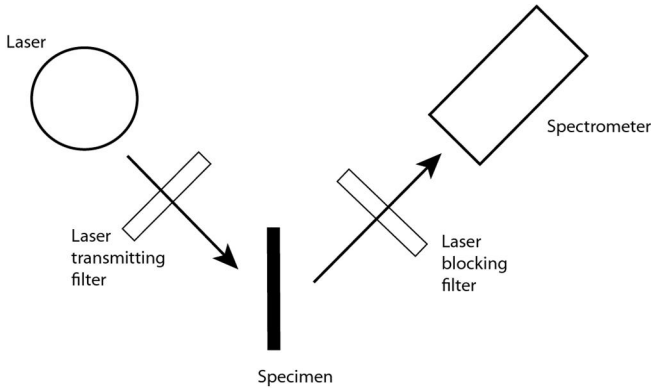

Figure 4.11. Schematic diagram of the measurement arrangement in Raman spectroscopy.

With the strain measurements of aluminum inclusions, obtained using the XRD method, it was possible to determine the stresses in the composite laminate by using the Eshelby model [31]. Eshelby model is used for predicting residual stresses in two-phased materials such as composites. The XRD- technique gives more information than MRS, because with MRS it is only possible to find the longitudinal strains of fibres. In case of non-transparent composites, low penetration depth of the laser beam in the MRS-technique limits the applicability of the technique. [30]

In the XRD technique, the needed equipment are the X-ray source and the X-ray detector. The strains are measured from the diffracted X-rays from the test specimen (Figure 4.12). When the diffraction angle and the lattice spacing of the crystal planes in the material are known in the stress free state, it is possible to calculate the stress state by using the measured diffraction angle. The penetration depth of the X-rays limits the strain measurement depth. For aluminum-alloys, iron and nickel, 50 % of the radiation is diffracted from the depth of 0.005 mm. XRD enables to measure strains as a function of depth in high resolution. The increase of the diffraction angle increases the precision of the technique. With XRD it is possible to find only elastic strains because only elastic deformation changes the lattice spacing of the crystal planes from where the X-rays are diffracted. [32]

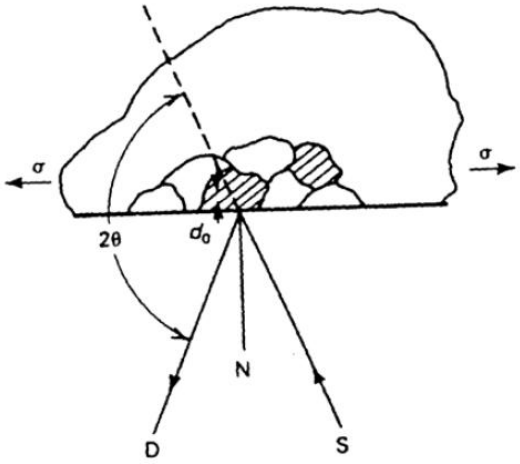

Figure 4.12. Schematic diagram of the XRD technique. Symbol S is the source and D is the detector of the x-ray. Symbol N represents the normal of the surface and 2θ is the diffraction angle. Quantity d_0 is the distance between crystal planes. [32]

MRS is based on inelastic scattering of monochromatic light produced usually with a laser. The frequency of the laser is usually close to the infrared or ultraviolet range. Information about certain molecular vibration, which changes due to the stress state of the material, is obtained from the scattered light. The scattered light is recorded with a spectroscope and unnecessary wavelengths of the light are filtered out. [30]

Benedikt et al. found out that the results were more accurate when using the MRS technique in their case. Accuracy of the method depends highly on the material and shape of the inclusions which are used as sensors for strain and stress measurements. The strain transfer to the fibres was better than to the Al inclusions. The benefit of the Al inclusions is that all three principal strains can be measured from them. From fibres it is possible to find only axial strains. [30]

In the research done by Benedikt et al., the Al inclusions were painted in between the structural layer of the composite. Another possible way is to mix the inclusions to the resin. However, the inclusions may affect to the thermal and mechanical properties of the composite and thus the obtained results for residual stresses may be inaccurate. [30]

Another possible way to find internal strains of the composites is to use optical fibres with Bragg gratings. Bragg gratings reflect narrow range of wavelengths, called the Bragg wavelengths, and the rest of the wavelengths are transmitted through the gratings (Figure 4.13). The reflected wavelengths change, when the distance between the Bragg gratings changes. The strain can be then determined from the wavelength shift after deformation of the optical fibre (Figure 4.14) [38].

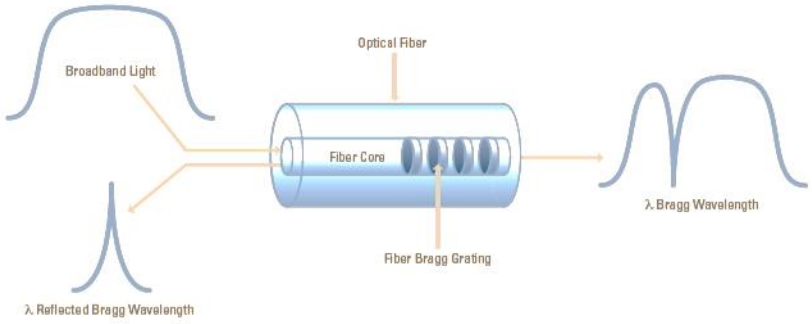

Figure 4.13. Schematic of the reflecting Bragg wavelengths due to Bragg gratings. [42]

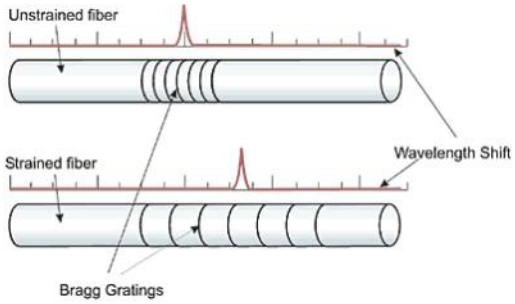

Figure 4.14. Optical fiber Bragg gratings and Bragg wavelengths before and after longitudinal deformation of the fibre. [43]

The optical fibre Bragg gratings can be calibrated in the longitudinal direction by using calibrated equipment to find the relation between the change in the wavelength and the actual strain. The calibration in the transverse direction is more complicated. In some studies the fibres are pressed in transverse direction and the effect of pressing to the gratings is investigated. Transverse strains of the optical fibres take place in many laminates because of the cure induced in-plane and out-of-plane shear stresses. Because of the shear strains in the optical fibre, the spectrum of the reflected light differs between laminates with different layup orientations (Figure 4.15). [37]

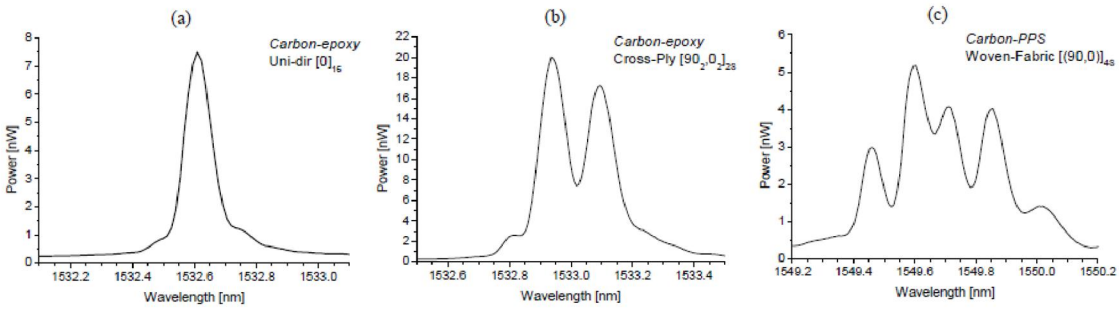

Figure 4.15. The spectrum of the reflected wavelengths from Bragg gratings in laminates with different layup orientations. [37]

5 Affecting residual stresses

There are various ways to affect formation of residual stresses in a composite laminate. The cure cycle must be optimized for the specific case especially in case of thick laminates to avoid residual stresses. The cure cycle optimization means finding the optimum heating rate, dwell time and cooling rate for the specific laminate. On the other hand the stacking sequence affects the final shape of the laminate after curing. The laminate can be distorted because of the cure induced residual stresses.

J.W. Kim et al. [27] introduced a modified cure cycle with cooling and reheating phases for carbon fabric phenolic composites in their study dealing the reduction of residual stresses in thick-walled composite cylinders. They used differential scanning calorimetry (DSC) in finding the degree of cure of the laminate. The idea of their work was to decrease the temperature difference between the solidification temperature and the room temperature to reduce thermal residual stresses. Their purpose was to keep the total curing time under the curing time recommended by the material manufacturer. In the curing process, the laminate was cooled abruptly by immersing the laminate in cool water. The cooling down phase was started when the degree of cure was 38 % and the temperature of the laminate was 125 °C. After the cooling phase, the laminate was reheated to the final post-cure temperature of 155 °C. With this procedure they managed to decrease the temperature difference between the solidification temperature and the room temperature by 29 % when compared to the cure cycle recommended by the material manufacturer. The developed cure cycle and the conventional cure cycle are shown in Figure 5.1. [27]

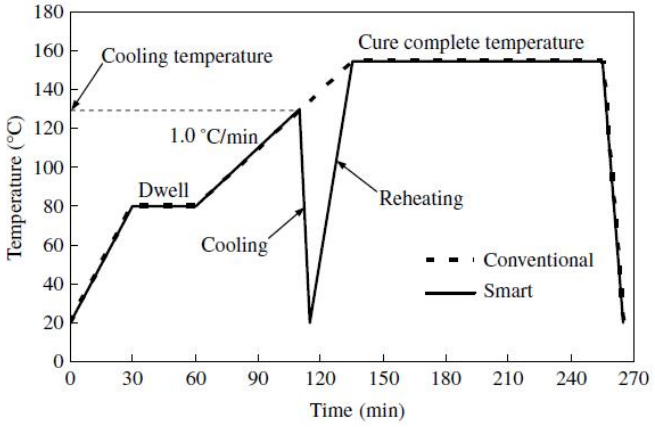

Figure 5.1. The cure cycle with cooling and reheating phases developed by Kim et al. (smart) and the conventional cure cycle recommended by the material manufacturer (conventional). [27]

Another possible way to modify the cure cycle is to lower the cure temperature. In some studies the low-temperature curing method has resulted to 25-30 % lower residual stresses when compared to the manufacturer recommended cure cycle. In the low-temperature curing method, the resin is cured until 50-70 % degree of cure is reached

and after this the post curing is carried out at a higher temperature to complete the curing process. As a drawback, the lower cure temperature leads to longer curing time. Another way to optimize the cure cycle is to reduce the heating rate so that the thermal expansion and cure shrinkage balance the effect of each other. This method does not lead to longer curing times. Russell et al. [28] investigated the latter method and its effect on residual stress formation of 3501-6/AS4 prepreg (Hexcel). They used the single fibre technique to find the curing condition where the stresses begin to grow and DSC to determine the temperature where low heating rate was initiated. The low heating rate was started at the temperature where exotherm initiates. In their study this temperature was 100 °C. The low heating rate was maintained to the temperature of 177 °C to avoid volumetric changes as thermal expansion and cure shrinkage balance each other. In their case, the thermal expansion and cure shrinkage balanced out at some point of the cure cycle, after which the shrinkage began to be larger than thermal expansion, which lead to shrinking of the resin as can be seen in Figure 5.2. [28]

The viscosity of the resin increased due to gelation at the point where cure shrinkage began to dominate. Shortly after gelation, the tension in the fibre began to grow as can be seen in Figure 5.2. At this point the degree of cure was 55 %. By using this kind of cure cycle with low heating rate sudden changes in volume of the resin were managed to even up and the shrinkage of the resin after the bonding of the resin and fibre was reduced. These issues resulted in lower residual stresses. [28]

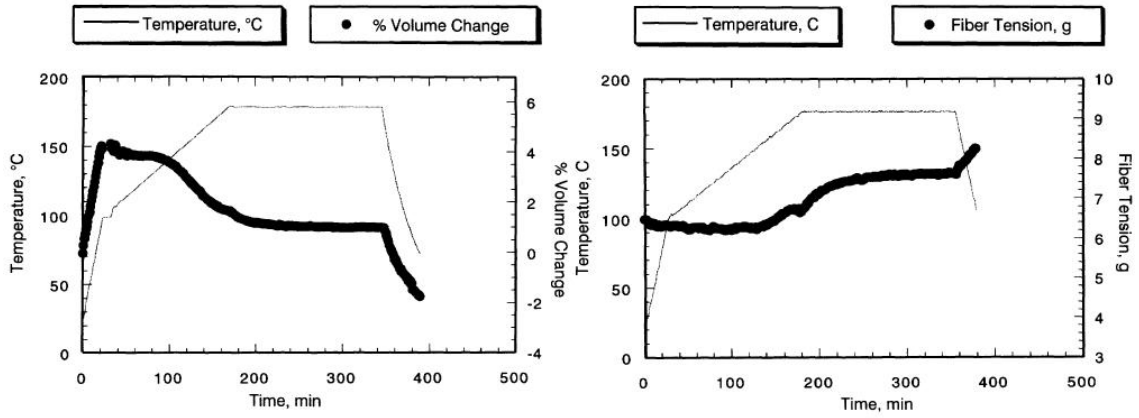

Figure 5.2. Volume change and fiber tension when low heating rate is used in curing of 3501-6/AS4 prepreg. [28]

With further research Russell et al. found an optimum cure cycle for the materials they used. By using this cure cycle, the thermal expansion of the matrix is compensating the effect of the cure shrinkage, which results in minimum fibre tension in the end of the cure process. The purpose of the modified cure cycle was to reduce the cure shrinkage, which happens after the gelation of the resin and the fibre and matrix bonding. This was obtained by increasing the temperature at the point where fibre-matrix interface developed, in which case the thermal expansion compensated the magnitude of the cure shrinkage. This way the fiber tension was steady until the cool-down as shown in Figure 5.3 and the residual stresses were reduced in the end of the cure cycle. Slow heating rate

enables the residual stresses to relieve during the cure process. Temperature in this cure cycle was raised rapidly to the hold temperature of 140 °C which was held until the fibre-matrix bonding. By using higher temperature in the beginning of the cure cycle, the fibre-matrix bonding started at lower degree of cure. When the degree of cure is low, the stresses are able to relax because of the lower stiffness of the matrix. [28]

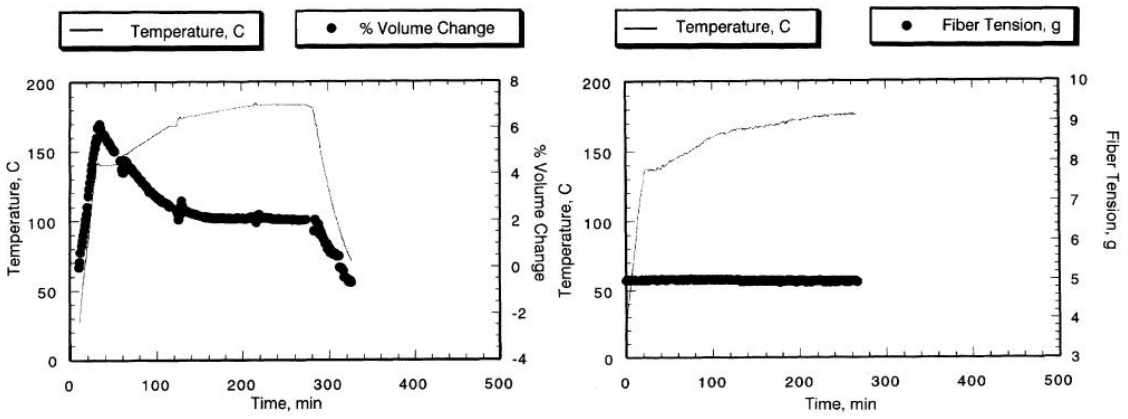

Figure 5.3. Volume change and fibre tension when optimized cure cycle is used for 3501-6/AS4 carbon/epoxy. [28]

In case of thick laminates, the heating rate must be slow enough to prevent the high exothermic peaks during the cure. Temperature rise due to exothermic reaction may cause differences in the degree of cure between the core and the surfaces of the laminate, which leads to formation of residual stresses. The internal thermal gradient can be decreased by using optimized heating rate. During the cooling, the stress formation caused by the internal temperature gradients can be avoided by using slow enough cooling rate. When the internal gradients in temperature, degree of cure and fibre volume fraction are avoided, the residual stresses of a thick laminate are similar to the ones in a thin laminate.

Matrix material has an impact on the residual stresses as well. In the case of thermosetting resins, the cure shrinkage after the bonding of the reinforcing fibres and the resin causes compressive stresses to the fibres. The amount of the shrinkage can be decreased by using particulate fillers such as silica, talc and calcium carbonate.

In case of thermoplastics, a low cooling rate gives more time for residual stresses to relax and reduces the internal gradient in temperature, as well as in degree of cure. A lower cooling rate leads also to a lower glass transition temperature. For amorphous polymers, a lower glass transition temperature leads to lower residual stresses. For semi-crystalline thermoplastics, a higher cooling rate results in a lower crystallinity level when shrinkage of the polymer is lower. However, the larger amount of amorphous content curing with high cooling rate leads to higher residual stresses. [18] Thus, the optimum cooling rate must be found for semi-crystalline polymers.

6 Experiments

In the experimental part of the thesis selected methods for residual stress determination are evaluated. The test specimens are similar in all tests, which makes it possible to compare the results with each other. Three different test methods are used in the study. The methods are the hole-drilling-method, layer-removal-method and unsymmetrical laminate. The selection of the methods was based on the availability of the equipment. The results of the experiments were compared to thermal stresses calculated with the ESAComp-software. In the case of post-cured laminates (50 °C) a temperature change of -30 °C was used in thermal stress analyses and in the case of elevated temperature cure (70 °C) a temperature change of -50 °C was used. The ESAComp calculates the thermal stresses by using the directional thermal expansions and CLT.

6.1 Materials and manufacturing

The test specimens are laminated plates and manufactured of glass-fibre reinforced epoxy. The reinforcement fabric is unidirectional and made of stitched E-glass roving. The specimens are manufactured using the vacuum resin infusion technique. The materials and manufacturing information are shown in the test programme in Table 6.1.

Table 6.1. Programme for evaluating different residual stress determination methods.

Test type	Cure temp.	Number of specimens	Measurements	Stacking sequence	Dimensions	Materials	Manufacturing
Hole-Drilling	Room temp. 20°C/24h + post-cure 50°C/15h	6	-Strains with strain gage rosette in 0°, 90°, 225°	$[0_4/90_4/0_4]$	L: 100 mm W: 100 mm T: ~ 10 mm	E-glass UD-reinforcement - 960g/m^2 , 2400tex in 0°-direction - 40g/m^2 , 68tex in 90°- direction Epoxy-resin - Araldite LY5052 resin - Aradur HY5052 hardener	Vacuum resin infusion at vacuum pressure of -0.5 bar
Layer-Removal		3	-Strains with strain gage rosette in 0°, 90°, 45°				
Unsymmetrical Laminate		2	-Midplane strains with embedded strain gage rosette in 0°, 90°, 45° -Curvatures	$[0_4/90_4]$	L: 200 mm W: 200 mm T: ~ 6 mm		
Layer-Removal for unsymmetrical laminate		4	-Strains with UD strain gage in 0° and 90°		L: 100 mm and 200 mm W: 50 mm T: ~ 6 mm		
Hole-Drilling	Elevated temp. cure 70°C/15h Heating mats on both sides of the laminate	6	-Strains with strain gage rosette in 0°, 90°, 225°	$[0_4/90_4/0_4]$	L: 100 mm W: 100 mm T: ~ 10 mm		Vacuum resin infusion at vacuum pressure of -0.5 bar
Unsymmetrical Laminate		2	-Midplane strains with embedded strain gage rosette in 0°, 90°, 45° -Curvatures	$[0_4/90_4]$	L: 200 mm W: 200 mm T: ~ 6 mm		

The needed material properties of a ply were calculated by using the ESAComp-software. ESAComp uses the so-called rule-of-mixtures expressions in approximation of the in-plane stiffness properties of a ply. The material properties applied are shown in Table 6.2 for the cured matrix, the reinforcing fabric and the ply. The material properties of the matrix are assumed to be the same for the both cure processes. The material properties of the matrix and the fabric are received from the manufacturers of the materials.

Table 6.2. Material properties for the matrix, the reinforcing fabric and one ply.

Material	E_1 [MPa]	E_2 [MPa]	G_{12} [MPa]	ν_{12}	ν_{21}	α_1 [/°C]	α_2 [/°C]
epoxy matrix	3100	3100	1148	0.35	0.35	$71 \cdot 10^{-6}$	$71 \cdot 10^{-6}$
E-glass fabric	40000	10000	3000	0.3		$5 \cdot 10^{-6}$	$5 \cdot 10^{-6}$
ply	21550	4730	1660	0.325	0.0714	$9.75 \cdot 10^{-6}$	$48 \cdot 10^{-6}$

The schematics of the laminates for the test specimens are shown in Figure 6.1.

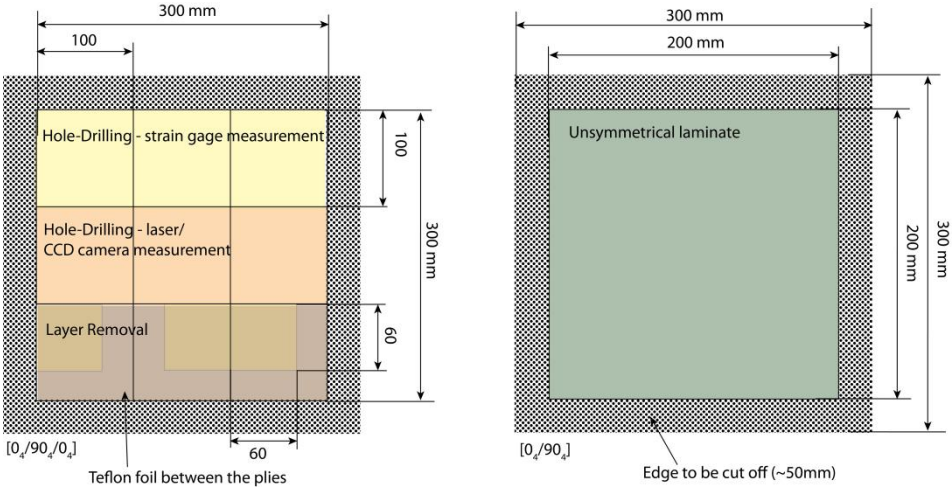

Figure 6.1. Schematics of the laminates used in evaluation of different residual stress determination methods.

The laminates were cured in as uniform temperature as possible to achieve even residual stresses in the laminate. The post-cure of room temperature cured laminates was done in an oven in the 50 °C temperature for 15 hours after the laminate had cured in room temperature for 24 hours. The elevated temperature curing was done by using heating mats on both sides of the laminate. The heating mats were controlled with the Envic controller device. A low heating ramp, 1 °C/min, was used to keep the temperature of the laminate even through the thickness. The cooling ramp was also 1 °C/min to avoid the thermal gradient between the core and the surfaces during the cooling. The manufacturing of the elevated temperature cured laminates is shown in Figure 6.2.

Figure 6.2. The elevated temperature cure by using heating mats. The heating mats were placed under the mold and on top of the vacuum bag. The system was covered with thermal insulation to keep the temperature changes low during the cure temperature hold.

The idea of using the elevated temperature cure was to create higher residual stresses than in the room temperature cure/post-cure process. When the post-cure is used, the fibre-matrix interaction has already taken place during the room temperature cure phase. During the room temperature phase the cure shrinkage is the only factor that induces internal stresses to the laminate. The final curing takes place during the post-cure in an elevated temperature and after this the total residual stresses form due to temperature change during the cool down to ambient temperature. Before the post-cure, the stiffness of the thermoset has already increased which leads to stress formation during the heating to the post-cure temperature. Thus the stress-free temperature is not the post-cure temperature but somewhere in between the ambient and post-cure temperatures.

In the elevated temperature cure, the curing was done completely in the elevated temperature and the total residual stresses were formed by the cure shrinkage and the temperature change from the cure temperature to the ambient temperature.

In the layer removal method, a Teflon foil was placed between every layer to the edge of each specimen. In this way it is possible to remove plies one by one with a sharp tool. The removing of layers was done one ply at a time in the fibre direction. The locations of the Teflon foils are shown in Figure 6.3

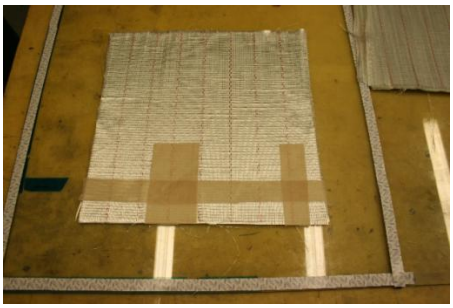

Figure 6.3. Teflon foil strips were placed between the plies to prevent the adhesion between the plies in the edge of the layer removal specimens.

In the case of an unsymmetrical laminate, the midplane strains were measured by using an embedded strain gage rosette in the laminate. Kyowa strain gage rosettes of the type KFG-5-120-D17-11L3M2S were used. The cables of the strain gage are vinyl coated and the maximum operating temperature is 80 °C. The strains were measured from the strain gage during the injection and during the cure and the post-cure. In experiments, three different locations for the strain gage rosette were used. In the first (1) test, the rosette was attached to a 50x50 mm and 0.05 mm thick steel foil and it was placed in the midplane of the laminate during the lay-up. In the second (2) test, the rosette was attached to the steel foil as well, but this time it was placed on the bottom of the laminate. Attaching the strain gage rosette to the steel foil was used to help the alignment of the rosette. In the third (3) test, the rosette was attached directly on the first glass-fibre fabric layer on the bottom of the laminate. The different locations of the strain gages are shown in Figure 6.4.

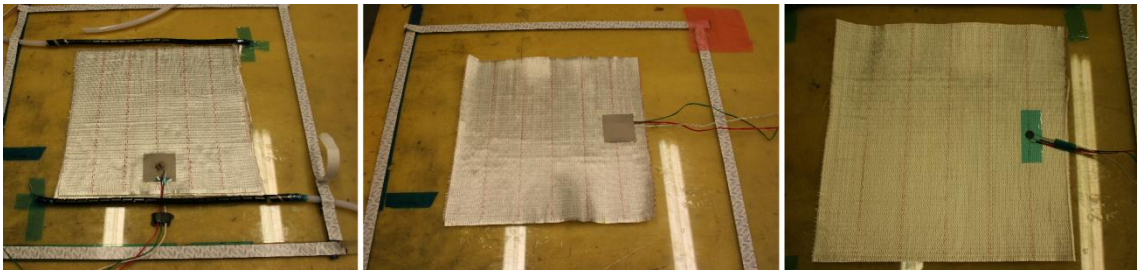

Figure 6.4. The locations of the embedded strain gages. The first (1) location of the gage is shown on the left-hand side, the second (2) in the middle and the third on the right-hand side. The reinforcement ply in (2) and (3) was turned over after attaching the strain gage, so that the strain gage locates in between the mold and the ply.

In the third (3) test, the scatter of the measurements was smallest of the three tests. Thus it can be presumed that the strain gage readings were the most accurate in the third test. Because the strain gage was located on the bottom of the laminate, the alignment of the rosette was easy to check to find out possible errors in the strains due to misalignment of the rosette.

In all tests, the strain data was logged with Peekel Instruments Autolog 3000 and Signasoft software. The data logging equipment can be seen in Figure 6.5.

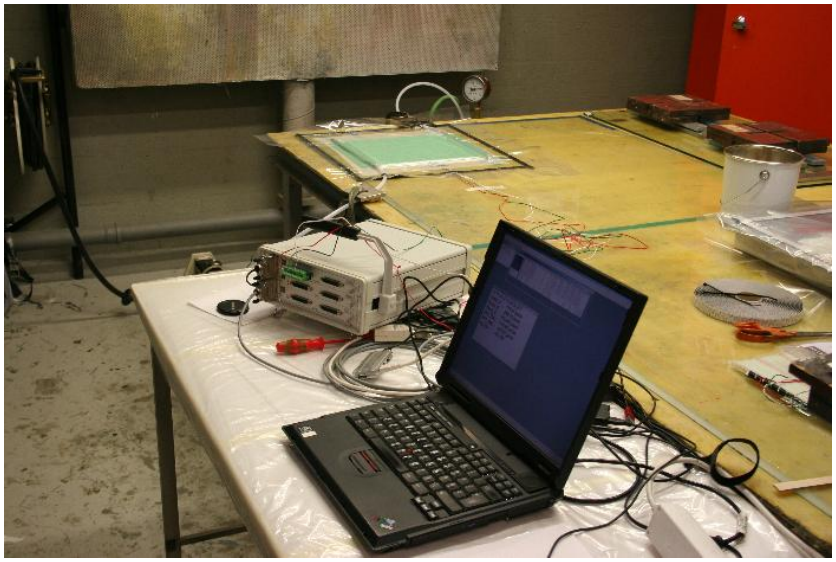

Figure 6.5. The strain data logging equipment. In the figure the strain data of an embedded strain gage is being recorded.

6.2 Hole-drilling method

6.2.1 Theory

In the through-hole-drilling method, the strains are measured after drilling a through hole to the specimen. The strains around the hole are measured from the surface of the specimen in three planar directions. The equations for the through-hole drilling method are originally introduced by Pagliaro and Zuccarello. [39]

Using the Hooke´s law, the relation between the ply strains and ply stresses in the global coordinate system LT can be written in the following form:

$$\begin{Bmatrix} \sigma_{L,k} \\ \sigma_{T,k} \\ \tau_{LT,k} \end{Bmatrix} = \left[\tilde{Q}\right]_k \begin{Bmatrix} \varepsilon_L \\ \varepsilon_T \\ \varepsilon_{LT} \end{Bmatrix} \quad 6.1$$

where $k = 1,2,..n$ and $\left[\tilde{Q}\right]_k$ is the stiffness matrix of kth ply in the global coordinate system, given by the following equation:

$$\left[\tilde{Q}\right]_k = \begin{bmatrix} \frac{E_L^k}{1-\nu_{LT}^k \nu_{TL}^k} & \frac{\nu_{TL}^k E_L^k}{1-\nu_{LT}^k \nu_{TL}^k} & \frac{\eta_{L,LT}^k}{G_{LT}^k} \\ \frac{\nu_{LT}^k E_T^k}{1-\nu_{LT}^k \nu_{TL}^k} & \frac{E_T^k}{1-\nu_{LT}^k \nu_{TL}^k} & \frac{\eta_{T,LT}^k}{G_{LT}^k} \\ \frac{\eta_{L,LT}^k}{G_{LT}^k} & \frac{\eta_{T,LT}^k}{G_{LT}^k} & G_{LT}^k \end{bmatrix} = [T]^{-1}[Q]_k[T]^{-T} \quad 6.2$$

where E_L^k and E_T^k are the Young´s modulus, G_{LT}^k is the shear modulus, ν_{LT}^k and ν_{TL}^k are the Poisson´s ratios, $\eta_{L,LT}^k$ and $\eta_{T,LT}^k$ are the Lekhnitskii´s coefficients of the kth ply in global coordinate system. $[Q]_k$ is the stiffness matrix of the ply in the local coordinate system and $[T]$ is the coordinate transformation matrix, stated as follows:

$$[Q]_k = \begin{bmatrix} \frac{E_1^k}{1-\nu_{12}^k \nu_{21}^k} & \frac{\nu_{21}^k E_1^k}{1-\nu_{12}^k \nu_{21}^k} & 0 \\ \frac{\nu_{12}^k E_2^k}{1-\nu_{12}^k \nu_{21}^k} & \frac{E_2^k}{1-\nu_{12}^k \nu_{21}^k} & 0 \\ 0 & 0 & G_{12}^k \end{bmatrix} \quad 6.3$$

$$[T] = \begin{bmatrix} cos^2\theta & sin^2\theta & 2sin\theta cos\theta \\ sin^2\theta & cos^2\theta & -2sin\theta cos\theta \\ -sin\theta cos\theta & sin\theta cos\theta & cos^2\theta - sin^2\theta \end{bmatrix} \quad 6.4$$

where E_1^k, E_2^k, G_{12}^k, ν_{12}^k and ν_{21}^k are the elastic constants of the ply in the local coordinate system and θ is the angle between the principal axis of the local and global coordinate systems.

The following normalized stiffness matrix $[a^*]$ is needed for the elastic properties of the laminate:

$$[a^*] = [A^*]^{-1} \quad 6.5$$

where:

$$[A^*] = \frac{1}{h}[A] = \frac{1}{h} \cdot \sum_{i=1}^{n} \left[\tilde{Q}\right]_k \cdot (z_i - z_{i-1}) \quad 6.6$$

The elastic properties of the laminate can be calculated with the following equations, if the elastic properties of each ply are known:

$$E_L = \frac{1}{a_{11}^*} \quad 6.7$$

$$E_T = \frac{1}{a_{22}^*} \quad 6.8$$

$$G_{LT} = \frac{1}{a_{66}^*} \quad 6.9$$

$$\nu_{LT} = -\frac{a_{12}^*}{a_{11}^*} \quad 6.10$$

$$\nu_{TL} = -\frac{a_{12}^*}{a_{22}^*} \quad 6.11$$

Lekhnitskii´s coefficients for each ply are obtained from the relations of the compliance matrix elements as follows:

$$\eta_{L,LT}^k = \frac{S_{16}^k}{S_{11}^k} \quad 6.12$$

$$\eta_{T,LT}^k = \frac{S_{26}^k}{S_{22}^k} \quad 6.13$$

where S_{nn}^k are obtained as follows:

$$[S]^k = \begin{bmatrix} S_{11} & S_{12} & S_{16} \\ S_{21} & S_{22} & S_{26} \\ S_{16} & S_{26} & S_{66} \end{bmatrix} = \left[\tilde{Q}\right]_k^{-1} \quad 6.14$$

Normalized stresses of the laminate are obtained by using the following relation:

$$\begin{Bmatrix} \sigma_L \\ \sigma_T \\ \tau_{LT} \end{Bmatrix} = E_L \begin{bmatrix} \frac{\bar{E}}{\bar{E}-\bar{\nu}^2} & \frac{\bar{E}}{\bar{E}-\bar{\nu}^2} & 0 \\ \frac{\bar{\nu}}{\bar{E}-\bar{\nu}^2} & \frac{1}{\bar{E}-\bar{\nu}^2} & 0 \\ 0 & 0 & \frac{\bar{G}}{\bar{E}} \end{bmatrix} \begin{Bmatrix} \varepsilon_L \\ \varepsilon_T \\ \varepsilon_{LT} \end{Bmatrix} \quad 6.15$$

where $\bar{E}$, $\bar{G}$ and $\bar{\nu}$ are the dimensionless elastic constants that are obtained from the relations of the elastic properties of the laminate as follows:

$$\bar{E} = \frac{E_L}{E_T}, \bar{\nu} = \nu_{LT} \text{ and } \bar{G} = \frac{G_{LT}}{E_T} \qquad \text{if } E_L > E_T \quad 6.16$$

$$\bar{E} = \frac{E_T}{E_L}, \bar{\nu} = \nu_{TL} \text{ and } \bar{G} = \frac{G_{LT}}{E_L} \qquad \text{if } E_T > E_L \quad 6.17$$

The relation between the measured strains and laminate strains is now obtained with the following relation:

$$\begin{Bmatrix}\varepsilon_1\\ \varepsilon_2\\ \varepsilon_3\end{Bmatrix} = \begin{bmatrix}c_{11} & c_{12} & c_{13}\\ c_{21} & c_{22} & c_{23}\\ c_{31} & c_{32} & c_{33}\end{bmatrix}\begin{bmatrix}\frac{\bar{E}}{\bar{E}-\bar{\nu}^2} & \frac{\bar{E}}{\bar{E}-\bar{\nu}^2} & 0\\ \frac{\bar{\nu}}{\bar{E}-\bar{\nu}^2} & \frac{1}{\bar{E}-\bar{\nu}^2} & 0\\ 0 & 0 & \frac{\bar{G}}{\bar{E}}\end{bmatrix}\begin{Bmatrix}\varepsilon_L\\ \varepsilon_T\\ \varepsilon_{LT}\end{Bmatrix} = [C][\bar{E}]\begin{Bmatrix}\varepsilon_L\\ \varepsilon_T\\ \varepsilon_{LT}\end{Bmatrix} \quad 6.18$$

where the matrix $[C]$ contains the dimensionless influence coefficients and ε_1, ε_2 and ε_3 are the strains measured with the strain gage rosette. The coefficients are dependent on the elastic properties of the material and the strain-gage-rosette geometry. They can be determined whether by using FEM-model or analytical solution. In this study the coefficients are determined with the analytical calculation method, which is based on the Lekhnitskii´s complex potentials method. The method gives a generic solution for the strain-stress relation of an orthotropic material. The "principal complex parameters" for the complex potential method are stated as follows:

$$\mu_{1,2} = \pm Re\left[\sqrt{-\frac{\bar{E}}{2\bar{G}} + \bar{\nu} \mp \frac{\sqrt{-4\bar{E}\bar{G}^2+(\bar{E}-2\bar{G}\bar{\nu})^2}}{2\bar{G}}}\right] + i \cdot \left|Im\left[\sqrt{-\frac{\bar{E}}{2\bar{G}} + \bar{\nu} \mp \frac{\sqrt{-4\bar{E}\bar{G}^2+(\bar{E}-2\bar{G}\bar{\nu})^2}}{2\bar{G}}}\right]\right| \quad 6.19$$

The relaxed strains, measured with the strain gages, can be stated with the following equation:

$$\varepsilon_{x'} = \frac{1}{E_L}\left\{\begin{array}{l}\left(Re\left[\frac{a}{F_1(\theta)} - \frac{b}{F_2(\theta)}\right]\sigma_L + Re\left[\frac{i\mu_2 a}{F_1(\theta)} - \frac{i\mu_1 b}{F_2(\theta)}\right]\sigma_T + Re\left[\frac{(i+\mu_2)a}{F_1(\theta)} - \frac{(i+\mu_1)b}{F_2(\theta)}\right]\tau_{LT}\right)\cos^2\theta +\\ \left(Re\left[\frac{c}{F_1(\theta)} - \frac{d}{F_2(\theta)}\right]\sigma_L + Re\left[\frac{i\mu_2 c}{F_1(\theta)} - \frac{i\mu_1 d}{F_2(\theta)}\right]\sigma_T + Re\left[\frac{(i+\mu_2)c}{F_1(\theta)} - \frac{(i+\mu_1)d}{F_2(\theta)}\right]\tau_{LT}\right)\sin^2\theta +\\ \left(Re\left[\frac{e}{F_1(\theta)} - \frac{f}{F_2(\theta)}\right]\sigma_L + Re\left[\frac{i\mu_2 e}{F_1(\theta)} - \frac{i\mu_1 f}{F_2(\theta)}\right]\sigma_T + Re\left[\frac{(i+\mu_2)e}{F_1(\theta)} - \frac{(i+\mu_1)f}{F_2(\theta)}\right]\tau_{LT}\right)\sin\theta\cos\theta\end{array}\right\} \quad 6.20$$

where a, b, c, d, e and f are dimensionless complex constants that are dependent on the dimensionless elastic properties. $F_1(\theta)$ and $F_2(\theta)$ are dependent on the strain gage geometry and the measuring arrangement as shown in Figure 6.6. The dimensionless complex constants are stated as follows:

$$a = \frac{(i+\mu_1)(\mu_1{}^2-\bar{\nu})}{\mu_1-\mu_2} \quad 6.21$$

$$b = \frac{(i+\mu_2)(\mu_2{}^2-\bar{\nu})}{\mu_1-\mu_2} \quad 6.22$$

$$c = \frac{(i+\mu_1)(\bar{E}-\bar{\nu}\mu_1{}^2)}{\mu_1-\mu_2} \quad 6.23$$

$$d = \frac{(i+\mu_2)(\bar{E}-\bar{\nu}\mu_2{}^2)}{\mu_1-\mu_2} \quad 6.24$$

$$e = \frac{(i+\mu_1)\bar{E}\mu_1}{(\mu_1-\mu_2)\bar{G}} \quad 6.25$$

$$f = \frac{(i+\mu_2)\bar{E}\mu_2}{(\mu_1-\mu_2)\bar{G}} \quad 6.26$$

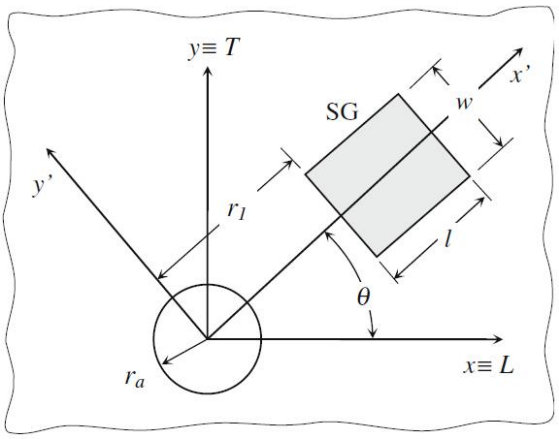

Figure 6.6. Coordinate system and notations for influence coefficients determination. [39]

The functions $F_1(\theta)$ and $F_2(\theta)$ are given by:

$$F_{1,2}(\theta) = \frac{A}{\int_{-w/2}^{w/2}\int_{r_l}^{r_l+l} f_{1,2}^{-1}(x',y')dx'dy'} \quad 6.27$$

where A is the area of each strain gage in the rosette and $f_{1,2}(x,y)$ depends on the radius of the drilled hole and the principal complex parameters as follows:

$$f_{1,2}(x,y) = \begin{cases} \frac{x+\mu_{1,2}y}{r_a}\sqrt{\frac{(x+\mu_{1,2}y)^2}{{r_a}^2} - \left(1+{\mu_{1,2}}^2\right)} & \forall \ |\zeta_{1,2}| \geq 1 \\ -\frac{x+\mu_{1,2}y}{r_a}\sqrt{\frac{(x+\mu_{1,2}y)^2}{{r_a}^2} - \left(1+{\mu_{1,2}}^2\right)} & \forall \ |\zeta_{1,2}| < 1 \end{cases} \quad 6.28$$

where x and y are the coordinates of the strain measurement point in the principal coordinate system. The strain measurement point is considered to be the center of the strain gage. The function $\zeta_{1,2}$ is:

$$\zeta_{1,2}(x,y) = \frac{x+\mu_{1,2}y+\sqrt{(x+\mu_{1,2}y)^2-{r_a}^2(1+{\mu_{1,2}}^2)}}{r_a(1-i\cdot\mu_{1,2})} \quad 6.29$$

Finally, combining Equations 6.1 and 6.18, the stress state of the each ply is obtained:

$$\begin{Bmatrix} \sigma_{L,k} \\ \sigma_{T,k} \\ \tau_{LT,k} \end{Bmatrix} = \left[\tilde{Q}\right]_k [\bar{E}]^{-1}[C]^{-1} \begin{Bmatrix} \varepsilon_1 \\ \varepsilon_2 \\ \varepsilon_3 \end{Bmatrix} \quad 6.30$$

where ε_1, ε_2 and ε_3 are the strains obtained with strain gages 1, 2 and 3 shown in Figure 6.7.

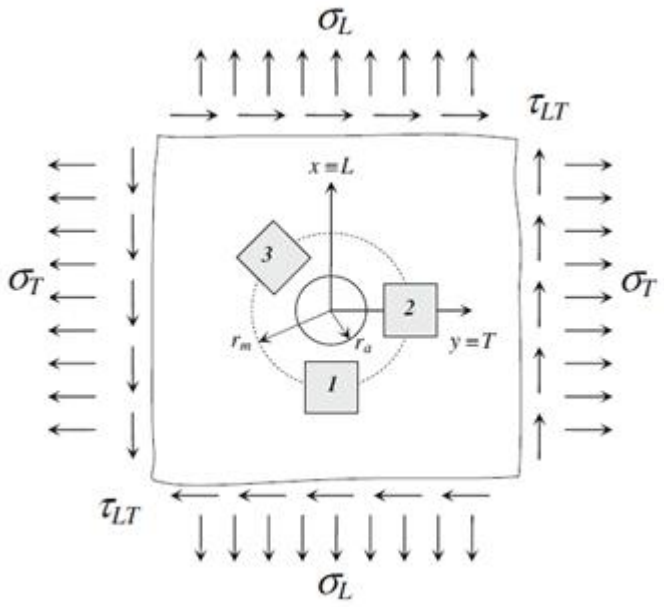

Figure 6.7. Coordinate system and sample geometry for strain gage locations. [39]

6.2.2 Test procedures

In the hole-drilling method the through-hole drilling approach was used instead of incremental hole-drilling. The repeatability of the through-hole drilling method seemed to be better when the existing devices of Laboratory of Lightweight Structures in Aalto University were used. By using the manual controlled column type drill, the accurate increments could have been hard to achieve. In addition, the thickness of the plies may vary and the brad point drill bit is not useful for the incremental hole-drilling method. The influence coefficients were calculated for this case by using the method introduced by Pagliaro and Zuccarello [39]. In the study, triaxial strain gages KFG-3-120-D28-11L3M2S, were used. The recommended hole diameter for the strain gage rosette is 3 mm.

In the experiments, the hole was drilled by using a regular column-type drilling machine. A brad point drill bit was used for making the centering of the hole easier. The specimen was held in its position by using a polyurethane frame that was clamped from its sides (Figure 6.8). This way, the initial stress state of the specimen was not distracted before the drilling. Drilling speed was 2900 r/min and feed was roughly 0.25 mm/sec.

Proper feed was found out experimentally by testing different feeds and evaluating the hole quality.

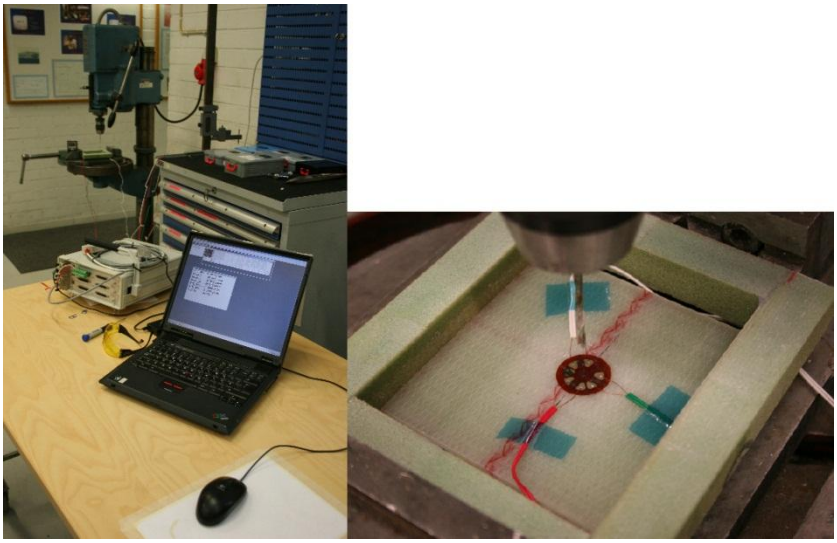

Figure 6.8. Hole-drilling test arrangement and the clamping of the specimen during the drilling.

The strains were measured constantly during the drilling with the measuring frequency f = 1 Hz. After drilling, the clamping of the specimen was removed and the specimen was left for cooling down for 20 minutes. An average strain from time period of the last 60 seconds was used in the strain calculations.

Three tests were done for the two types of laminates, i.e. for the post-cured laminate and for the laminate cured in elevated temperature. The stacking sequences of the laminates were the same.

6.2.3 Results and discussion

The strains for the post cured laminate and the elevated temperature cured laminate are shown in Table 6.3 and in Table 6.4, respectively. The strains had some scatter but nevertheless the trend was evident. The difference between the strains in different specimens was between 29.7-56.5 % of the maximum strains. The relatively large scatter may be caused by the small differences in the laminate properties in different locations or subtle differences in the hole locations. The first test in both specimen sets did not succeed due to inaccuracy in the hole location. The released strains of the successfully performed specimens followed similar trend, thus it was reasonable to take an average of the strains and use that for the stress calculations.

6.2.3.1 Post-cured laminate

Table 6.3. Strains on the surface of the post-cured laminate after through-hole-drilling. The average strains were used in the calculations.

	$\varepsilon_{0°}$ [m/m]	$\varepsilon_{90°}$ [m/m]	$\varepsilon_{225°}$ [m/m]
HD2-50pc	5.11E-04	3.91E-04	3.23E-04
HD3-50pc	2.84E-04	1.70E-04	1.60E-04
Average	**3.98E-04**	**2.81E-04**	**2.42E-04**

The stresses of the post-cured laminate, defined by using Equation 6.30, are shown in Figure 6.9. The results are compared to the calculated stresses due to temperature change during the cooling down from the post-cure temperature to room temperature. The stresses due to chemical shrinkage may increase the total residual stresses. The specific chemical shrinkage effects are not known for the materials that were used in this study. The chemical shrinkage of epoxy is normally 2-7 % [6]. Despite the chemical shrinkage is not taken into account, the stresses given by the hole-drilling method seem to be large. In addition, the hole-drilling method gives here only compressive stresses, which is not a possible situation when the laminate is not under an external compressive force.

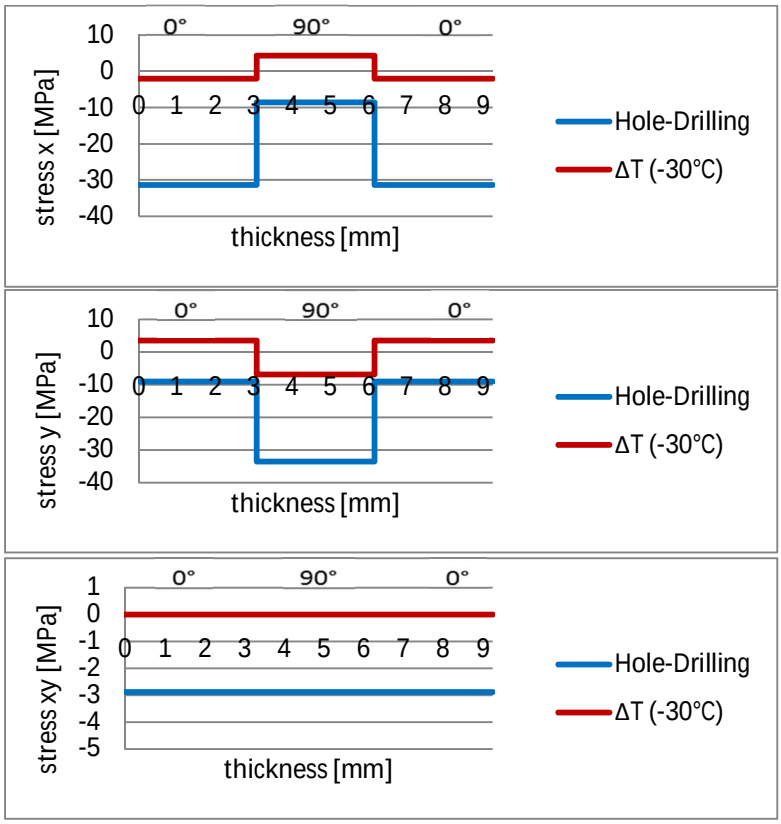

Figure 6.9. Residual stresses for the post-cured laminate in the xy-coordinate system. The stresses determined by using the through-hole-drilling method (blue lines) compared to thermal stresses computed with the ESAComp-software (red lines).

6.2.3.2 Elevated temperature cured laminate

Table 6.4. Strains on the surface of the elevated temperature cured laminate after through-hole-drilling. The average strains were used in the calculations.

	$\varepsilon_{0°}$ [m/m]	$\varepsilon_{90°}$ [m/m]	$\varepsilon_{225°}$ [m/m]
HD2-70ec	4.40E-04	4.49E-04	3.59E-04
HD3-70ec	7.55E-04	6.39E-04	5.58E-04
Average	**5.98E-04**	**5.44E-04**	**4.58E-04**

The residual stresses of the elevated temperature cured laminate are shown in Figure 6.10. The difference between the results of the hole-drilling method and thermal stresses determined with the ESAComp are even larger than for the post-cured laminate.

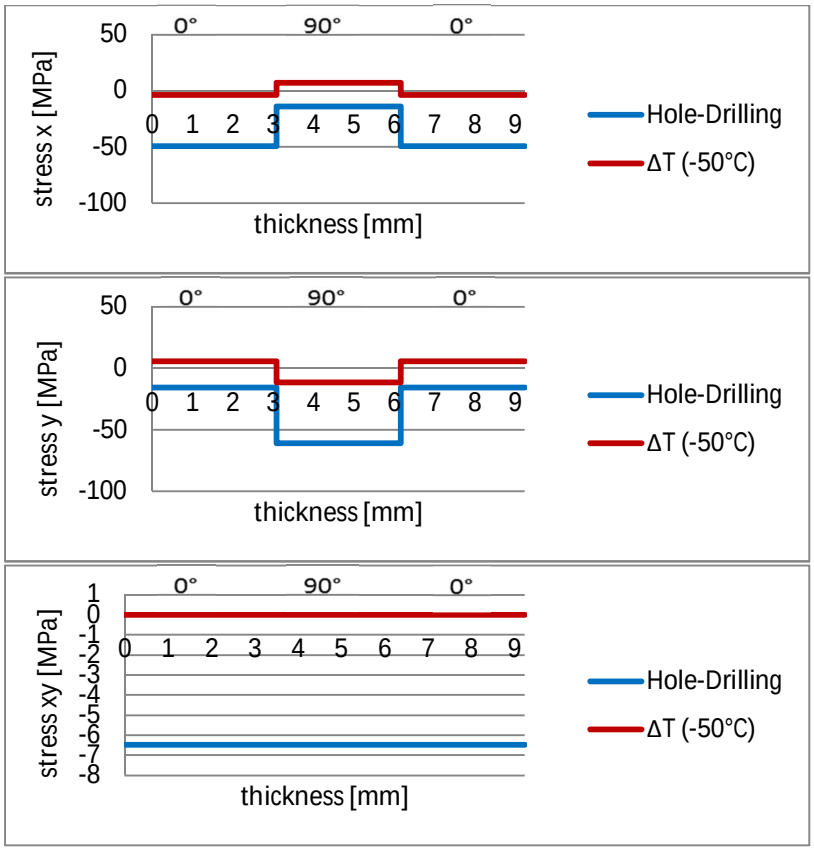

Figure 6.10. Residual stresses for the elevated temperature cured laminate in the xy-coordinate system. The stresses determined by using the through-hole-drilling method (blue lines) compared to thermal stresses computed with the ESAComp-software (red lines).

The results indicate that the through-hole-drilling method with a 3 mm hole diameter is not suitable for finding residual stresses of a thick laminate. As Pagliaro and Zuccarello

stated, the ratio (h/r_m) between the thickness of the laminate and the mean radius of the strain gage rosette affects the accuracy of the influence coefficients [39]. The ratio h/r_m in this study is 9.24/5.5=1.68. According to Pagliaro and Zuccarello the error in the influence coefficients is between 5-7 %, when the ratio h/r_m<0.25. Thus, if the target is to minimize the error in the influence coefficients, the thickness of the laminate should be less than 1.375 mm if a similar rosette as in this study is used.

6.2.4 Electronic Speckle Pattern Interferometry (ESPI)

The hole-drilling approach using Electronic Speckle Pattern Interferometry (ESPI) was tested with a cooperation of the Finnish company Stresstech Oy. The ESPI method uses laser light and CCD camera for producing the interference fringe pattern. The surface strains are obtained from the fringe pattern and the internal planar residual stresses are calculated from the surface strains.

Stresstech Oy has developed the Prism residual stress measurement device, which is based on the ESPI. While the thesis was being done, the Prism device was able to determine the residual stresses of an isotropic material. The calculation method for the orthotropic materials such as composites was under development. However, some tests were done for the composite materials. The test specimens were similar than in the hole-drilling method using strain gages for surface strain measurement. The test arrangement is shown in Figure 6.11.

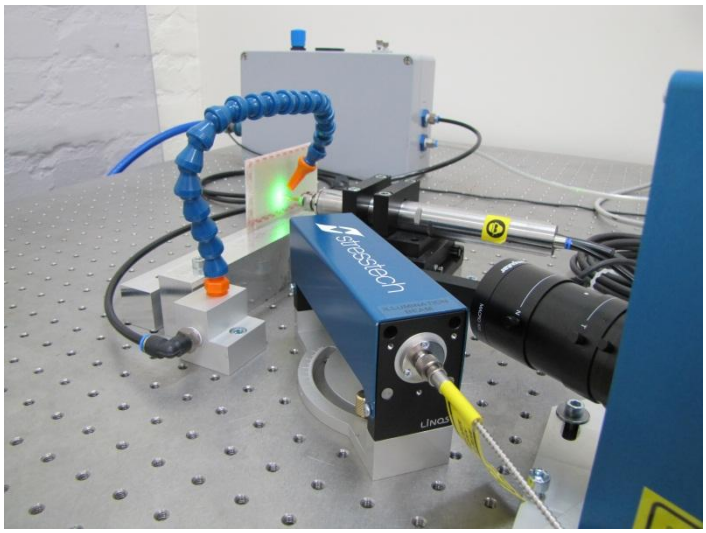

Figure 6.11. The laser illuminator is in the middle of the figure with the Stresstech label on it. The optics of the CCD camera can be seen on the right hand side, where the reference light source locates as well. The specimen is clamped between the aluminum bars and the green laser is pointed on the analysis area. The swivel pipe is used for blowing pressurized air to the specimen surface to remove the drilling dust during the drilling.

With the Prism, the hole-drilling procedure can be fully automated and the hole-drilling can be done in several steps or in one depth to obtain the stress profile. The software calculates the stress profile automatically. The results are obtained as figures and graphs. The fringe pattern also illustrates the distribution of the surface strains. A fringe pattern from the experiments is shown with a FEM model contour plot in Figure 6.12. The FEM-model is generated with the Abaqus 6.10-software. The only stress state applied to the FEM-model is the through the thickness uniform temperature change of 50 °C, which represents the elevated temperature cure at 70°C. The hole diameter in the FEM-model is 3 mm.

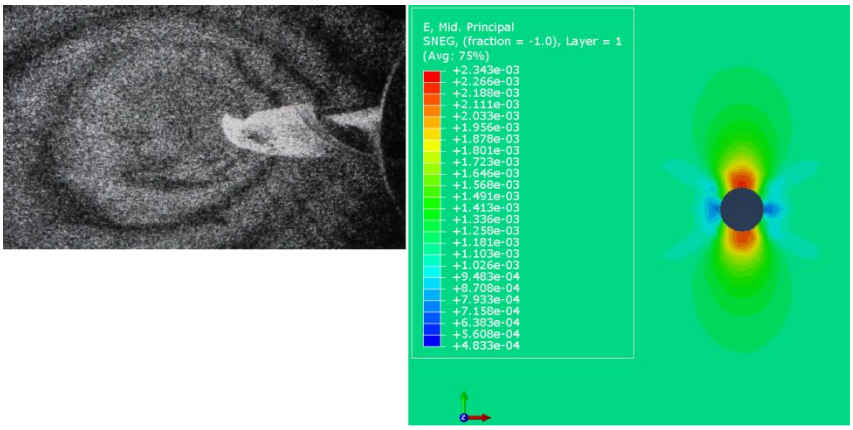

Figure 6.12. On the left hand side is the fringe pattern from the Prism device after one drilling increment of 1.58 mm which is roughly the thickness of two plies. On the right hand side the FEM model of the elevated temperature (70 °C) cured laminate with a through hole is shown. The contours illustrate the average principal surface strains.

The fringe pattern from the experiment and the contour plot of the average principal strains obtained with the FEM-model should contain similar contours after the through hole is drilled. The FEM model was not used for stress calculations but the surface strains in Figure 6.12 can be seen to be somewhat equal to the measured strains in Table 6.4.

During the experiments, the fine drilling dust attached to the surfaces of the specimen and the camera optics and the laser lens. The drilling dust leads to excess noise in the fringe pattern, thus some noise reduction method is needed. Also, because the calculation method was not yet ready, the residual stress profile was not obtained.

In the ESPI method there are several advantages, compared with the hole-drilling method by using strain gages for surface strain measurement. The ESPI method obtains surface strains from larger area than strain gages, which gives more accurate results. Possible inaccuracy in strain gage installation is avoided. Also, the analysis area can be determined after the drilling, thus an exact hole location is not required. When the strain gage is used, even a slight inaccuracy in the hole location leads to variation in measured surface strains and error in the stress calculation.

6.3 Layer-removal method

6.3.1 Theory

In the layer removal method, strain gages are attached to the surface of the specimen and layers are removed from the opposite side of the specimen. The strains are measured after every layer removal. The stress state of the removed layers can be calculated with the method introduced by N. Ersoy and Ö. Vardar [40]. The calculation of the stresses is based on the deformation caused by the layer removal (Figure 6.13). When the layers are removed one by one from the top to the bottom of the laminate, the through the thickness stress profile is obtained.

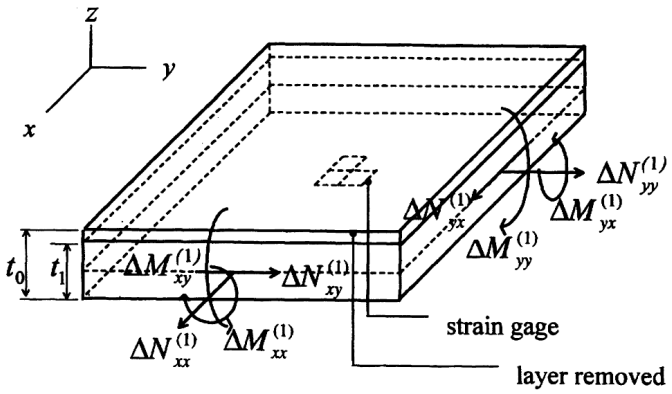

Figure 6.13. Strain measurement arrangement in the layer removal method. Determination of the stress state of the removed layer is based on the deformation caused by layer removal. [40]

When the first layer is removed, the changes in the strains are obtained. The changes in strains after kth layer removal can be stated as:

$$\{\Delta\varepsilon\}^k = \begin{Bmatrix} \varepsilon_x^k - \varepsilon_x^{k-1} \\ \varepsilon_y^k - \varepsilon_y^{k-1} \\ \gamma_{xy}^k - \gamma_{xy}^{k-1} \end{Bmatrix} \tag{6.31}$$

When the change in the strain after the first layer removal $\{\Delta\varepsilon\}^1$ is assumed to be caused by average stresses $\{\sigma\}^1$, the change in the in-plane loads and moments in the remaining laminate can be stated as follows:

$$\{\Delta N\}^1 = (t^0 - t^1) \cdot \{\sigma\}^1 \tag{6.32}$$

$$\{\Delta M\}^1 = (t^0 - t^1) \cdot \{\sigma\}^1 \cdot \frac{t^0}{2} \tag{6.33}$$

where t^0 and t^1 are the laminate thicknesses before and after the first layer removal and $\frac{t^0}{2}$ is the moment arm:

$$\frac{t^0}{2} = \left[\frac{(t^0+t^1)}{2} - \frac{t^1}{2}\right] \quad 6.34$$

The midplane strains and curvatures of the remaining laminate due to the first layer removal are:

$$\begin{Bmatrix}\Delta\varepsilon_0^1\\ \Delta\kappa^1\end{Bmatrix} = \begin{bmatrix}A^1 & B^1\\ B^1 & D^1\end{bmatrix}^{-1}\begin{Bmatrix}\Delta N^1\\ \Delta M^1\end{Bmatrix} = \begin{bmatrix}A^1 & B^1\\ B^1 & D^1\end{bmatrix}^{-1}\begin{Bmatrix}(t^0-t^1)\cdot\{\sigma\}^1\\ (t^0-t^1)\cdot\{\sigma\}^1\cdot\frac{t^0}{2}\end{Bmatrix} \quad 6.35$$

where A^1, B^1, and D^1 are the stiffness matrices of the remaining laminate.

The corresponding strain distribution through the thickness of the remaining laminate is:

$$\{\Delta\varepsilon(z)\}^1 = \{[e]^1 + z[f]^1\}\cdot\{\sigma\}^1 \quad 6.36$$

where $[e]^1$ and $[f]^1$ are stated as follows:

$$[e]^1 = (t^0-t^1)[A^1]^{-1} + (t^0-t^1)\frac{t^0}{2}[B^1]^{-1} \quad 6.37$$

$$[f]^1 = (t^0-t^1)[B^1]^{-1} + (t^0-t^1)\frac{t^0}{2}[D^1]^{-1} \quad 6.38$$

The change in the measured strains can now be written as follows:

$$\left\{\Delta\varepsilon\left(\frac{t^1}{2}\right)\right\}^1 = \left\{[e]^1 + \frac{t^1}{2}[f]^1\right\}\cdot\{\sigma\}^1 \quad 6.39$$

Thus, the stresses in the first layer that is removed can be calculated with Equation 6.40 as follows:

$$\{\sigma\}^1 = \left\{[e]^1 + \frac{t^1}{2}[f]^1\right\}^{-1}\cdot\left\{\Delta\varepsilon\left(\frac{t^1}{2}\right)\right\}^1 \quad 6.40$$

In general form, the residual stresses of the removed kth layer can be written as follows:

$$\{\sigma\}^k = \left\{[e]^k + \frac{t^k}{2}[f]^k\right\}^{-1}\cdot\left\{\Delta\varepsilon\left(\frac{t^k}{2}\right)\right\}^k \quad 6.41$$

where:

$$[e]^k = (t^{k-1}-t^k)[A^k]^{-1} + (t^{k-1}-t^k)\frac{t^{k-1}}{2}[B^k]^{-1} \quad 6.42$$

$$[f]^k = (t^{k-1}-t^k)[B^k]^{-1} + (t^{k-1}-t^k)\frac{t^{k-1}}{2}[D^k]^{-1} \quad 6.43$$

The changes in the residual stresses of the remaining ith layer, when the kth layer is removed, can be calculated with the following equation:

$$\{\Delta\sigma\}^{(i,k)} = [\bar{Q}]^i\cdot\{[e]^k\cdot\{\sigma\}^k\} + \frac{1}{2}(t^{i-1}+t^i-t^k)[\bar{Q}]^i\cdot\{[f]^k\cdot\{\sigma\}^k\} \quad 6.44$$

For finding the total residual stresses of the kth layer, the change in the stresses of the remaining layers must be subtracted from the stresses of the kth layer. Thus, the total residual stresses of the kth layer are:

$$\{\sigma\}_{total}^{k} = \{\sigma\}^{k} - \sum_{k=1}^{i-1}\{\Delta\sigma\}^{(i,k)} \quad 6.45$$

6.3.2 Test procedures

Residual stress tests were done for a similar laminate than in the hole-drilling method. During the layup of the layers, a strip of Teflon-foil was placed in between every layer to the edge of the specimen. The strips formed initial cracks between the layers and this helped removing of the layers. The layers were removed with a sharp knife, having a 2 mm thick blade. Because of the thickness of the blade, the layers were removed mostly by ripping, which appeared to be a good way to remove the layers most completely. The layers were removed starting from the top of the laminate since the strain gage was attached to the mold side due to better surface quality. The test setup and one of the specimens after layer removal is shown in Figure 6.14. The wooden slot is used for holding the laminate in place during the layer removal. After removing a layer the laminate was placed into the wooden slot to a vertical position, where it could freely deform. The strains were logged for 60 seconds after each layer removal and an average strain from this period was used in stress calculations.

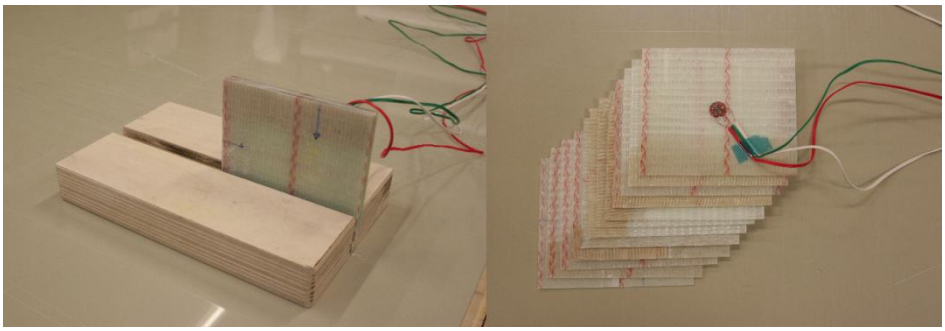

Figure 6.14. A test specimen before and after layer removal.

6.3.3 Results and discussion

The released strains were quite consistent between the three post-cured specimens. In the stress calculation, the change in the measured surface strains after each layer removal is used for determining the stresses of the removed layer. The changes in the measured strains are shown in the x- and y- directions for the three post-cured specimens in Figure 6.15.

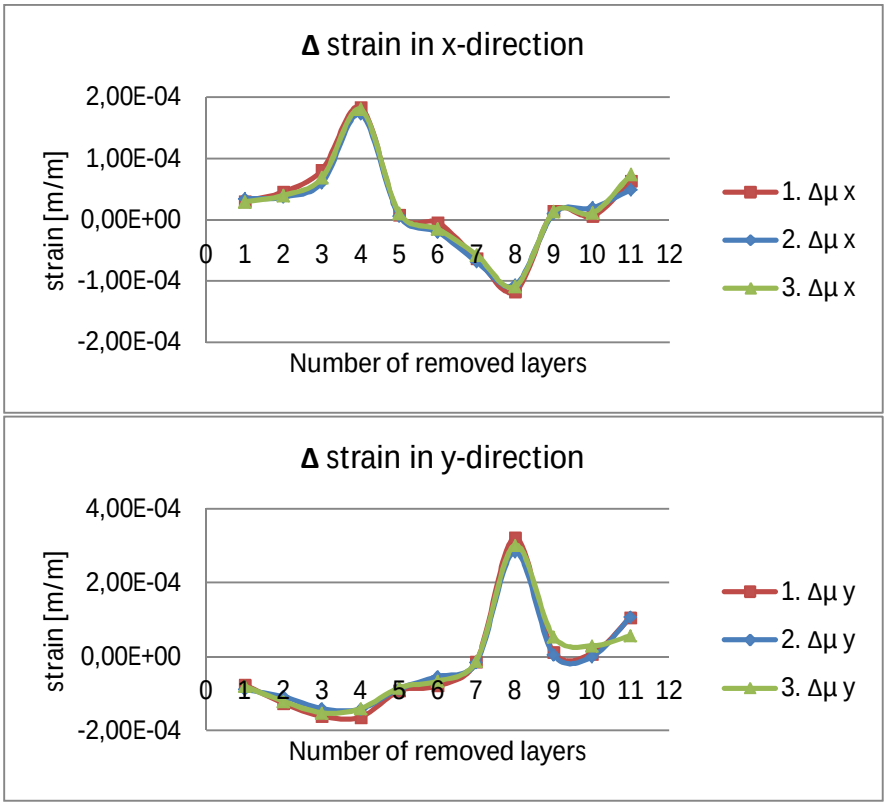

Figure 6.15. Changes in the surface strains in two directions for the three post-cured specimens. The strains are logged after each layer removal.

In the stress calculations, the average strains from the three specimens were used. The stresses are compared to thermal stresses, which are determined by using the ESAComp software. The residual stresses for the post-cured laminate are shown in Figure 6.16. If the strains are assumed to be distributed evenly on every adjacent layer in the same orientation, the results of the experimental method are quite close to the calculated ones. The largest differences between calculated stresses and layer-removal method stresses are 23 % in the x-direction and 71 % in the y-direction.

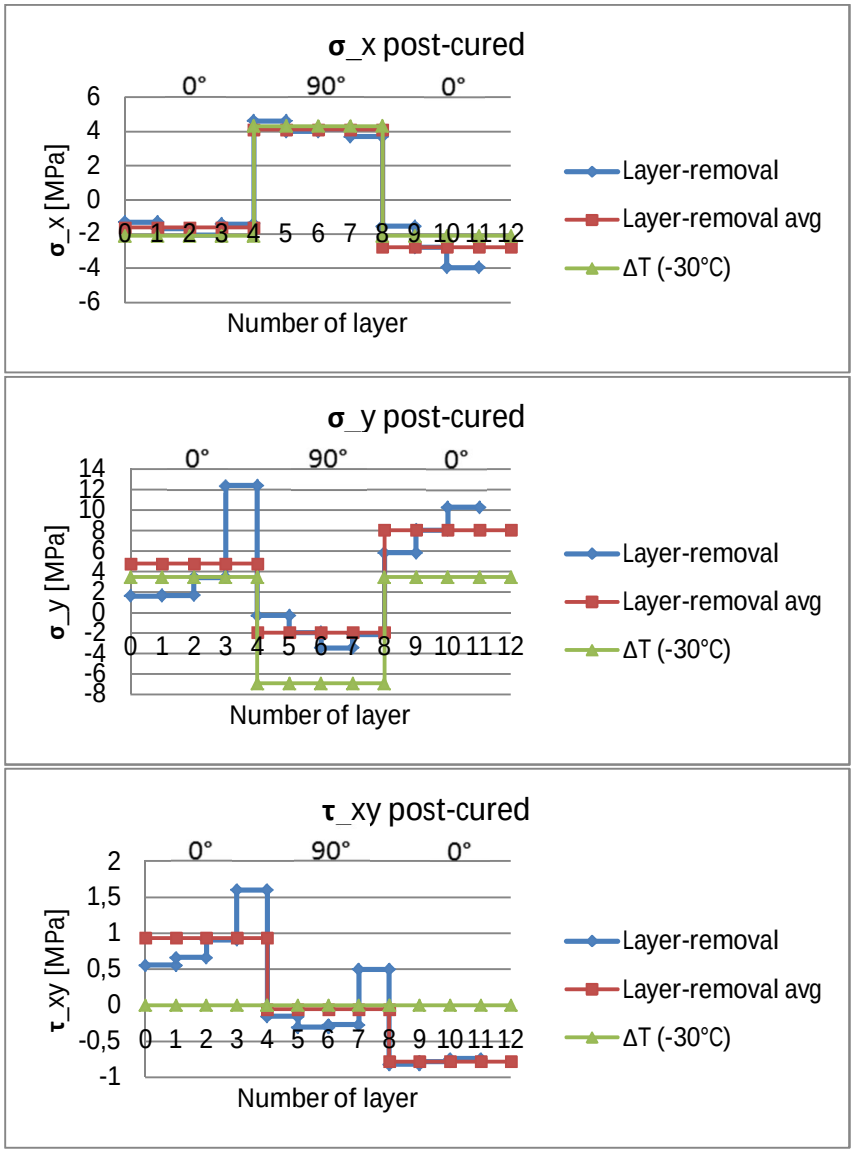

Figure 6.16. Residual stresses of the post-cured (50 °C) laminate. The stresses are determined by using the layer removal method, which are compared to the calculated thermal stresses. The "Layer-removal" graph describes the stresses of the removed ply and the "Layer-removal avg" describes the average stresses of the adjacent plies in the same orientation.

The layer-removal method gives a different stress level to the top layers and to the bottom layers of the laminate, while the calculated thermal stresses are identical in the layers with same fibre orientation. The friction between the laminate and tooling may cause difference to the residual stresses between the top and the bottom of the laminate. The stresses seem to relieve more effectively in the x-direction immediately after the first layer removal. In the y-direction, the stresses seem to relieve abruptly after removing the fourth layer after which the fibre orientation is 90°. The stresses may relieve in the x-direction more effectively because the initial flexural stiffness is four times higher in the x-direction than in the y-direction.

Instead of repeating this test for the elevated temperature cured laminate, tests were done for a post-cured unsymmetrical laminate. The laminate stacking sequence was similar than in the unsymmetrical laminate case in Section 6.4 in this study. The results of the layer-removal method for the unsymmetrical laminate are presented in Section 6.4.

6.4 Unsymmetrical laminate

An unsymmetrical laminate warps due to residual stresses after cooling down to ambient temperature from the cure temperature. The target was to determine the initial residual stresses of the straight laminate because the warping takes place due to this stress state. After warping the stress distribution changes and part of the stresses relax. The calculated stresses describe a situation where the warping of the laminate is prevented.

In the experiments, embedded strain gages were used for finding out the midplane strains during the cure. However, this method did not give reliable results. The deviation between the strain gage readings was high and some of the results were not consistent. The inconsistent strain gage readings may be a result of slight bending of the strain gage due to small gaps between the unidirectional roving. The calculation of the stresses was done by using only the laminate curvatures.

6.4.1 Theory

The laminate was able to warp freely after the cure. Because the laminate has plies only in the x- and y-directions, it can be assumed that the warping happens around the neutral axis of the laminate. The neutral axis locates in the neutral plane, which locates in different depth in x- y- and xy-directions. The location of the neutral plane is calculated with the following equation:

$$z_{np_{x,y}} = \frac{\sum_{i=1}^{n} E_i z_i}{\sum_{i=1}^{n} E_i} \quad 6.46$$

where $z_{np_{xy}}$ is the neutral plane in x- and y-directions and E_i is the directional stiffness of each ply and z_i is the coordinate of the ply in thickness direction.

The normal force acting in the plies can be calculated as follows:

$$N_{x,y} = \frac{\pm M_{x,y}}{z_{np_{x,y}}} \quad 6.47$$

where $M_{x,y}$ is the bending moment around the neutral axis of the laminate.

The curvatures are considered being caused by the bending moments around the neutral axis. The bending moment can be calculated by using the bending stiffness matrix and the measured curvatures as follows:

$$\{M\}_{xy} = [D]\{\kappa\}_{xy} \quad 6.48$$

where $[D]$ is the bending stiffness matrix and $\{\kappa\}_{xy}$ is the measured curvature vector in the global coordinate system.

The bending stiffness matrix is stated as follows:

$$[D] = \frac{1}{3}\sum_{i=1}^{n}[\bar{Q}]_i \cdot ({z_i}^3 - {z_{i-1}}^3) \quad 6.49$$

where $[\bar{Q}]_i$ is the rotated reduced stiffness matrix of the ply in the global coordinate system. The ply notations, used in previous equations, are shown in Figure 6.17. The rotated reduced stiffness matrix $[\bar{Q}]_i$ is stated as follows:

$$[\bar{Q}]_i = [T]_i^{-1}[Q]_i[T]_i^{-T} \quad 6.50$$

where $[T]_i$ is the coordinate transformation matrix of the ply and $[Q]_i$ is the reduced stiffness matrix of the ply in its principal coordinate system.

The strains in the global coordinate system are then calculated with the normal force vector from Equation 6.47 as follows:

$$\{\varepsilon\}_{xy} = [A]^{-1}\{N\}_{xy} \quad 6.51$$

where $[A]$ is the extensional stiffness matrix calculated as follows:

$$[A] = \sum_{i=1}^{n}[\bar{Q}]_i \cdot (z_i - z_{i-1}) \quad 6.52$$

The stresses in the global coordinate system can be now calculated for each ply as follows:

$$\{\sigma\}_{xy,i} = [\bar{Q}]_i\{\varepsilon\}_{xy} \quad 6.53$$

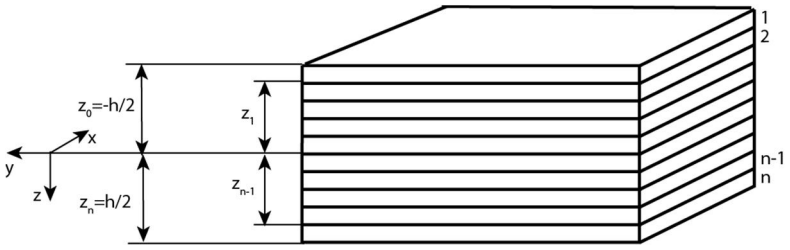

Figure 6.17. Ply notations and principal coordinate system of a laminate.

6.4.2 Test procedures

The curvatures were measured with the Carl Zeiss Calypso 3D CNC measuring device in Aalto University at Department of Engineering Design and Production. The device and measuring setup are shown in Figure 6.18. The curvatures were determined in three different planar directions.

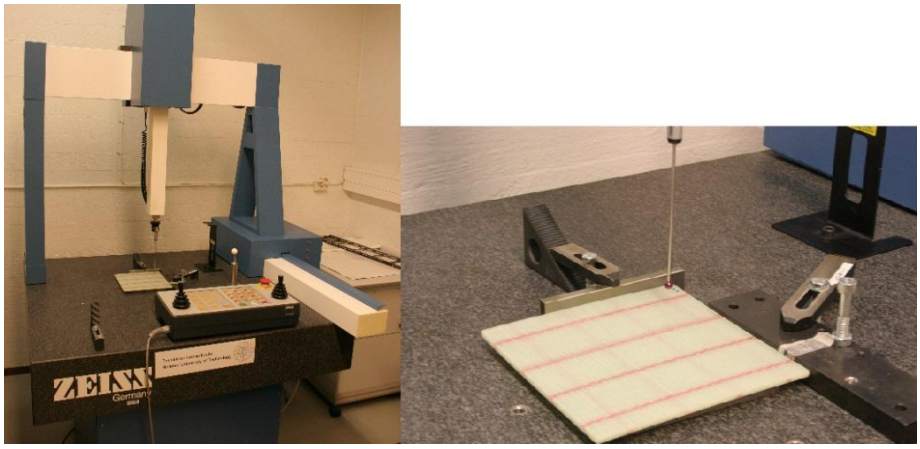

Figure 6.18. Curvature measuring setup of an unsymmetrical laminate by using Carl Zeiss Calypso CNC measuring device.

The specimens in the layer-removal method for the unsymmetrical laminate were of the size 50x100 mm and 50x200 mm. The specimens are shown in Figure 6.19. The strains were measured with longitudinal strain gages, thus the strains for shear stress calculation were not obtained.

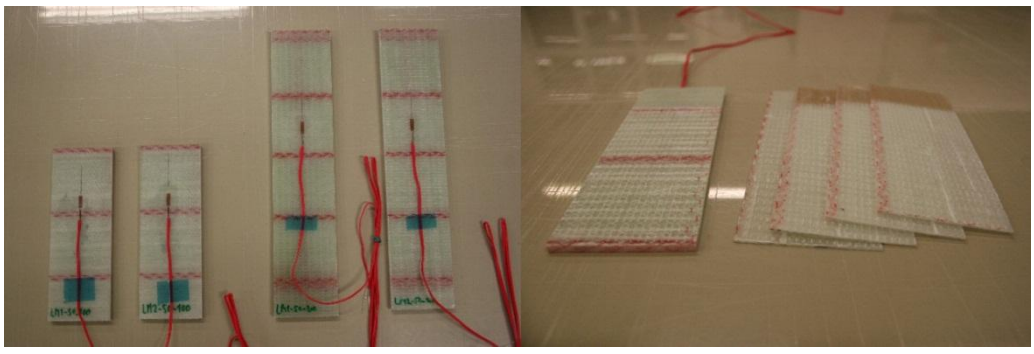

Figure 6.19. Unsymmetrical laminate specimens for layer-removal method. In the right-hand side, the layers are removed until the midplane of the laminate.

6.4.3 Results and discussion

The results of the calculation are shown in Figure 6.20. The results are compared to the test results of the layer-removal method and thermal stresses calculated by using the ESAComp software. The layer-removal was done in this case only to the midplane of the laminate and the stresses were assumed to be similar but acting to the opposite direction in the residual layers.

In the layer removal, when the four unidirectional plies are removed until the midplane is reached, the last ply mostly carries the stresses which are relaxed by removing the previous plies. When the stresses are then calculated, the fourth ply stresses are the highest in the x- and the y-directions as can be seen in Figure 6.20. When the stresses are assumed to be evenly distributed on all four plies in the same orientation, the stresses are convergent with the thermal stress analysis results that are obtained with the ESAComp software. The shrinkage of epoxy was earlier found to be 2-7 % after the gelation of the resin [6]. Most of the stresses are caused by the temperature change after the cure in which case the determined stresses should be close to thermal stresses obtained with the ESAComp.

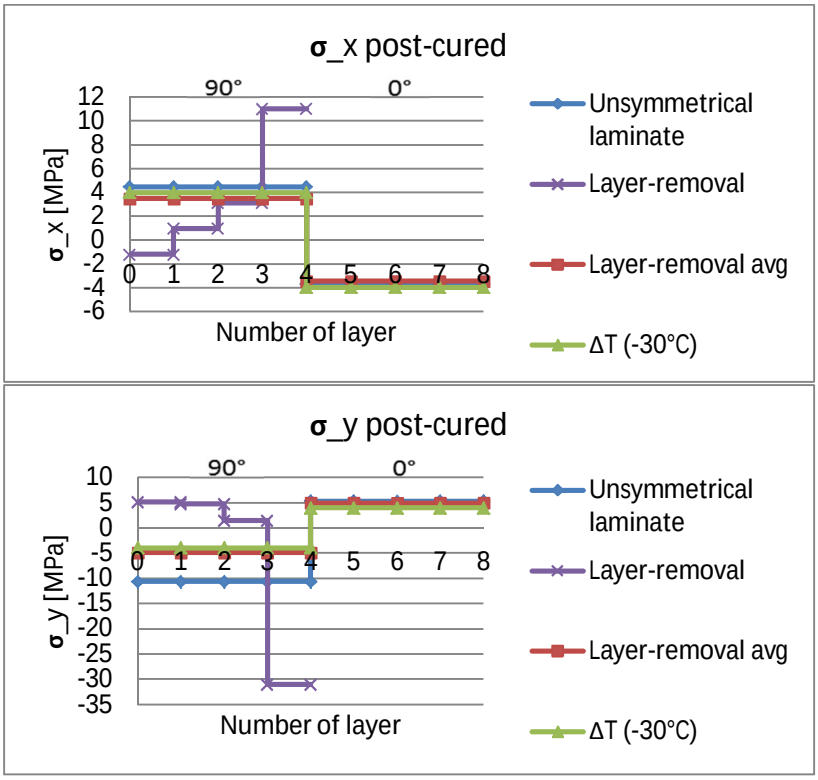

Figure 6.20. Residual stresses of the post-cured (50 °C) unsymmetrical laminate. The stresses are determined by using the method described in this chapter and by using the layer-removal method and the ESAComp-software. The stresses are shown here from the top to the bottom of the laminate.

The calculations were repeated for the elevated temperature cured (70 °C) unsymmetrical laminate. The layer-removal method was done however only for the post-cured laminate. The results for the elevated temperature cured unsymmetrical laminate are shown in Figure 6.21.

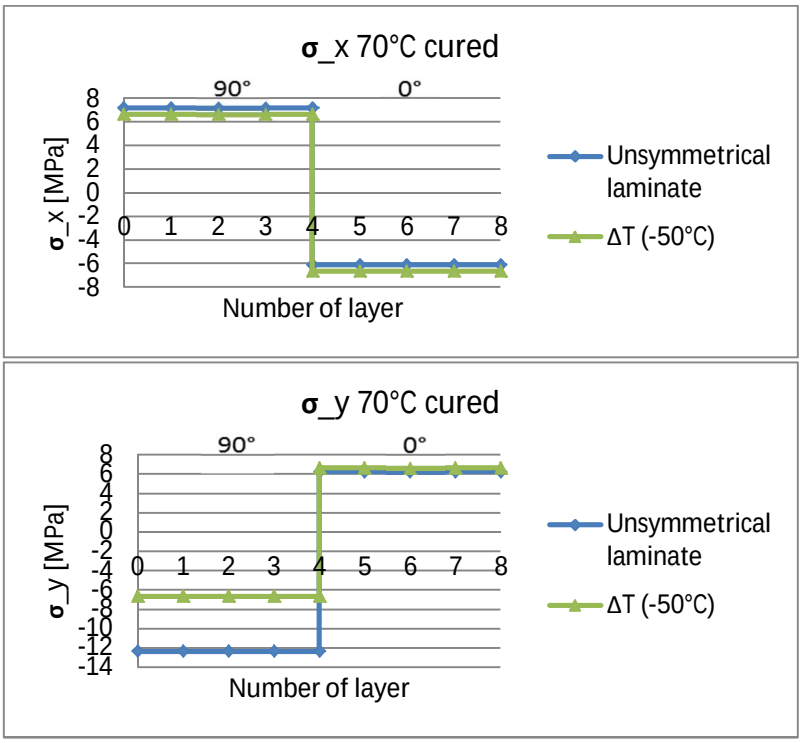

Figure 6.21. Residual stresses of the elevated temperature (70 °C) cured laminate. The stresses are determined by using the method described in this chapter and by using ESAComp software. The stresses are presented from the top to the bottom of the laminate.

The differences between the methods are in the range of 8 % to 50 % from the maximum stresses. The stress calculation from the curvature-bending moment relation gives similar results with the thermal stress analysis in the x-direction but in the y-direction the difference is large. The difference is presumably caused by two different factors. Firstly, the effect of midplane strains is not taken into account in calculations because of the inconsistent strain information. Secondly, the friction between the mold and laminate has certain effect on the development of the residual stresses during the cure.

7 Case study: Ring slitting method for a composite tube

An additional task of the thesis work was to determine the stress state of different layers in a laminated tube made of glass fibre reinforced plastic. The tubes were manufactured by filament winding and they were designed to represent a hydrometallurgical reactor structure. The tubes are composed of a sealing layer and structural layer. The sealing layer is designed to withstand the elevated temperature and the chemicals used in the process. The structural layer is designed to carry the pressure loading applied in the long-term test of the structure.

There were in total 16 different specimens to study. The specimens consisted of four different structures with four different resins. The structures of the specimens are presented in Figure 7.1. The reinforcement fibres were made of E-glass and they were in UD form in two different areal weights and as a mat made of discontinuous fibres in two different areal weights. The UD formed layers were used in the load carrying layers of the laminate and the mat formed layers were used in the sealing and surface layers of the laminate.

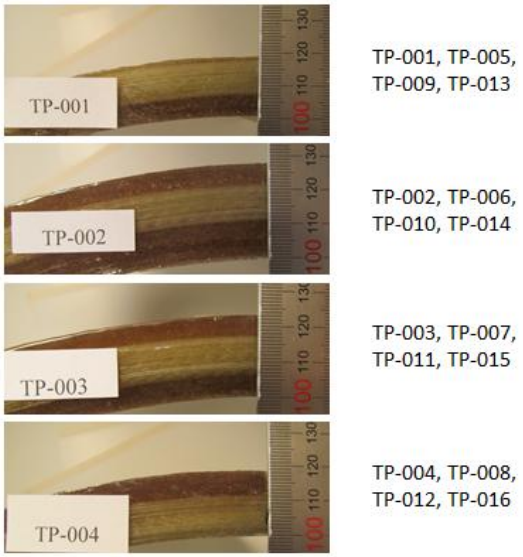

Figure 7.1. The layers of the test specimens. The darker layers are the sealing and the surface layers of the tube and the lighter section is the load carrying part of the tube.

The behavior that the resins in this study have in common is that their heat distortion temperature is high and their chemical resistance is good. The elastic modulus and the coefficient of thermal expansion of the layers are different after the resin is cured. This results in residual stresses when the laminate is cooled down to room temperature from the cure temperature. The elastic properties of the resins are different, which is one factor that causes variation in residual stresses between the samples. The higher the elastic modulus of the resin is, the more the stress relaxation is hindered after the cure.

Another factor is that the amount of cure shrinkage may vary between the resins. The shrinking of the resin causes compressive stress to the fibres. The amount of resin shrinkage is higher when the resin is in liquid form and in this phase the residual stresses will not develop because of the low elastic modulus of the resin. After the resin has turned into its solid form due to polymerisation, the residual stresses begin to develop. The reinforcement fibres are being under compressive stress after the cure of the resin. This leads to a tensile stress in the polymer matrix. The mechanical and thermal properties of the resins and the possible differences in cure cycles and layup process are the reasons to the differences in residual stress states of the samples with the same stacking sequence. The known properties of the resins are shown in Table 7.1.

Table 7.1. Mechanical and known shrinkage properties of the resins according to manufacturers.

Resin	Elastic modulus [GPa]	Tensile strength [MPa]	Volume shrinkage [%]
Resin A	3.4	90	7.5
Resin B	3.5	88	
Resin C	3.7	72	
Resin D	3.3	85	

The method used for determining the residual stresses was the ring slitting method, which is introduced in the Section 4.1. Firstly, the needed mechanical properties of the laminate layers, shown in appendix B, were determined by using the ESAComp 4.1-software. For stress measurements, 25 mm wide rings were cut from the tubes, one of each resin-layup combination. The holes for the steel studs were drilled (Figure 7.2) and the studs were attached. The distance between the studs was measured with a slide caliper after which the rings were cut open in between the studs. The distance between the studs was measured again after cutting and the residual stress driven displacement was determined from the difference of the measured distances between the studs. An average value of the displacement measured from the outer and inner studs was used in calculation of the stresses. One of the ring shaped specimens and the hole drilling procedure is shown in Figure 7.2. An example of the displacement measurement is shown in Figure 7.3.

Figure 7.2. Drilling of the holes for the measurement studs.

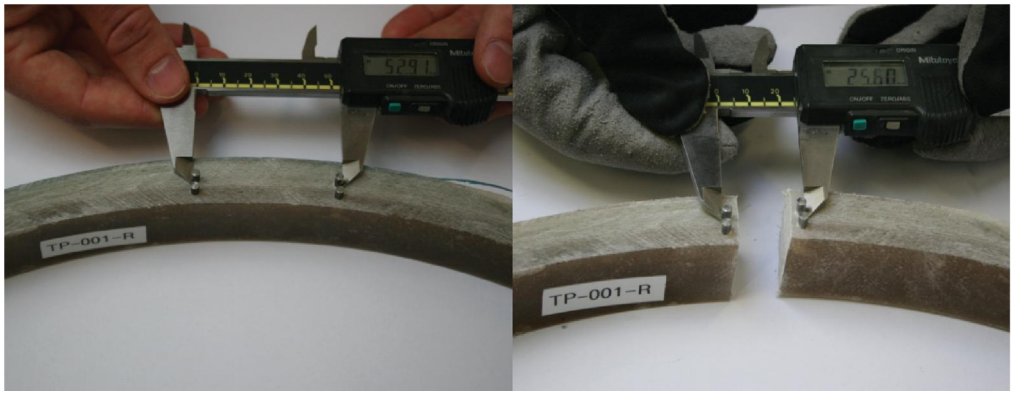

Figure 7.3. Measurement for determining the residual stress driven displacement.

The calculation of the stresses is based on the idea of a curved beam bending calculation. The stresses are considered being formed because of a bending moment affecting the ring. The variation in the elastic properties is taken into account by calculating the stresses piecewise. With the calculation method it was possible to determine the stresses in the radial and tangential (hoop) direction. A calculation tool for Mathcad 15.0 was developed for determining the residual stresses with this technique. This calculation tool is presented in appendix B.

The radial stresses were found to be lower than the hoop stresses. The maximum of the radial stress was locating roughly in the midplane of the laminate being naturally zero on the boundaries. The radial stresses of the laminates are shown in Figures 7.4-7.7. The laminates with the same stacking sequence are shown in same figures, so that the differences can be considered as differences in the resin behavior, when the curing and layup conditions are assumed to be similar in all specimens. All of the stresses are presented from inner to outer radius of the ring.

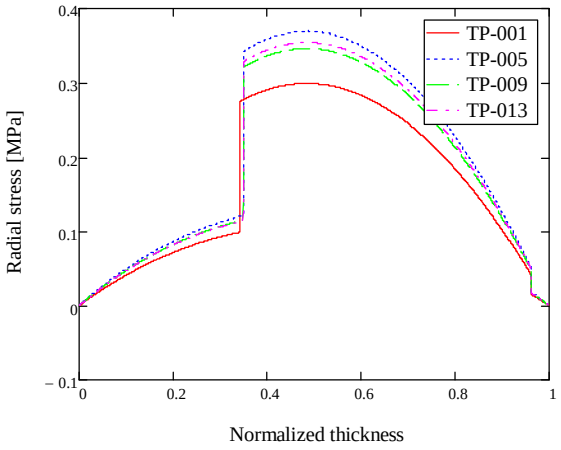

Figure 7.4. Radial stresses of the specimens with the stacking sequence 1.

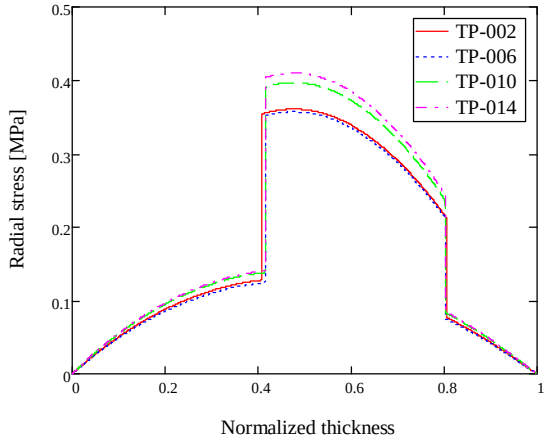

Figure 7.5. Radial stresses of the specimens with the stacking sequence 2.

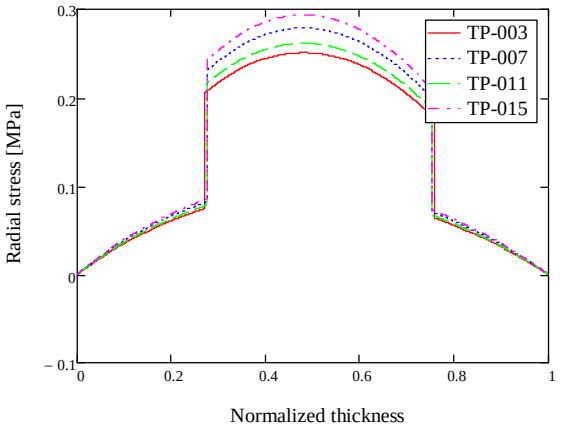

Figure 7.6. Radial stresses of the specimens with the stacking sequence 3.

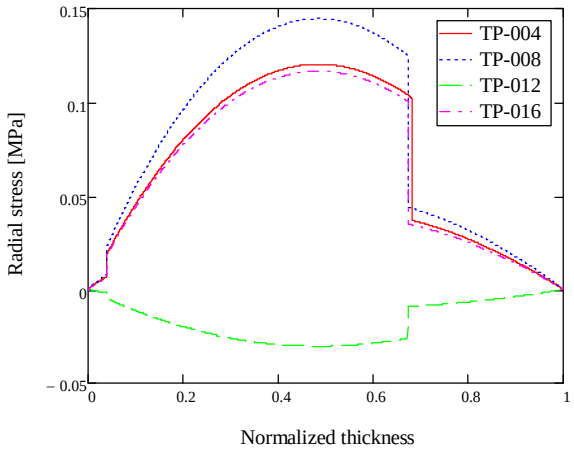

Figure 7.7. Radial stresses of the specimens with the stacking sequence 4.

The maximum of the radial stresses is located in the load carrying layer of the laminates. The maximum value of the radial stress was tensile almost in all cases. Only one stacking sequence-resin combination (TP-012) shown in Figure 7.6 resulted in a compressive radial stress. In the same specimen (TP-012) the absolute value of the stress was the smallest. According to these results the biggest radial residual stress was in the sample TP-014, where the stress was 0.41 MPa. The radial stresses were very small when compared to the tensile strength of the resins. There were no reinforcing fibres in the radial direction of the laminates, thus the strength of the laminate in that direction is close to the strength of the matrix.

The tangential residual stresses of the laminates were significantly higher than the radial stresses. Tangential stresses obtained by using the calculation tool are shown in Figures 7.8-7.11. According to the calculations the highest stresses were locating near the interface of the inner or outer sealing layer and the support layer of the laminates. Tangential stress was zero roughly at the midplane of each laminate.

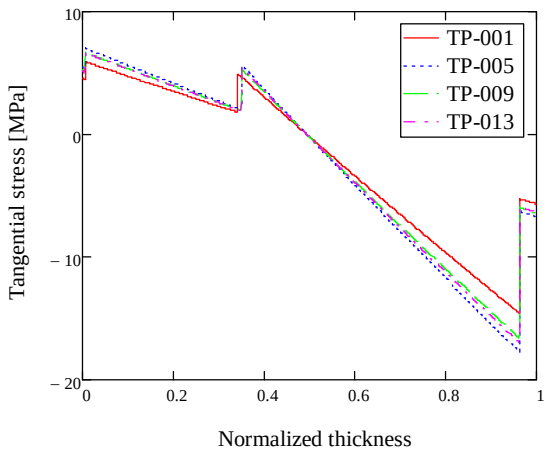

Figure 7.8. Tangential stresses of the specimens with the stacking sequence 1.

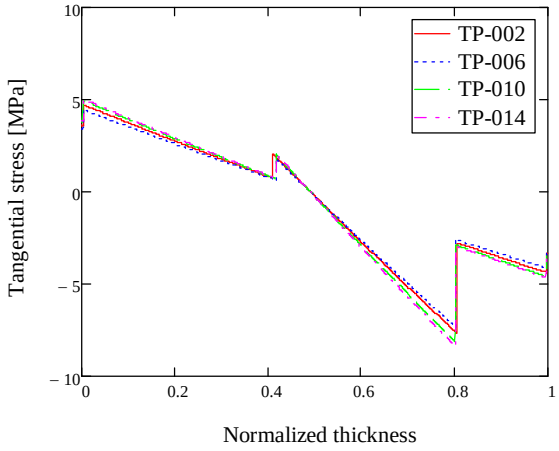

Figure 7.9. Tangential stresses of the specimens with the stacking sequence 2.

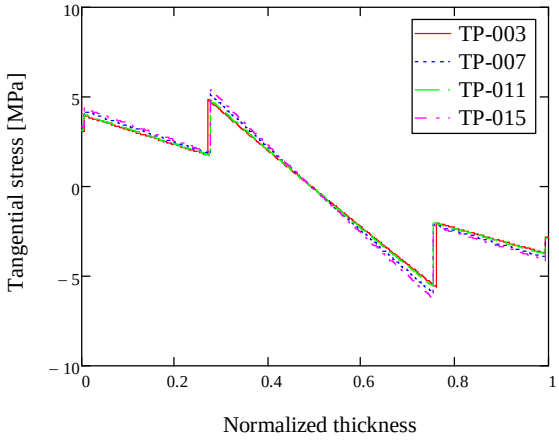

Figure 7.10. Tangential stresses of the specimens with the stacking sequence 3.

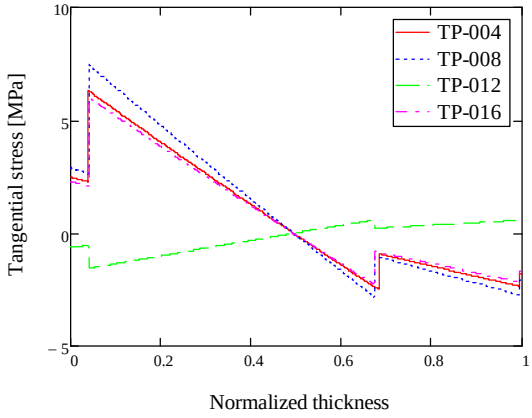

Figure 7.11. Tangential stresses of the specimens with the stacking sequence 4.

The highest value of the tangential stress was found in the specimen TP-005, where the highest tangential stress was compressive stress, which magnitude was 17.62 MPa. The lowest tangential stress level was found in the specimen TP-012. The highest tangential tensile stress, which was 7.47 MPa, was found in the specimen TP-008. Considering all the specimens the first layup sequence resulted in highest compressive peak stresses locating near the interface of the support layer and the outer sealing layer. The highest tensile stresses were found at the first and the last layup sequence except for the specimen TP-012.

The residual stresses were found to be lowest in the specimen TP-012 in both radial and tangential directions. In TP-012, the stresses were found to be very small and acting to the opposite direction when compared to the other specimens. The reason for this kind of behavior could be in different curing parameters. The section of the tube, where the specimen TP-012 was cut, could be post-cured incompletely. More research should be done to find out the reason for the behavior of the specimen.

Comparing the stresses to the tensile strength in hoop direction, the magnitude of the tangential residual stresses can be estimated. The accurate strength properties of the laminates are not known at this phase of the study, thus calculated values are used. Nevertheless, suggestive magnitude was found out. The highest percentages of the tangential residual stresses are about 4.5 % of the tensile strength. The highest percentages locate in the inner and outer layers of the laminate or at the interface of the support layer and the inner or outer sealing layer.

The effect of the residual stresses seems to be relatively low when compared to the strength of the laminate. The macro level effects of the residual stresses can be taken into account in design by using additional factor of safety. Another concern occurring due to residual stresses is the microcracking of the laminate. In some cases the aging of the matrix material due to hygrothermal effects has caused degradation of the material properties that leads to microcracking only due to residual stresses. [41] Microcracks may form pathways for corrosive agents, which may cause further degradation of materials and lower the strength of the load carrying support layer in this particular case.

A FEM-model was made for evaluating the accuracy of the stress values obtained by using the equations. The FEM-model was generated with Abaqus 6.10-software. The model consisted of a ring that was initially open from one side. The ring was partitioned and the partition properties were determined with the “composite layups” tool in Abaqus. The initial stress state of the ring shaped laminates was obtained by adding a forced displacement to the free ends of the ring and solving the stress state after this. The displacement was pointed to the hoop direction of the ring and it was equal to the displacement which was measured from the slit rings. The FEM-model enables also determining of the axial stresses by adding a forced axial displacement to the free end of the ring. In Figure 7.12, the FEM-model of the specimen TP-001 is shown and the distribution of the tangential stresses can be seen as color indications.

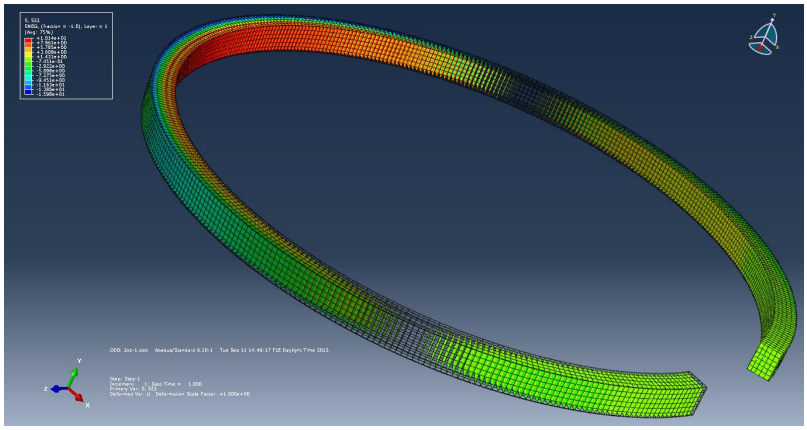

Figure 7.12. FEM results of the specimen TP-001 with forced displacement in hoop direction. The colors illustrate the tangential stress distribution of the ring.

The residual stresses from the FEM-model of specimen TP-001 in the radial and tangential directions are shown in Figures 7.13 and 7.14.

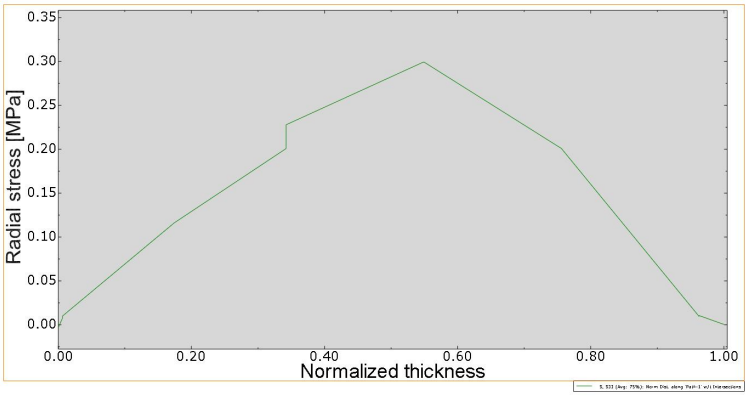

Figure 7.13. Radial residual stress obtained with FEM for specimen TP-001.

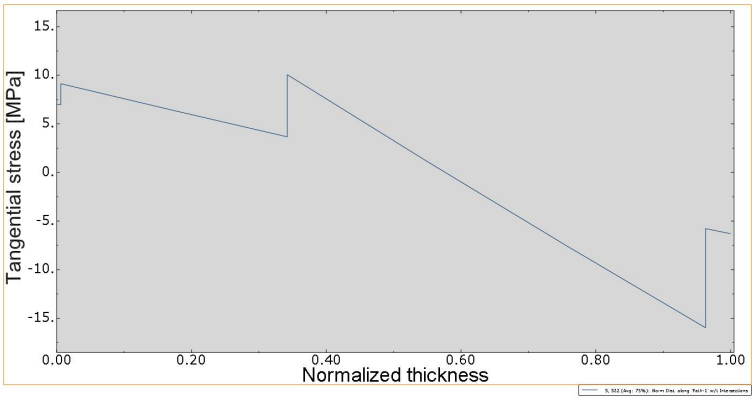

Figure 7.14. Tangential residual stress obtained with FEM for specimen TP-001.

The stress distributions were quite similar between these two stress determination methods. The maximum and minimum values had a small difference between the analytical method and the FEM-calculation. The differences of the maximum stresses between the FEM and the analytical method were under 1 % in the radial stresses and 10 % in the tangential stresses.

8 Conclusions

Most of the tested experimental methods gave credible results. The experimental method results were compared partly to thermal stresses and partly to the FEM calculation results. Comparing the experimental results to thermal stresses is reasonable because the cure shrinkage of the epoxy is low and the curing temperature was uniform through the thickness due to really slow heating and cooling ramps.

The hole-drilling method was found not to be suitable for determining the residual stresses of a thick laminate. The method has restrictions, because the relation between the released internal stresses and the surface strains is valid only to some depth, which can be called the limiting depth. The limiting depth depends on the surface strain measuring technique, that is, whether the strains are measured with strain gages or with optical interferometry. The limiting depth depends also on the material properties and thus it should be determined for each case separately. In the particular case of the thesis, the results of the hole-drilling method were not reliable. Nevertheless the hole-drilling method could be the most potential residual stress determination method from the tested ones. By utilizing the ESPI in surface strain measurement, the test procedure and the measurements are more precise than with strain gages. The test procedure also takes less time compared to using strain gages.

The prices of the hole-drilling residual stress measurement devices are high due to expensive components and small production series. The price of a complete system using the strain gage measurement or the ESPI measurement is around 50 000-80 000 €. If the suitability of the devices can be expanded for wider range of materials, the demand could increase and the prices could lower.

From the layer removal method, it was possible to obtain similar stress profile than by calculating the thermal stresses due to cooling from the cure temperature to ambient temperature. The released stresses by removing a layer were not leading to strains on the opposite surface every time. In some cases the plies with same fibre orientations seemed to hold the stresses and the released stresses of these plies were found to be the largest. When an average stress state of the plies having the same fibre orientation was calculated, the stress profile and the stress values ended up to be similar with the thermal stresses.

The stress determination of an unsymmetrical laminate by using the stress induced deformations gets more difficult when the orientations of the plies increase. In the particular case in the thesis, there were only two fibre directions perpendicular to each other. The stresses were thought as being caused by normal forces, which were determined by using the bending moments. The bending moments were considered acting around the normal axis of the laminate in different directions. The described method is not necessarily compatible for a laminate with more fibre orientations because the stress distribution can be more complex. The measurement of the cure induced midplane strains by using the embedded strain gages did not give reliable results in this study. The reason for it could be the fairly rough laminate structure caused by the thick glass fibre roving. Under the vacuum, the strain gages formed to the shapes of the laminate surface and that affected the strain readings.

The results obtained with the ring slitting method were consistent with the stresses obtained by using the FEM modeling. The only drawback is that the axial stress state of a tube cannot be found by using this method. In a filament wound tube the axial stresses may also occur and they depend, for example on the winding angle and the fibre directions. In the ring slitting case, the FEM modeling was done by utilizing the hoop direction displacement of the cut open ring. In some cases it could be useful to combine experimental measurements and FEM modeling.

In the forthcoming research, the hole-drilling method for composite materials could be improved by utilizing the ESPI in the surface strain measurement. Also further developing of the non-destructive methods such as X-Ray Diffraction and Fiber Bragg grating sensors in the internal strain measurement could be useful. In the thesis, the stresses were considered being distributed evenly on the plies in the same orientation. One interesting field relating to residual stresses is the stress state in the interfaces of two adjacent plies. The hole-drilling method could be compatible for finding the interface stresses when adequate accuracy in the strain measurement and drilling is used.

9 References

[1] M. Zarrelli, A. Skordos. Investigation of cure induced shrinkage in unreinforced epoxy resin. Plastics, Rubber and Composites Processing and Applications, 2002, 377-384

[2] R. Rothon, Particulate-Filled Polymer Composites, 2nd Edition, Rapra Technology Limited, 2003

[3] Materials World Modules, http://www.materialsworldmodules.org/resources/polimarization/2-polymers+monomers.html#Part2. 8.6.2012

[4] Substances & Technologies, http://www.substech.com/dokuwiki. 8.6.2012.

[5] O. Saarela, I. Airasmaa, J. Kokko, M. Skrifvars, V. Komppa. Komposiittirakenteet. Muoviyhdistys ry. 2007.

[6] L. Khoun, P. Hubert. Characterizing the cure shrinkage of an epoxy resin in situ. Society of plastic engineers, 2010. (http://www.4spepro.org/pdf/002583/002583.pdf). 9.7.2012

[7] C. Li, K. Potter. In situ measurement of chemical shrinkage of MY750 epoxy resin by a novel gravimetric method. Composite Science and Technology. Volume 64, Issue 1, January 2004, Pages 55-64.

[8] M. R. Wisnom, L. G. Stringer, R.J. Hayman, M.J. Hinton. Curing stresses in thick polymer composite components Part I: Analysis. International Committee on Composite Materials. DERA, University of Bristol. 1999.

[9] P. Olivier, M. Cavarero. Comparison between longitudinal tensile characteristics of thin and thick thermoset composite laminates: influence of curing conditions. Computers and Structures 76 (2000) 125-137.

[10] M.A. Seif, U.A. Khashaba, R. Rojas-oviedo. Residual stress measurements in CFRE and GFRE composite missile shells. Computers and Structures 79 (2007) 261-269.

[11] J.A. Nairn, S. Hu, J.S. Bark. A critical evaluation of theories predicting microcracking in composite laminates. Journal of material science 28 (1993) 5099-5111.

[12] G.S. Schajer, L. Yang. Residual-stress measurement in orthotropic materials using the hole-drilling method.

[13] A.G. Ghasemi, M. Akbarzadeh. Calibration coefficients for residual stress measurements in composite materials using finite element method. American Journal of engineering and applied sciences 5 (1) 25-28. 2012.

[14] M.M. Shokrieh, A.R. Ghasemi K. Simulation of central hole drilling process for measurement of residual stresses in isotropic, orthotropic and laminated composite plates. Journal of composite materials 41 (2007) 435.

[15] C.B. Smith. Effect of elliptic or circular holes on the stress distribution in plates of wood or plywood considered as orthotropic materials. USDA Forest Products Lab. 1944.

[16] P.G. Ifju, B.C. Kilday, X. Niu, S-C. Liu. A novel method to measure residual stresses in laminated composites. Techomic publishing Co., Inc. 1999

[17] A.S. Khan, X. Wang. Strain measurements and stress analysis. Prentice Hall. 2001.

[18] P.P. Parlevliet, H.E.N. Bersee, A. Beukers. Residual stresses in thermoplastic composites – A study of literature – Part I: Formation of residual stresses. Science direct. Composites: Part A 37 (2006) 1847-1857.

[19] A.S. Nielsen, R. Pyrz. The effect of cooling rate on thermal residual strains in carbon/polypropylene microcomposites. Science and engineering of composite materials. Vol.7 No.1-2. 1998.

[20] H. Nuriel N. Klein, G. Marom. The effect of the transcrystalline layer on the mechanical properties of composite materials in the fibre direction. Composites science and technology. Vol.59, Issue 11. 1999.

[21] R.G Treuting, W.T Read. A mechanical determination of biaxial stress in sheet materials. Journal of applied physics 22, 130. 1951.

[22] M.P.I.M. Eijpe, P.C. Powell. Residual stress evaluation in composites using a modified layer removal method. Composite structures, vol. 37, p.335-342. 1997.

[23] D.N. Betts, A.I.T. Salo, C.R. Bowen, H.A. Kim. Characterisation and modeling of the cured shapes of arbitrary layup bistable composite laminates. Composite structures, 92, p.1694-1700. 2010.

[24] M-L. Dano, M.W. Hyer. Thermally-induced deformation behavior of unsymmetric laminates. International journal of solids and structures, vol. 35, issue 17, p.2101-2120. 1998.

[25] M.W. Hyer, A. Jilani. Predicting the deformation charasteristics od rectangular unsymmetrically laminated piezoelectric materials. Smart material structures 7, p. 784-791. 1998.

[26] J.W. Kim, D.G. Lee. Measurement of residual stresses in thick composite cylinders by the radial-cut-cylinder-bending method. Composite structures 77, p. 444-456. 2007.

[27] J.W. Kim, J.H. Lee, H.G. Kim, H.S. Kim, D.G. Lee. Reduction of residual stresses in thick-walled composite cylinders by smart cure cycle with cooling reheating. Composite structures 75, p. 261-266. 2006.

[28] J.D. Russell, M.S. Madhukar, M.S. Genidy, A.Y. Lee. A new method to reduce cure-induced stresses in thermoset polymer composites, Part III: Correlating stress history to viscosity, degree of cure and cure shrinkage. Journal of composite materials, Vol.34, No.22. 2000

[29] G. Fernlund, A. Poursartip, G. Twigg, C. Albert. Residual stress, spring-in and warpage in autoclaved composite parts. Convergent Manufacturing Technologies Inc. 2003.

[30] B. Benedikt, M. Lewis, P. Rangaswamy. Measurement and modeling of internal stresses at microscopic and mesoscopic levels using Micro Raman Spectroscopy and X-Ray Diffraction. International Centre for Diffraction Data. 2006.

[31] G. Bruno, R. Fernandez. The dependence of the Eshelby model predictions on the microstructure of metal matrix composites. Acta Materialia. Vol. 55, Issue 4, p.1267-1274. 2007.

[32] P.S. Prevéy. X-Ray diffraction residual stress techniques. Metals Handbook 10. Metals Park: American society for metals. p.380-392. 1986.

[33] S. Timoshenko, J.N. Goodier. Theory of Elasticity. McGraw-Hill Book Company Inc. 1951.

[34] J. Mathar. Determination of initial stresses by measuring the deformation around drilled holes. Trans ASME 56(4):249–254. 1934.

[35] C.B. Prasad, R. Prabhakaran, S. Thompkins. Determination of Calibration Constants for the Hole-Drilling Residual Stress Measurement Technique Applied to Orthotropic Composites. Composite Structures, Part 1: Theoretical Considerations. 1987

[36] Y. Watanabe, M. Nishida, T. Hanabusha. X-Ray in situ residual stress measurement of fiber reinforced plastic composite. International Centre for Diffraction Data 2009 ISSN 1097-0002.

[37] G. Luyckx, E. Voet, N. Lammens, J. Degrieck. Strain measurements of composite laminates with embedded fibre Bragg gratings: Criticism and opportunities for research. Sensors, 11, 384-408. 2011.

[38] M. Kreuzer. Strain measurement with fiber Bragg grating sensors. HBM, Darmstadt, Germany. (http://micronoptics.com/uploads/library/documents/FBGS_StrainMeasurement_mo.pdf). 19.10.2012

[39] P. Pagliaro, B. Zuccarello. Residual stress analysis of orthotropic materials by the through-hole drilling method. Experimental mechanics 47. p. 217-236. 2007.

[40] N. Ersoy, Ö. Vardar. Measurement of residual stresses in layered composites by compliance method. Journal of composite materials 34:575. 2000.

[41] Man-Hee Han, J.A. Nairn. Hygrothermal aging of polyimide matrix composite laminates. Composites Part A, 34. p.979-986. Materials science and engineering, University of Utah. 2003.

[42] National Instruments Corporation. Fundamentals of FBG Optical Sensing. http://www.ni.com/white-paper/11821/en. 20.10.2012.

[43] Brigham Young University. Fiber Bragg Gratings. Photonics/Optics Laboratory. http://www.photonics.byu.edu/. 20.10.2012.

10 Appendices

APPENDIX A: Calibration factors for the equations used in the hole drilling method

APPENDIX B: Mathcad 15.0 residual stress calculation tool for ring slitting method

Appendix A. Calibration factors for the equations used in the hole drilling method

Calibration factors C_{ij} for different orthotropic materials calculated by Schajer and Yang (1994). The first row of the headings in the table is used when materials $E_x > E_y$ and the second row when $E_y > E_x$. [12]

E_x/E_y	ν_{xy}	G_{xy}/E_y	c_{11}	c_{13}	c_{21}	c_{22}	c_{23}	c_{31}	c_{33}
E_y/E_x	ν_{yx}	G_{xy}/E_x	c_{33}	c_{31}	c_{23}	c_{22}	c_{21}	c_{13}	c_{11}
1	0	0,1	-0,591	0,169	-0,291	1,18	-0,291	0,169	-0,591
1	0,25	0,1	-0,583	0,123	-0,314	1,097	-0,314	0,123	-0,583
1	0,5	0,1	-0,575	0,076	-0,336	1,013	-0,336	0,076	-0,575
1	0,75	0,1	-0,568	0,03	-0,357	0,93	-0,357	0,03	-0,568
1	0	0,2	-0,514	0,193	-0,188	0,844	-0,188	0,193	-0,514
1	0,25	0,2	-0,503	0,146	-0,205	0,788	-0,205	0,146	-0,503
1	0,5	0,2	-0,491	0,098	-0,221	0,699	-0,221	0,098	-0,491
1	0,75	0,2	-0,478	0,049	-0,235	0,609	-0,235	0,049	-0,478
1	0	0,3	-0,474	0,205	-0,146	0,757	-0,146	0,205	-0,474
1	0,25	0,3	-0,46	0,157	-0,16	0,665	-0,16	0,157	-0,46
1	0,5	0,3	-0,445	0,109	-0,172	0,572	-0,172	0,109	-0,445
1	0	0,4	-0,45	0,213	-0,123	0,692	-0,123	0,213	-0,45
1	0,25	0,4	-0,433	0,164	-0,135	0,598	-0,165	0,164	-0,433
1	0	0,5	-0,433	0,218	-0,108	0,65	-0,108	0,218	-0,433
2	0	0,15	-0,453	0,156	-0,226	1,156	-0,345	0,185	-0,743
2	0,25	0,15	-0,448	0,122	-0,244	1,097	-0,357	0,153	-0,737
2	0,5	0,15	-0,443	0,088	-0,263	1,038	-0,369	0,122	-0,73
2	0,75	0,15	-0,438	0,053	-0,281	0,978	-0,38	0,09	-0,723
2	0	0,3	-0,403	0,18	-0,144	0,865	-0,225	0,207	-0,631
2	0,25	0,3	-0,396	0,145	-0,159	0,802	-0,233	0,175	-0,621
2	0,5	0,3	-0,389	0,11	-0,174	0,739	-0,24	0,143	-0,611
2	0,75	0,3	-0,382	0,074	-0,188	0,675	-0,247	0,11	-0,6
2	0	0,45	-0,377	0,193	-0,111	0,751	-0,177	0,217	-0,576
2	0,25	0,45	-0,369	0,158	-0,124	0,686	-0,182	0,185	-0,563
2	0,5	0,45	-0,36	0,122	-0,137	0,62	-0,187	0,152	-0,55
2	0,75	0,45	-0,35	0,085	-0,149	0,554	-0,191	0,119	-0,536
2	0	0,6	-0,361	0,201	-0,092	0,689	-0,15	0,223	-0,541
2	0,25	0,6	-0,351	0,165	-0,105	0,623	-0,154	0,191	-0,527
4	0	0,2	-0,35	0,137	-0,186	1,212	-0,435	0,195	-0,949
4	0,25	0,2	-0,347	0,112	-0,201	1,171	-0,441	0,174	-0,944
4	0,5	0,2	-0,344	0,088	-0,16	1,129	-0,447	0,152	-0,938
4	0,75	0,2	-0,341	0,063	-0,232	1,087	-0,453	0,131	-0,932
4	0	0,4	-0,318	0,162	-0,116	0,91	-0,288	0,215	-0,787
4	0,25	0,4	-0,314	0,136	-0,13	0,866	-0,291	0,193	-0,778

4	0,5	0,4	-0,31	0,11	-0,143	0,821	-0,294	0,171	-0,77
4	0,75	0,4	-0,306	0,84	-0,156	0,776	-0,296	0,149	-0,761
4	0	0,6	-0,301	0,175	-0,088	0,792	-0,229	0,223	-0,707
4	0,25	0,6	-0,296	0,149	-0,101	0,746	-0,23	0,201	-0,696
4	0,5	0,6	-0,291	0,122	-0,112	0,7	-0,231	0,179	-0,685
4	0,75	0,6	-0,286	0,096	-0,124	0,653	-0,231	0,157	-0,674
4	0	0,8	-0,291	0,183	-0,073	0,728	-0,196	0,228	-0,659
4	0,25	0,8	-0,285	0,157	-0,084	0,681	-0,196	0,206	-0,646
4	0,5	0,8	-0,279	0,13	-0,095	0,634	-0,196	0,184	-0,633
4	0	1	-0,283	0,189	-0,063	0,687	-0,175	0,231	-0,626
8	0	0,3	-0,263	0,123	-0,138	1,224	-0,508	0,207	-1,16
8	0,25	0,3	-0,262	0,105	-0,15	1,194	-0,51	0,192	-1,155
8	0,5	0,3	-0,26	0,087	-0,162	1,164	-0,513	0,177	-1,149
8	0,75	0,3	-0,258	0,068	-0,174	1,135	-0,515	0,163	-1,144
8	0	0,6	-0,244	0,146	-0,084	0,935	-0,343	0,222	-0,939
8	0,25	0,6	-0,242	0,127	-0,095	0,903	-0,343	0,207	-0,931
8	0,5	0,6	-0,239	0,108	-0,105	0,871	-0,342	0,192	-0,923
8	0,75	0,6	-0,236	0,089	-0,116	0,839	-0,342	0,177	-0,914
8	0	0,9	-0,234	0,158	-0,062	0,823	-0,278	0,228	-0,834
8	0,25	0,9	-0,231	0,139	-0,072	0,79	-0,276	0,213	-0,824
8	0,5	0,9	-0,228	0,12	-0,082	0,757	-0,275	0,198	-0,814
8	0,75	0,9	-0,224	0,1	-0,092	0,724	-0,273	0,183	-0,803
8	0	1,2	-0,227	0,166	-0,05	0,763	-0,242	0,231	-0,771
8	0,25	1,2	-0,224	0,147	-0,06	0,729	-0,24	0,216	-0,76
8	0,5	1,2	-0,22	0,127	-0,069	0,696	-0,237	0,201	-0,748
16	0	0,4	-0,199	0,105	-0,109	1,323	-0,634	0,213	-1,45
16	0,25	0,4	-0,198	0,092	-0,118	1,301	-0,634	0,203	-1,446
16	0,5	0,4	-0,196	0,079	-0,127	1,28	-0,634	0,193	-1,441
16	0,75	0,4	-0,195	0,065	-0,136	1,259	-0,634	0,182	-1,437
16	0	0,8	-0,187	0,126	-0,062	1,019	-0,437	0,225	-1,147
16	0,25	0,8	-0,186	0,113	-0,071	0,997	-0,435	0,214	-1,14
16	0,5	0,8	-0,184	0,099	-0,079	0,974	-0,433	0,204	-1,133
16	0,75	0,8	-0,182	0,085	-0,088	0,952	-0,432	0,193	-1,126
16	0	1,2	-0,181	0,138	-0,044	0,903	-0,36	0,228	-1,006
16	0,25	1,2	-0,179	0,124	-0,052	0,88	-0,357	0,218	-0,997
16	0,5	1,2	-0,177	0,109	-0,06	0,856	-0,354	0,207	-0,988
16	0,75	1,2	-0,175	0,095	-0,068	0,833	-0,351	0,197	-0,979
16	0	1,6	-0,177	0,145	-0,034	0,84	-0,318	0,23	-0,923
16	0,25	1,6	-0,175	0,131	-0,042	0,816	-0,315	0,22	-0,913
16	0,5	1,6	-0,173	0,116	-0,049	0,762	-0,311	0,209	-0,902
16	0,75	1,6	-0,171	0,102	-0,057	0,768	-0,308	0,198	-0,892
16	0	2	-0,175	0,15	-0,027	0,801	-0,292	0,231	-0,867

Appendix B. Mathcad 15.0 residual stress calculation tool for ring slitting method

The equations that are needed in residual stress calculation are presented. Similar equations were used for every specimen in this study. As the material properties are changing through the thickness, the elastic modulus and the thicknesses of the layers must be taken into account in the calculations.

Variable explanations:

$\delta_{inner\ pair}$ = displacement measured from the inner studs
$\delta_{outer\ pair}$ = displacement measured from the outer studs
r_{pIN} = radius to the inner studs
r_{pOUT} = radius to the outer studs
δ *(average)* = average displacement from inner and outer pair
r (average) = average radius to the measurement point
t = overall thickness of the laminate
a = inner radius of the ring
b = outer radius of the ring
α = angle measuring the displacement
n = coefficient (values in the table, simplifying the residual stress equations)

Elastic modulus:
E_{CR}=Chemical Resistant layer (SM)
E_{SealIN}=Sealing layer INNER (M300)
E_{Sup}=Support layer (U480 & UD256)
$E_{SealOUT}$=Sealing layer OUTER (M300)
E_{Sur}=Surface layer (SM)

In equations:
$E_n(r_n)$ = elastic modulus as a function of radius
$M_{r\_n}(r_n)$ = residual moment in the ring as a function of radius

Measured displacements, material properties and geometry that are needed in calculations are filled in the table. The calculation tool uses the output values from this table to determine the residual stresses through the thickness of the laminate.

$$\begin{pmatrix} \delta \\ r_p \\ t \\ a \\ b \\ \alpha \\ n \\ E_{CR} \\ E_{SealIN} \\ E_{Sup} \\ E_{SealOUT} \\ E_{Sur} \\ t_{CR} \\ t_{SealIN} \\ t_{Sup} \\ t_{SealOUT} \\ t_{Sur} \end{pmatrix} :=$$

Loop end displacements

Residual stress measurements

	Distance between studs							
	before cutting		after cutting					
	inner pair	outer pair	inner pair	outer pair	$\delta_{inner\ pair}$	$\delta_{outer\ pair}$	r_{pIN}	r_{pOUT}
TP-001	52,94	52,91	26,90	25,60	-26,04	-27,31	255	260
TP-002	52,96	52,94	39,42	39,20	-13,54	-13,74	255	260
TP-003	52,96	52,99	38,88	38,70	-14,08	-14,29	255	260
TP-004	52,86	52,89	41,35	41,29	-11,51	-11,60	255	260
TP-005	52,86	52,79	21,38	20,70	-31,48	-32,09	255	260
TP-006	52,91	53,06	40,25	40,15	-12,66	-12,91	255	260
TP-007	53,04	53,21	38,17	38,03	-14,87	-15,18	255	260
TP-008	52,92	53,09	39,56	39,60	-13,36	-13,49	255	260
TP-009	52,86	52,38	23,28	22,77	-29,58	-29,61	255	260
TP-010	52,87	53,13	38,73	38,86	-14,14	-14,27	255	260
TP-011	52,89	53,15	39,02	39,01	-13,87	-14,14	255	260
TP-012	52,85	52,96	55,65	55,74	2,80	2,78	255	260
TP-013	52,93	53,03	22,60	21,94	-30,33	-31,09	255	260
TP-014	52,95	53,07	38,28	38,21	-14,67	-14,86	255	260
TP-015	53,04	53,03	37,26	36,99	-15,78	-16,04	255	260
TP-016	53,10	52,94	42,23	42,04	-10,87	-10,90	255	260

Variables for residual stress calculation							Elastic modulus for different layers [Mpa]					Thicknesses of the layers [mm]					
δ (average)	r (average)	t	a	b	α	n	Chemical Resistant	Sealing Inner	Support	Sealing Outer	Surface	Chemical Resistant	Sealing Inner	Support	Sealing Outer	Surface	
-26,68	257,5	19,3125	250	269,3125	-0,10359	185444	7200	9480	26230	9480		0,12	6,49	11,9825	0,72		TP-001
-13,64	257,5	30,2625	250	280,2625	-0,05297	1117813	7200	9480	26230	9480	7200	0,12	12,27	11,9825	5,77	0,12	TP-002
-14,19	257,5	24,4825	250	274,4825	-0,05509	478890	7200	9480	26230	9480	7200	0,12	6,49	11,9825	5,77	0,12	TP-003
-11,56	257,5	18,5925	250	268,5925	-0,04487	159300		9480	26230	9480	7200		0,72	11,9825	5,77	0,12	TP-004
-31,79	257,5	19,6425	250	269,6425	-0,12344	198446	7120	9310	26320	9310		0,12	6,79	11,9825	0,75		TP-005
-12,79	257,5	31,0925	250	281,0925	-0,04965	1245554	7120	9310	26320	9310	7120	0,12	12,83	11,9825	6,04	0,12	TP-006
-15,03	257,5	25,0525	250	275,0525	-0,05835	525063	7120	9310	26320	9310	7120	0,12	6,79	11,9825	6,04	0,12	TP-007
-13,43	257,5	18,8925	250	268,8925	-0,05214	169832		9310	26320	9310	7120		0,75	11,9825	6,04	0,12	TP-008
-29,60	257,5	19,6425	250	269,6425	-0,11493	198446	7320	9510	26500	9510		0,12	6,79	11,9825	0,75		TP-009
-14,21	257,5	31,0925	250	281,0925	-0,05517	1245554	7320	9510	26500	9510	7320	0,12	12,83	11,9825	6,04	0,12	TP-010
-14,01	257,5	25,0525	250	275,0525	-0,05439	525063	7320	9510	26500	9510	7320	0,12	6,79	11,9825	6,04	0,12	TP-011
2,79	257,5	18,8925	250	268,8925	0,010835	169832		9510	26500	9510	7320		0,75	11,9825	6,04	0,12	TP-012
-30,71	257,5	19,6425	250	269,6425	-0,11926	198446	6920	9110	26140	9110		0,12	6,79	11,9825	0,75		TP-013
-14,77	257,5	31,0925	250	281,0925	-0,05734	1245554	6920	9110	26140	9110	6920	0,12	12,83	11,9825	6,04	0,12	TP-014
-15,91	257,5	25,0525	250	275,0525	-0,06179	525063	6920	9110	26140	9110	6920	0,12	6,79	11,9825	6,04	0,12	TP-015
-10,89	257,5	18,8925	250	268,8925	-0,04227	169832		9110	26140	9110	6920		0,75	11,9825	6,04	0,12	TP-016

Modulus of elasticity for different layers of specimen TP-001:

$$E_1(r_1) := \begin{cases} E_{CR_1} & \text{if } 0 \le \frac{(r_1 - a_1)}{t_1} \le \frac{(t_{CR_1})}{t_1} \\ E_{SealIN_1} & \text{if } \frac{(t_{CR_1})}{t_1} \le \frac{(r_1 - a_1)}{t_1} \le \frac{(t_{CR_1} + t_{SealIN_1})}{t_1} \\ E_{Sup_1} & \text{if } \frac{(t_{CR_1} + t_{SealIN_1})}{t_1} \le \frac{(r_1 - a_1)}{t_1} \le \frac{(t_{CR_1} + t_{SealIN_1} + t_{Sup_1})}{t_1} \\ E_{SealOUT_1} & \text{if } \frac{(t_{CR_1} + t_{SealIN_1} + t_{Sup_1})}{t_1} \le \frac{(r_1 - a_1)}{t_1} \le \frac{(t_{CR_1} + t_{SealIN_1} + t_{Sup_1} + t_{SealOUT_1})}{t_1} \end{cases}$$

Residual moment for specimen TP-001:

$$M_{r.1}(r_1) := \frac{\frac{1}{E_1(r_1)^{-1}}}{\left[\frac{\frac{-\alpha_1}{8\cdot\pi}}{\left[\left[(b_1)^4 - 2\cdot\left[\frac{(a_1)^2}{(b_1)^{-2}}\right] + (a_1)^4\right] - \frac{\left[\frac{4\cdot(a_1)^2}{(b_1)^{-2}}\right]}{\left(\ln\left(\frac{b_1}{a_1}\right)\right)^{-2}}}{2\cdot\left[(b_1)^2 - (a_1)^2\right]}\right]^{-1}}\right]^{-1}}$$

Radial residual stress for specimen TP-001:

$$\sigma_{r1}(r_1) := \frac{-4\cdot M_{r.1}(r_1)}{n_1}\cdot\left[\frac{(a_1)^2\cdot(b_1)^2}{{r_1}^2}\cdot\ln\left(\frac{b_1}{a_1}\right) + (b_1)^2\cdot\ln\left(\frac{r_1}{b_1}\right) + (a_1)^2\cdot\ln\left(\frac{a_1}{r_1}\right)\right]$$

Tangential residual stress for specimen TP-001:

$$\sigma_{\theta 1}(r_1) := \frac{-4\cdot M_{r.1}(r_1)}{n_1}\cdot\left[\frac{-(a_1)^2\cdot(b_1)^2}{{r_1}^2}\cdot\ln\left(\frac{b_1}{a_1}\right) + (b_1)^2\cdot\ln\left(\frac{r_1}{b_1}\right) + (a_1)^2\cdot\ln\left(\frac{a_1}{r_1}\right) + \left[(b_1)^2 - (a_1)^2\right]\right]$$